ENZYME-LIKE CATALYSIS BY SINGLE CHAIN NANOPARTICLES THAT USE TRANSITION METAL COFACTORS

BY

THAO MEE XIONG

DISSERTATION

Submitted in partial fulfillment of the requirements
for the degree of Doctor of Philosophy in Chemistry
in the Graduate College of the
University of Illinois Urbana-Champaign, 2021

Urbana, Illinois

Doctoral Committee:

Professor Steven C. Zimmerman, Chair
Associate Professor Jefferson Chan
Associate Professor Alison R. Fout
Professor Jeffrey S. Moore

ABSTRACT

A strategy to improve the catalytic activity of transitional metal-based catalysis in the complex biological environment mimics metalloenzymes by folding a polymer chain around a metal center to form single chain nanoparticles (SCNPs). Herein I report two strategies for the preparation of transition metal-SCNPs. First, we developed a noncovalently cross-linked amphiphilic polymer with covalently attached catalyst that allows substrate binding for higher catalytic activity. Next, I developed a modular approach in which a noncovalently cross-linked SCNP formed from the folding of an amphiphilic polymer selectively binds catalyst "cofactors" and substrates to increase their proximity and resultant catalytic activity. The polymers were synthesized by free radical polymerization and post-polymerization functionalization with amines and characterized by NMR, GPC, and DLS. Fluorescence studies demonstrated the SCNP's ability to increase the catalytic activity of a Cu-catalyzed alkyne-azide cycloaddition reaction and the Ru-catalyzed cleavage of allylcarbamate groups compared to the free catalysts. A small library of Cu and Ru catalysts with different alkyl chain lengths, functional groups, and charges was used to develop a structure-activity relationship. Ligand binding to the SCNP was identified and characterized by NOESY and STD NMR experiments. These results demonstrate the potential of this plug-and-play strategy for obtaining functional transition metal-SCNPs.

We also utilized polymers for ketal-based cross-linked polyamide microcapsules. Under acidic conditions, the microcapsules degrade and release anticorrosion active agents. They were embedded in commercially available coatings to obtain self-protecting coatings.

ACKNOWLEDGMENTS

I would like to first thank my advisor, Professor Steven C. Zimmerman, for his patience and support throughout the completion of my doctoral degree requirements. I would also like to thank my committee members Professor Jefferson Chan, Professor Alison R. Fout, and Professor Jeffrey S. Moore for their advice and encouragement. I am thankful for all the wonderful members of the Zimmerman group, who created a collaborative and inclusive work environment. In particular, I would like to thank my collaborators and peer mentors Dr. Yugang Bai, Dr. Junfeng Chen, Dr. Edzna S. Garcia, and Dr. Ephraim G. Morado for their advice on research and professional development, and my undergraduate research assistant Ariale J. Alzona for her help synthesizing chemical compounds. I wish to thank Professor Emeritus Kimiko Gunji and the members of the Chado Urasenke Tankokai Urbana-Champaign Association for providing a welcoming space outside of lab. Finally, I would like to thank my family and friends for their unconditional support.

This work would not have been possible without funding from the National Science Foundation (NSF CHE-1709718). I would like to thank Dr. Dean Olson, Dr. Lingyang Zhu, Nikki Duay, and the School of Chemical Sciences NMR (SCS-NMR-UIUC) Lab for access to NMR instrumentation and their technical support.

TABLE OF CONTENTS

CHAPTER 1: INTRODUCTION TO SINGLE CHAIN NANOPARTICLES

1.1 Single Chain Nanoparticles

Conducting transition metal-catalyzed bioorthogonal reactions inside cells has enabled the intracellular synthesis of drugs and dyes for potential applications in therapy and imaging, respectively.[1-3] Successful intracellular catalysis requires the catalyst to enter the cell and to function under physiological conditions and often under dilute concentrations. However, most transition metal catalysts have poor water solubility and low stability in biologically relevant media. Recently reported approaches use metal nanoparticles and polymers to achieve intracellular delivery and catalysis.[4] For example, Rotello and coworkers designed AuNPs functionalized with a monolayer of hydrophobic alkyl segments for catalyst encapsulation and observed Ru- and Pd-catalyzed cleavage of allylcarbamate groups.[5] Lipshutz and coworkers demonstrated that micelles obtained from the assembly of surfactants promote a myriad of reactions in water, including Ru-catalyzed olefin metathesis and Pd-catalyzed cross-coupling reactions.[6]

A strategy that more closely resembles how nature achieves catalysis mimics metalloenzymes by folding a polymer chain around a metal center.[7] Single chain nanoparticles (SCNPs) are composed of a polymer scaffold that has been folded via intramolecular covalent bonds or noncovalent interactions to form particles with diameters ranging from 1 – 100 nm. They have been utilized to catalyze the oxidation of sulfides,[8] reduction of amides,[9] living radical polymerization,[10] hydroxylation of phenol,[11] depropargylation[12] and amination[13] reactions, and a myriad of other chemical transformations under aqueous conditions.[14] Our group has developed several catalytic SCNPs, including Cu-SCNPs that promote the Cu-catalyzed azide-alkyne cycloaddition (CuAAC) reaction in water and in cells.[15, 16] The Cu-SCNPs are cross-linked by

ionic bonds. Our group has also reported a Ru-SCNP that catalyzes the reduction of azido groups and has demonstrated potential for concurrent and tandem catalysis with enzymes such as β-galactosidase (βGal).[17] The Ru-SCNP is cross-linked by covalent bonds.

I envision a simpler approach in which the SCNP is not covalently cross-linked. Random amphiphilic copolymers have been reported by Sawamoto and coworkers[18] to undergo single-chain folding in water. A recent review by Knight and coworkers[19] highlights recent advances in the development of protein-mimetic synthetic macromolecules, including the assembly of random amphiphilic copolymers. The micelle-like structure has a hydrophilic outer shell and hydrophobic pockets. In the first strategy, we design a non-covalently cross-linked Ru-SCNP for catalyzing the cleavage of allylcarbamate groups.[20] Still, these and other reported examples involve covalently attaching the catalyst to the polymer, which requires the synthesis of a new polymeric scaffold for each reaction of interest. The second strategy utilizes a modular approach in which the SCNP is not covalently attached to the catalyst but is able to selectively bind the catalyst and its substrates for higher catalytic activity.[21] The SCNP is formed from folding of an amphiphilic polymer under dilute aqueous conditions and is utilized to produce Cu-SCNPs for CuAAC and Ru-SCNPs for Ru-catalyzed cleavage of allylcarbamate groups. These strategies offer the potential for more rapidly expanding the chemist's toolbox of transition metal-SCNPs.

1.2 References

1. Lang, K.; Chin, J. W. Bioorthogonal Reactions for Labeling Proteins. *ACS Chem. Biol.* **2014**, *9*, 16-20.
2. Patterson, D. M.; Nazarova, L. A.; Prescher, J. A. Finding the Right (Bioorthogonal) Chemistry. *ACS Chem. Biol.* **2014**, *9*, 592-605.

3. Li, J.; Chen, P. R. Development and Application of Bond Cleavage Reactions in Bioorthogonal Chemistry. *Nat. Chem. Biol.* **2016**, *12*, 129-137.

4. Bai, Y.; Chen, J.; Zimmerman, S. C. Designed Transition Metal Catalysts for Intracellular Organic Synthesis. *Chem. Soc. Rev.* **2018**, *47*, 1811-1821.

5. Tonga, G. Y.; Jeong, Y.; Duncan, B.; Mizuhara, T.; Mout, R.; Das, R.; Kim, S. T.; Yeh, Y.-C.; Yan, B.; Hou, S.; Rotello, V. M. Supramolecular Regulation of Bioorthogonal Catalysis in Cells Using Nanoparticle-Embedded Transition Metal Catalysts. *Nat. Chem.* **2015**, *7*, 597-603.

6. Lipshutz, B. H.; Ghorai, S.; Abela, A. R.; Moser, R.; Nishikata, T.; Duplais, C.; Krasovskiy, A.; Gaston, R. D.; Gadwood, R. C. TPGS-750-M: A Second-Generation Amphiphile for Metal-Catalyzed Cross-Couplings in Water at Room Temperature. *J. Org. Chem.* **2011**, *76*, 4379-4391.

7. Rothfuss, H.; Knofel, N. D.; Roesky, P. W.; Barner-Kowollik, C. Single-Chain Nanoparticles as Catalytic Nanoreactors. *J. Am. Chem. Soc.* **2018**, *140*, 5875-5881.

8. Zhang, Y.; Wang, W.; Fu, W.; Zhang, M.; Tang, Z.; Tan, R.; Yin, D. Titanium(IV)-Folded Single-Chain Polymeric Nanoparticles as Artificial Metalloenzyme for Asymmetric Sulfoxidation in Water. *Chem. Comm.* **2018**, *54*, 9430-9433.

9. Mavila, S.; Rozenberg, I.; Lemcoff, N. G. A General Approach to Mono- and Bimetallic Organometallic Nanoparticles. *Chem. Sci.* **2014**, *5*, 4196-4203.

10. Azuma, Y.; Terashima, T.; Sawamoto, M. Self-Folding Polymer Iron Catalysts for Living Radical Polymerization. *ACS Macro Lett.* **2017**, *6*, 830-835.

11. Thanneeru, S.; Duay, S. S.; Jin, L.; Fu, Y.; Angeles-Boza, A. M.; He, J. Single Chain Polymeric Nanoparticles to Promote Selective Hydroxylation Reactions of Phenol Catalyzed by Copper. *ACS Macro Lett.* **2017**, *6*, 652-656.

12. Liu, Y.; Pauloehrl, T.; Presolski, S. I.; Albertazzi, L.; Palmans, A. R. A.; Meijer, E. W. Modular Synthetic Platform for the Construction of Functional Single-Chain Polymeric Nanoparticles: From Aqueous Catalysis to Photosensitization. *J. Am. Chem. Soc.* **2015**, *137*, 13096-13105.

13. Knöfel, N. D.; Rothfuss, H.; Willenbacher, J.; Barner-Kowollik, C.; Roesky, P. W. Platinum(II)-Crosslinked Single-Chain Nanoparticles: An Approach Towards Recyclable Homogeneous Catalysts. *Angew. Chem. Int. Ed.* **2017**, *56*, 4950-4954.

14. Cole, J. P.; Lyon, C. K.; Berda, E. B. Single-Chain Nanoparticles. In *Bio-inspired Polymers*, Bruns, N.; Kilbinger, A. F. M., Eds. Royal Society of Chemistry: 2017; pp 107-140.

15. Bai, Y.; Feng, X.; Xing, H.; Xu, Y.; Kim, B. K.; Baig, N.; Zhou, T.; Gewirth, A. A.; Lu, Y.; Oldfield, E.; Zimmerman, S. C. A Highly Efficient Single-Chain Metal-Organic Nanoparticle Catalyst for Alkyne-Azide "Click" Reactions in Water and in Cells. *J. Am. Chem. Soc.* **2016**, *138*, 11077-11080.

16. Chen, J.; Wang, J.; Bai, Y.; Li, K.; Garcia, E. S.; Ferguson, A. L.; Zimmerman, S. C. Enzyme-like Click Catalysis by a Copper-Containing Single-Chain Nanoparticle. *J. Am. Chem. Soc.* **2018**, *140*, 13695-13702.

17. Chen, J.; Li, K.; Seon, J.; Shon, L. ; Zimmerman, S. C. Single-Chain Nanoparticle Delivers a Partner Enzyme for Concurrent and Tandem Catalysis in Cells. *J. Am. Chem. Soc.* **2020**, *142*, 4565–4569.

18. Terashima, T.; Sugita, T.; Fukae, K.; Sawamoto, M. Synthesis and Single-Chain Folding of Amphiphilic Random Copolymers in Water. *Macromolecules* **2014**, *47*, 589-600.

19. Barbee, M. H.; Wright, Z. M.; Allen, B. P.; Taylor, H. F.; Patteson, E. F.; Knight, A. S. Protein-Mimetic Self-Assembly with Synthetic Macromolecules. *Macromolecules* **2021**, *54*, 3585-3612.

20. Garcia, E. S.; Xiong, T. M.; Lifschitz, A.; Zimmerman, S. C. Tandem Catalysis Using an Enzyme and a Polymeric Ruthenium-Based Artificial Metallozyme. *Submitted* **2021**.

21. Xiong, T. M.; Garcia, E. S.; Chen, J.; Alzona, A. J.; Zimmerman, S. C. Enzyme-Like Catalysis by Single Chain Nanoparticles that Use Transition Metal Cofactors. *Submitted* **2021**.

CHAPTER 2: RUTHENIUM-CONTAINING SINGLE CHAIN NANOPARTICLES VIA NONCOVALENT CROSS-LINKING

Part of this chapter has been adapted and modified from the following publication: Garcia, E. S.; **Xiong, T. M.**; Lifschitz, A.; Zimmerman, S. C. Tandem Catalysis Using an Enzyme and a Polymeric Ruthenium-Based Artificial Metallozyme. *Submitted* **2021**.

2.1 Design and Synthesis of Polymers

In the first strategy, we design a non-covalently cross-linked Ru-SCNP for catalyzing the cleavage of allylcarbamate groups (Scheme 2.1).[1] In 2006 Kitamura and coworkers reported a Ru

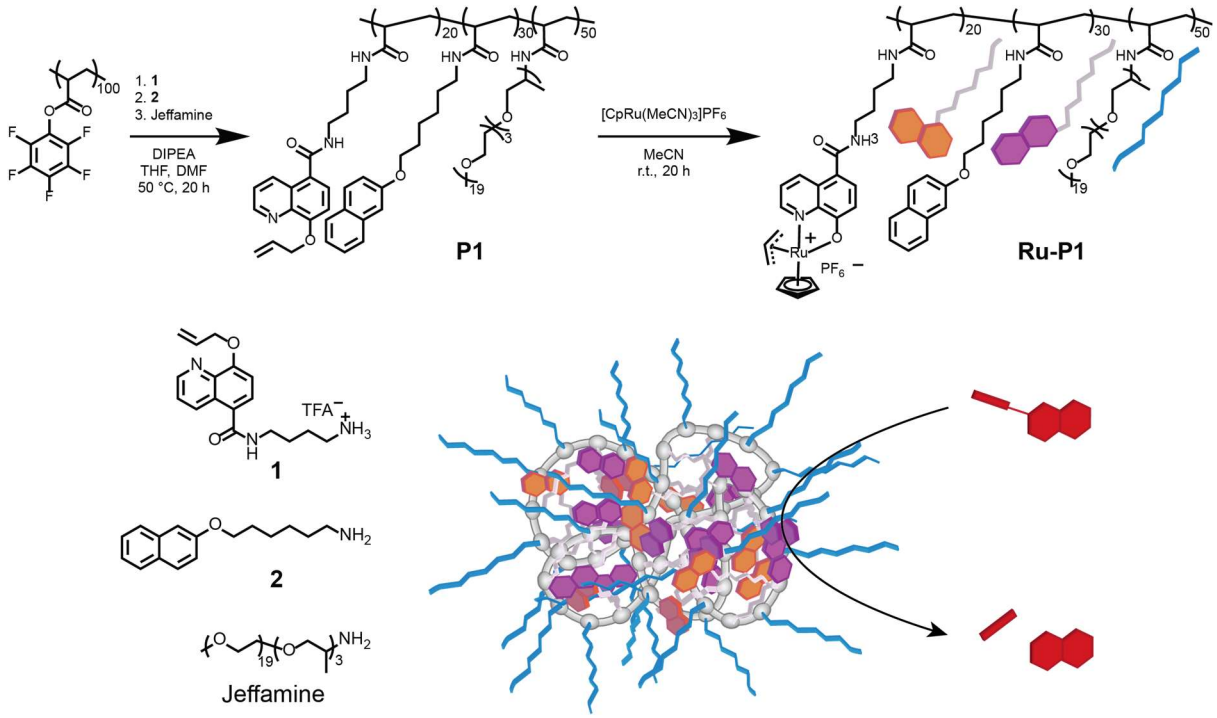

Scheme 2.1 Synthetic scheme for polymer **P1** and **Ru-P1** using post-polymerization functionalization of poly(pentafluorophenyl acrylate) with quinoline **1**, naphthalene **2**, and Jeffamine M-1000 followed by Ru coordination.

catalyst with a 2-quinolinecarboxylate ligand for the cleavage of allylcarbamate groups.[2] Meggers and coworkers optimized the Ru catalyst for the uncaging of alloc protected amines under aqueous conditions and inside living cells.[3, 4] We hypothesized that covalently attaching a derivative of their 8-hydroxyquinolate Ru complex to a random amphiphilic copolymer would improve its catalytic activity and allow enzyme-like substrate binding. We synthesized random amphiphilic polymer

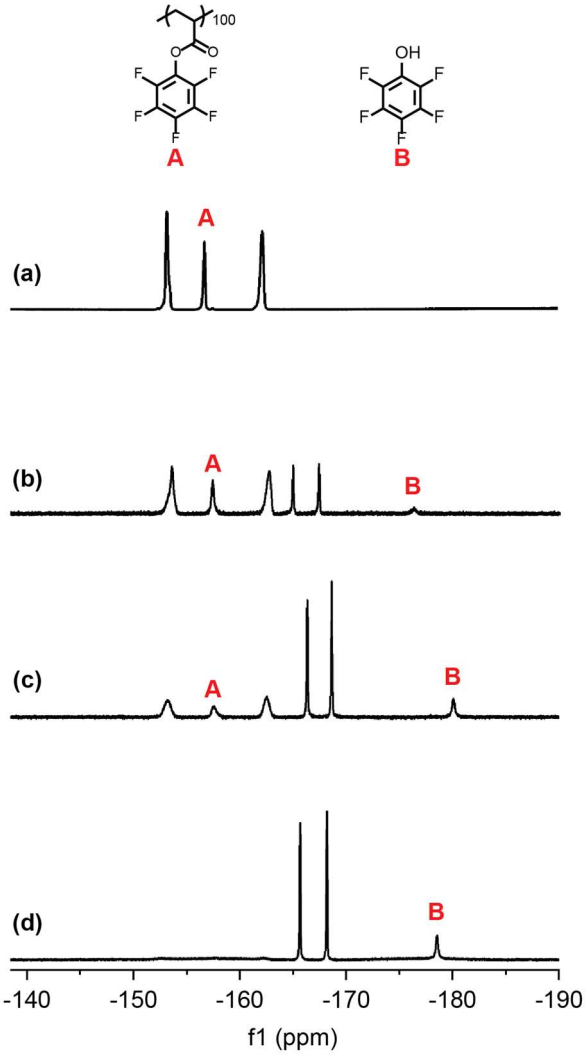

Figure 2.1 Stacked ^{19}F NMR spectra of **P1** (a) before addition of amines (0% conversion, $CDCl_3$) (b) 4 h after addition of quinoline **1** (23% conversion, $CDCl_3$) (c) 4 h after addition of 6-(2-naphthyloxy)-1-hexylamine **2** (57% conversion, $CDCl_3$) and (d) 16 h after addition of Jeffamine M-1000 (>95% conversion, $CDCl_3$).

P1 from precursor poly(pentafluorophenyl acrylate), which was obtained from reversible addition-fragmentation chain-transfer (RAFT) polymerization.[5] The degree of polymerization (DP) of the poly(pentafluorophenyl acrylate) was controlled by carefully controlling the ratio of monomer to chain transfer agent and characterization by gel permeation chromatography (GPC) indicated a DP of 100. The pendant activated ester groups readily undergo substitution in the presence of a hard nucleophile, such as an amine. This flexible and efficient approach to SCNPs was developed by Palmans, Meijer, and coworkers[6] and we have employed it to obtain Ru-SCNPs. Thus, amphiphilic polyacrylamide **Ru-P1** was obtained through post-polymerization functionalization using quinoline **1**, 6-(2-naphthyloxy)-1-hexylamine (**2**), and Jeffamine M-1000.

Hydrophilic Jeffamine M-1000 was added to provide water solubility, the naphthyl groups assist folding and provide a hydrophobic interior for substrate binding, and the quinoline groups allow coordination to the Ru catalyst. The target functionalization ratio of quinoline **1**/naphthalene

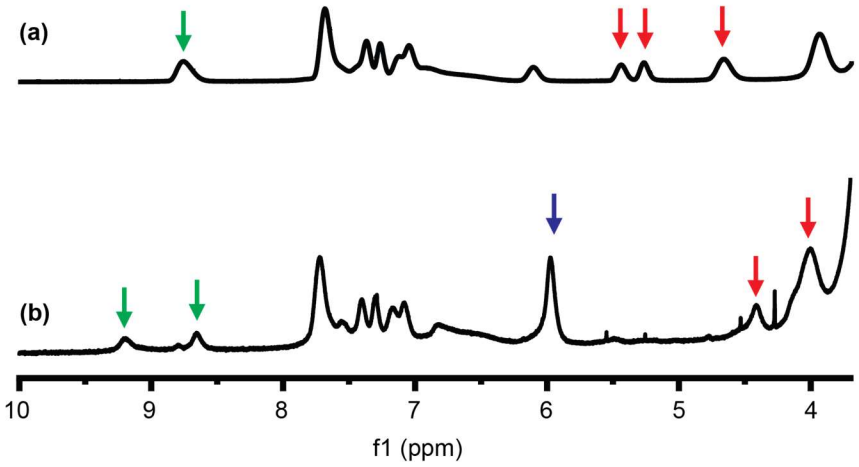

Figure 2.2 Stacked ^{1}H NMR spectra (CD_3CN) of **P1** (a) before and (b) 20 h after addition of $[CpRu(MeCN)_3]PF_6$. The resolution of quinoline protons (green arrows), appearance of a cyclopentadienyl peak (blue arrow), and upfield shift of the allyl protons on the ligand (red arrows) were observed after Ru coordination.

2/Jeffamine M-1000 was 20:30:50, respectively. The percent conversion was monitored by ^{19}F NMR to give an observed functionalization ratio of 23:34:43, which is consistent with the feed ratio of quinoline **1**, naphthalene **2**, and Jeffamine M-1000 (Figure 2.1). Polymer **P1** was further characterized by GPC to obtain a molecular weight, M_n = 54.8 kDa, and dispersity, $Đ$ = 1.2. The functionalized polymers were purified by precipitation from diethyl ether and dialysis against water and used in the next step to produce polymer **Ru-P1**. Polymer **Ru-P1** was obtained by treating polymer **P1** with $[CpRu(MeCN)_3]PF_6$. Ru coordination to the quinoline ligands was monitored by ^1H NMR (Figure 2.2). The allyl protons of quinoline side chain **1** underwent an upfield chemical shift, which suggested coordination to the electron dense Ru metal center. In addition, the appearance of a broad cyclopentadienyl peak at δ 6 ppm and resolution of quinoline

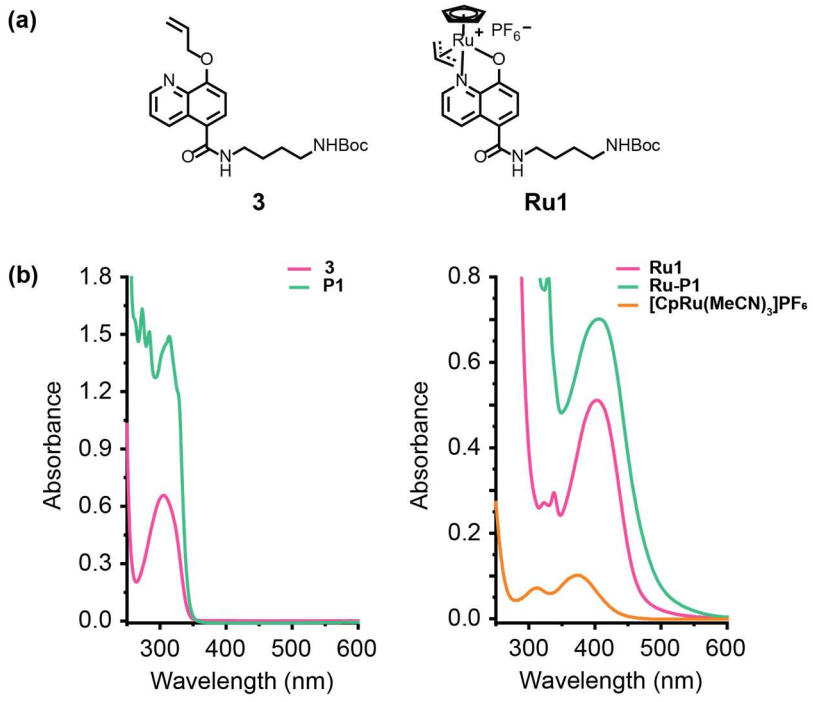

Figure 2.3 (a) Structure of small molecule models **3** and **Ru1** and (b) UV-vis spectra in MeCN of **3** (100 μM) and **P1** (0.5 mg/mL, 9.1 μM), **Ru1** (100 μM), **Ru-P1** (138 μM Ru), and $[CpRu(MeCN)_3]PF_6$ (100 μM).

protons at δ 9 ppm were observed. These proton chemical shifts are consistent with those observed for the small molecule catalyst **Ru1** (Figure 2.3a).

Next, we quantified the efficiency of the Ru coordination to **P1** using UV-vis spectroscopy (Figure 2.3b). We synthesized small molecule models **3** and **Ru1** and compared their absorption bands with those of polymers **P1** and **Ru-P1**. Ligand **3** and polymer **P1** have absorption bands below 350 nm. Small molecule catalyst **Ru1** has an absorption band at λ_{max} = 401 nm, which corresponds to the metal-to-ligand charge transfer (MLCT) process.[7] This absorption band was also observed for polymer **Ru-P1** and was used to estimate the amount of Ru loading per polymer. A calibration curve was generated from the UV-vis spectra of **Ru1** at various concentrations ranging from 5 μM to 200 μM. Based on the calibration curve and the M_n of **P1**, we calculated that **Ru-P1** contains 15 Ru per polymer on average.

2.2 Characterization of SCNPS

Under aqueous conditions, random amphiphilic copolymers may intramolecularly fold into SCNPs or intermolecularly aggregate to form micelles.[8-11] Sawamoto, Terashima and coworkers have extensively studied the self-folding of random amphiphilic copolymers into unimolecular micelles in water.[12-14] Because the polymers are not covalently cross-linked, their ability to form SCNPs is dependent on the concentration of the solution. Fluorescence spectroscopy was used to determine the critical micelle concentration (CMC) of polymers **P1** and **Ru-P1**. Samples of polymer **P1** or **Ru-P1** with 1 μM Nile red were prepared with concentrations ranging from 0.5 μg/mL (9.1 nM) to 1.0 mg/mL (18.2 μM). The fluorescence emission was measured (Figure 2.4a). Nile red does not fluoresce in polar solvents, but it exhibits strong fluorescence in hydrophobic environments.[15-17] Little to no fluorescence is observed before significant aggregation of

unimolecular micelles, but fluorescence emission increases exponentially after assembly of aggregates. The CMC, or the point at which this change occurs, was calculated as 0.025 ± 0.003 mg/mL (456 ± 55 nM) polymer for **P1** (Figure 2.4b). We were unable to determine a CMC value for **Ru-P1** due to interference of the dye fluorescence from the Ru catalyst.

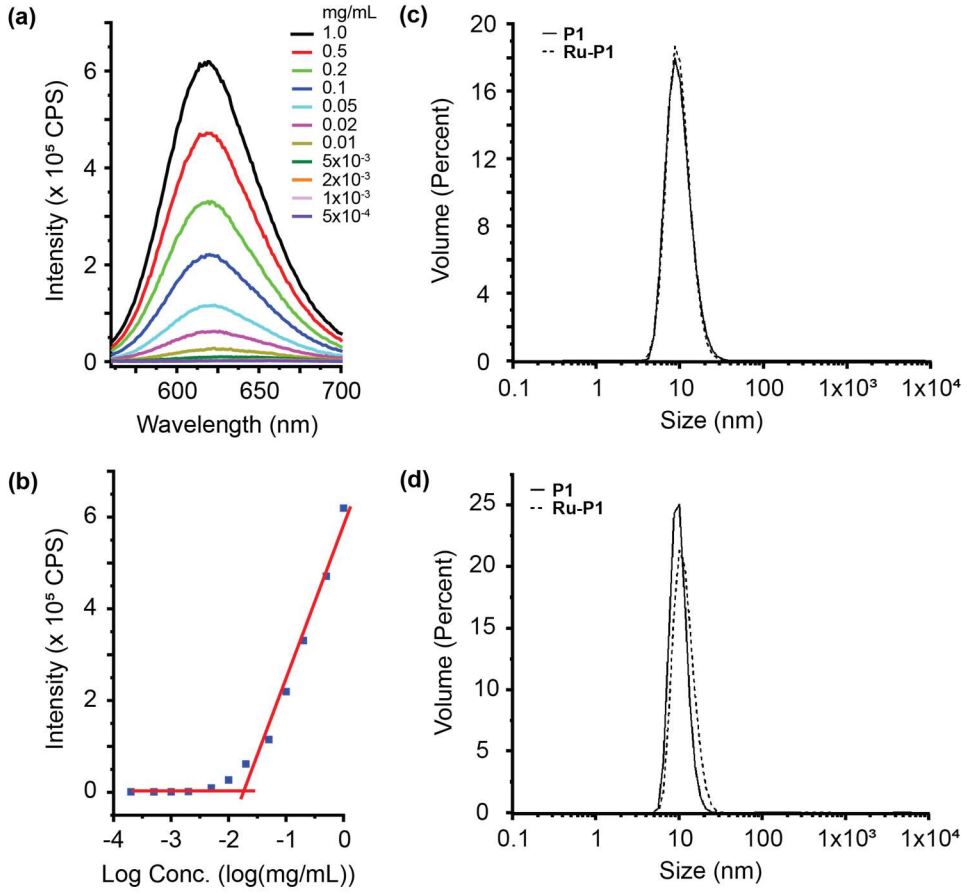

Figure 2.4 (a) Plot of fluorescence emission vs wavelength for Nile red with 0.5 µg/mL (9.1 nM) to 1.0 mg/mL (18.2 µM) polymer **P1** in water. [Nile red] = 1 µM. (b) Plot of fluorescence emission (λ_{em} = 619 nm) vs log concentration. Critical micelle concentration was calculated as 0.025 ± 0.003 mg/mL (456 ± 55 nM) polymer **P1**. [Nile red] = 1 µM. DLS size distribution by volume for (c) 0.1 mg/mL and (d) 0.02 mg/mL polymers **P1** and **Ru-P1** in PBS buffer.

Polymers **P1** and **Ru-P1** were further characterized by dynamic light scattering (DLS) at concentrations above and at the CMC (Figure 2.4c, d). Hydrodynamic diameters of 8.1 ± 1.3 nm and 8.6 ± 0.6 nm were observed for polymers **P1** and **Ru-P1**, respectively, at 0.1 mg/mL (1.8 μM) polymer. At 0.02 mg/mL (365 nm) polymer, hydrodynamic diameters of 9.6 ± 0.5 nm and 10.6 ± 0.5 were observed for polymers **P1** and **Ru-P1**, respectively. These sizes are consistent with what has been reported in the literature for polymers with similar molecular weights.[18]

2.3 SCNP Catalysis of a Ru-Mediated Deprotection

We analyzed the ability of polymeric catalyst **Ru-P1** to increase the catalytic activity of Ru-catalyzed cleavage of allylcarbamate groups compared to previously reported small molecule catalyst **Ru2**. We hypothesized that the SCNP would produce higher catalytic activity by selectively binding substrates and creating a high local concentration of them.[19, 20] The catalytic activity of polymer **Ru-P1** and small molecule catalyst **Ru2** was studied using the deprotection of caged coumarin **4** (Figure 2.5a). Substrate **4** is non-fluorescent but cleavage of the allylcarbamate group activates the fluorescence of coumarin.[21] By using fluorescence as a "turn on" property, the progress of the deprotection reaction was monitored by fluorescence spectroscopy. Polymer **Ru-P1** or small molecule catalyst **Ru2**, glutathione (GSH), and substrate **4** were added to PBS buffer, and fluorescence emission curves of the deprotection reaction were obtained over 20 min (Figure 2.5b). The concentration of Ru was varied between 10, 5 and 3 μM, which corresponded to concentrations of polymer **Ru-P1** above, at, and below the CMC at 830, 415, and 248 nM, respectively. The initial rate of reaction and percent conversion increased with increasing Ru concentration (Figure 2.5c). Overall, faster initial rates of reactions and higher percent conversion were observed with polymer **Ru-P1** compared with small molecule catalyst **Ru2**.

My collaborator Edzna S. Garcia also investigated the catalytic activity of polymer **Ru-P1** and small molecule catalyst **Ru2** under biologically relevant conditions, including PBS, Dulbecco's Modified Eagle Medium (DMEM), and HeLa cell lysate (not shown). We observed

(a)

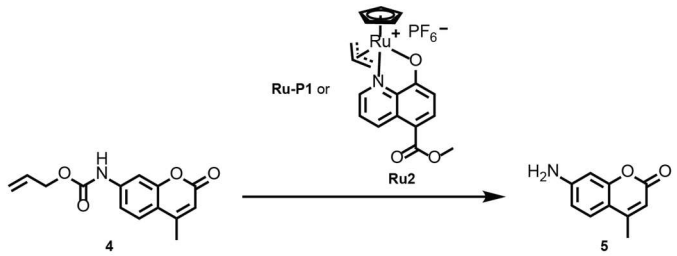

(b)

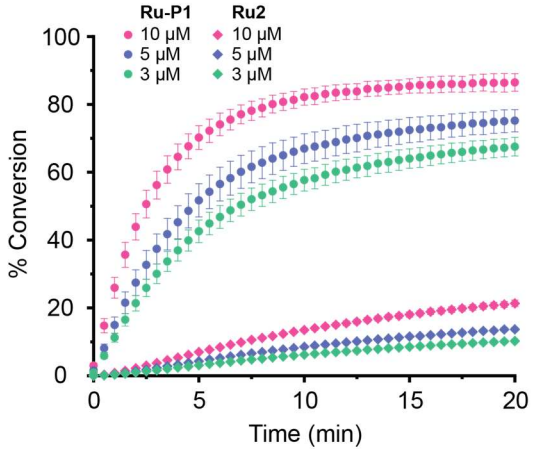

(c)

		Ru-P1		Ru2	
Ru (μM)	**4** (μM)	Rate (nM/s)	Conversion (%)	Rate (nM/s)	Conversion (%)
10	20	72 ± 9	86 ± 3	5.0 ± 0.2	21 ± 1
5	20	42 ± 7	75 ± 3	3.3 ± 0.1	14 ± 1
3	20	33 ± 4	68 ± 3	2.2 ± 0.1	10 ± <1

Figure 2.5 (a) Ru-catalyzed cleavage of allylcarbamate groups was measured by deprotection reaction of caged coumarin **4** (20 μM) with polymer **Ru-P1** or small molecule catalyst **Ru2** (3, 5, and 10 μM Ru) and GSH (300 μM). (b) Increase in fluorescence emission intensity at λ_{em} = 440 nm of Ru-catalyzed cleavage of allylcarbamate groups in PBS buffer vs. time. [GSH] = 300 μM (c) Observed percent conversions and initial rates obtained from fluorescence emission curves of catalysts **Ru-P1** and **Ru2** in PBS buffer. Standard deviation calculated from n = 3.

that polymer Ru-P1 performed better than small molecule catalyst Ru2 in the buffer solutions. However, the catalysts produced similar initial rates of reaction and percent conversions in cell lysate. We rationalize that the polymer's ability to bind substrates and provide a protective environment for the catalyst may decrease in cell lysate as a potential result of unfolding of the polymer in the complex biological environment. Finally, we demonstrated that polymer **Ru-P1** can achieve tandem catalysis with native enzyme β-galactosidase (βGal) (not shown).

2.4 Conclusions

In conclusion we developed a Ru-containing SCNP **Ru-P1** that does not require covalent cross-linking to improve catalysis in PBS and DMEM buffers. Under these conditions, polymer **Ru-P1** outperforms the free catalyst for the Ru-catalyzed cleavage of allylcarbamate groups. We also demonstrated its ability to perform tandem catalysis with native enzyme βGal to unlock a double-gated system to release a fluorescent probe. This simple strategy to obtain functional SCNPs has the potential to be applied to other transition metal catalysts to expand the chemist's toolbox for transition metal catalysis under aqueous conditions. In this approach, the SCNP does not require covalent cross-linking, but the Ru catalyst is covalently attached to the polymer via the quinoline ligand. An approach to further simplify the process of obtaining transition metal-SCNPs is to develop functional SCNPs that require neither covalent cross-linking nor covalent attachment of the catalyst. This method will be explored in Chapter 3.

2.5 Experimental Section

General Experimental Procedures

All reagents were purchased from Acros Organics, Cambridge Chemical Technologies, Chem- Impex International, Fisher Scientific, Oakwood Chemicals, Sigma-Aldrich, or TCI America, and used without further purification unless otherwise noted. For the synthetic procedures, 1,4-dioxane, DCM, DIPEA, and DMF were stored over activated 4 Å molecular sieves. NMR spectra were recorded using Varian UI400, U500, VXR500 and VNS750NB or Bruker CB500 and B600 spectrometers in the NMR Laboratory, School of Chemical Science, University of Illinois. NMR spectra were processed using MestReNova software and chemical shifts were in parts per million (ppm). All ^{1}H spectra were referenced to the residual solvent peak. Integration is provided and coupling constants (*J*) are reported in Hertz (Hz). Analytical gel permeation chromatography (GPC) experiments were performed on a Waters system equipped with a Waters 1515 isocratic pump, a Waters 2414 refractive index detector, and a Waters 2998 photodiode array detector. Separations were performed at 50 °C using DMF containing 0.1 M LiBr as the mobile phase. The molecular weights of all polymers were determined using dn/dc values for each sample calculated offline with the internal calibration system processed by the ASTRA 6 software (version 6.1.1, Wyatt Technology CA). Dynamic light scattering (DLS) characterization was performed using a Marvin Instrument Ltd. nanoZS Zetasizer with Zetasizer software. Fluorescence experiments were performed on a Horiba FluoroMax-4 fluorometer with FluorEssence (v3.5) software. Mass spectrometry was performed using a Waters Q-Tof Ultima mass spectrometer with MassLynx software. The raw data files were processed using OriginPro.

Synthetic Procedures

8-Hydroxyquinoline-5-carboxylic acid (S1). A modification of a reported procedure was followed for synthesis of compound **S1**.[22] To a 250-mL round bottom flask was added 3-amino-4-hydroxybenzoic acid (5.5 g, 33 mmol) and HCl (100 mL, 6 M aq. soln.). The suspension was magnetically stirred at 40 °C in an oil bath. To the suspension was added acrolein (3.3 mL, 49 mmol) dropwise via an addition funnel over 30 min. The mixture was refluxed at 105 °C for 2 h. The dark brown mixture was filtered via vacuum filtration. The pH of the dark brown filtrate was adjusted to pH = 9 with NH_4OH (28% aq. soln.). The basic mixture was filtered by vacuum filtration. The pH of the dark brown filtrate was adjusted to pH = 7 using HCl (10 M aq. soln.) and filtered by vacuum filtration. The pH of the filtrate was adjusted to pH = 6 with HCl (10 M aq. soln.) and filtered by vacuum filtration. The pH of the filtrate was adjusted by the dropwise addition of HCl (10 M aq. soln.) until solid precipitated out and the heterogeneous mixture was filtered. The process of adjusting the pH of the filtrate with HCl (10 M aq. soln.) and filtering was repeated until an orange solid was obtained (usually pH = 4-5). The pH = 5 filtrate was extracted with ethyl acetate and more yellow solid precipitated out. The orange solids were combined, washed twice with DCM, and dried under vacuum to afford 1.02 g (17%) of the product as a bright orange powder. ^{1}H NMR (500 MHz, DMSO-d_6): δ 9.47 (dd, J = 8.8, 1.6, 1H), δ 8.90 (dd, J = 4.0, 1.6, 1H), δ 8.24 (d, J = 8.2, 1H), δ 7.69 (dd, J = 8.8, 4.1, 1H), δ 7.12 (d, J = 8.2, 1H). ^{13}C NMR (126 MHz, DMSO-d_6): δ 167.63, 157.75, 148.11, 138.21, 134.51, 133.39, 128.05, 123.21, 116.68, 110.11. High resolution ESI-MS: m/z calculated for $C_{10}H_8NO_3^+$ ($[M+H]^+$): 190.0504; found 190.0495.

Allyl 8-(allyloxy)quinoline-5-carboxylate (S2). In a 50-mL round bottom flask, compound **S1** (1.0 g, 5.3 mmol) and K_2CO_3 (4.4 g, 32 mmol) were dissolved in DMF (15 mL). The mixture was magnetically stirred and allyl bromide (1.8 mL, 21 mmol) was added dropwise. The mixture was stirred at 50 °C for 16 h. To the reaction mixture was added water (20 mL) and ethyl acetate (20 mL). The layers were separated, and the aqueous layer was extracted twice with ethyl acetate (20 mL). The combined organic layers were washed 4 times with water (20 mL) and once with sat. aq. NaCl (20 mL). The organic layer was dried over Na_2SO_4, filtered, and concentrated by rotary evaporation. The crude was purified by silica gel column chromatography eluting with 30% (v/v) ethyl acetate in hexane to afford a pale yellow solid. The solid was washed with a minimal amount of diethyl ether to remove the yellow impurity and dried under vacuum to afford 550 mg (39%) of a white solid. ^{1}H NMR (500 MHz, $CDCl_3$): δ 9.47 (dd, *J* = 8.8, 1.7, 1H), 8.98 (dd, *J* = 4.1, 1.7, 1H), 8.35 (d, *J* = 8.4, 1H), 7.55 (dd, *J* = 8.8, 4.1, 1H), 7.06 (d, *J* = 8.4, 1H), 6.20 (ddt, *J* = 17.3, 10.7, 5.5, 1H), 6.09 (ddt, *J* = 17.3, 10.5, 5.7, 1H), 5.51-5.42 (m, 2H), 5.39-5.30 (m, *J* = 2H), 4.94 (dt, *J* = 5.6, 1.5, 2H), 4.88 (dt, *J* = 5.6, 1.5, 2H). ^{13}C NMR (126 MHz, $CDCl_3$): δ 165.91, 158.30, 149.43, 140.17, 134.53, 132.57, 132.33, 128.78, 123.05, 118.97, 118.38, 118.05, 107.51, 77.22, 70.07, 65.49. High resolution ESI-MS: *m*/*z* calculated for $C_{16}H_{16}NO_3^+$ ($[M+H]^+$): 270.1130; found 270.1118.

8-(Allyloxy)-7,8-dihydroquinoline-5-carboxylic acid (S3). In a 20-mL glass vial, compound **S2** (460 mg, 1.71 mmol) and $LiOH·H_2O$ (717 mg, 17.1 mmol) were dissolved in THF (2 mL), MeOH (2 mL), and water (1 mL). The mixture was stirred at room temperature for 12 h. Volatiles were removed by rotary evaporation and the solid was resuspended in water (5 mL). The pH of the slurry was adjusted to pH = 3 with HCl (1 M aq. soln.) and filtered via vacuum filtration to afford

374 mg (95%) of a white solid. ^{1}H NMR (500 MHz, DMSO-d_6): δ 12.95 (s, 1H), 9.41 (dd, J = 8.8, 1.7, 1H), 8.91 (dd, J = 4.0, 1.7, 1H), 8.27 (d, J = 8.4, 1H), 7.67 (dd, J = 8.7, 4.0, 1H), 7.27 (d, J = 8.4, 1H), 6.18 (ddt, J = 17.1, 10.7, 5.4, 1H), 5.53 (dq, J = 17.2, 1.6, 1H), 5.35 (dq, J = 10.5, 1.5, 1H), 4.85 (dt, J = 5.4, 1.5, 2H). ^{13}C NMR (126 MHz, DMSO-d_6): δ 167.56, 157.68, 149.02, 139.55, 133.89, 133.10, 132.54, 127.98, 123.06, 118.30, 118.28, 108.13, 69.17. High resolution ESI-MS: m/z calculated for $C_{13}H_{12}NO_3^+$ ($[M+H]^+$): 230.0817; found 230.0808.

Methyl 8-(allyloxy)quinoline-5-carboxylate (S4). In a 25-mL round bottom flask, compound **S3** (300 mg, 1.31 mmol) was dissolved in dry DCM (7.5 mL), and DMF (11.5 µL) and oxalyl chloride (285 µL, 3.27 mmol) were added. The mixture was stirred at room temperature for 1 h. Volatiles were removed under rotary evaporation and the resulting solid was washed with dry THF. The solid was dissolved in MeOH (10 mL) and the mixture was stirred at room temperature for 16 h. Volatiles were removed under rotary evaporation and the resulting solid was dissolved in ethyl acetate (10 mL) and washed with sat. aq. $NaHCO_3$ soln. (10 mL). The solution was dried over Na_2SO_4, filtered, and concentrated by rotary evaporation. The crude was purified by silica gel column chromatography eluting with 50% (v/v) ethyl acetate in hexane to afford a pale yellow oil. The oil was washed with hexane to afford 164 mg (52%) of a white crystalline solid. ^{1}H NMR (500 MHz, Acetone-d_6): δ 9.43 (dd, J = 8.8, 1.7, 1H), 8.92 (dd, J = 4.0, 1.7, 1H), 8.32 (d, J = 8.4, 1H), 7.65 (dd, J = 8.8, 4.0, 1H), 7.26 (d, J = 8.4, 1H), 6.23 (ddt, J = 17.3, 10.5, 5.2, 1H), 5.59 (dq, J = 17.2, 1.7, 1H), 5.34 (dq, J = 10.6, 1.5, 1H), 4.90 (dt, J = 5.1, 1.6, 2H), 3.94 (s, 3H). ^{13}C NMR (126 MHz, Acetone-d_6): δ 166.28, 158.66, 149.00, 140.33, 133.71, 133.12, 132.47, 128.40, 122.95, 117.91, 117.28, 107.83, 69.41, 51.30. High resolution ESI-MS: m/z calculated for $C_{14}H_{14}NO_3^+$ ($[M+H]^+$): 244.0974; found 244.0962.

***tert*-Butyl (4-(8-(allyloxy)quinoline-5-carboxamido)butyl)carbamate (3).** In a 25-mL round bottom flask, compound **S3** (800 mg, 3.49 mmol), EDC (803 mg, 4.19 mmol), HOBt (641 mg, 4.19 mmol), and *N*-boc-1,4-butanediamine[23] (788 mg, 4.19 mmol) were dissolved in DMF (15 mL). Triethylamine (1.7 mL, 12 mmol) was added and the mixture was stirred at room temperature for 16 h. The mixture was diluted with water (20 mL) and extracted three times with ethyl acetate (20 mL). The organic layers were washed four times with water (20 mL) and once with sat. aq. NaCl (20 mL). The organic layer was dried over Na_2SO_4, filtered, and concentrated by rotary evaporation. The crude was dissolved in minimal volume of DCM and the product was obtained by precipitation in diethyl ether (25 mL). The solid was dried under vacuum to afford 659 mg (47%) of the product as a beige solid. ^{1}H NMR (500 MHz, $CDCl_3$): δ 8.97 (dd, *J* = 4.1, 1.7, 1H), 8.85 (dd, *J* = 8.6, 1.8, 1H), 7.63 (d, *J* = 8.1, 1H), 7.50 (dd, *J* = 8.6, 4.1, 1H), 6.99 (d, *J* = 8.2, 1H), 6.27 (s, 1H), 6.19 (ddt, *J* = 17.4, 10.7, 5.4, 1H), 5.47 (dq, *J* = 17.2, 1.5, 1H), 5.36 (dq, *J* = 10.5, 1.4, 1H), 4.90 (dt, *J* = 5.5, 1.5, 2H), 4.63 (s, 1H), 3.54 (q, *J* = 6.6, 2H), 3.19 (q, *J* = 6.6, 2H), 1.73 – 1.66 (m, 2H), 1.63 (q, *J* = 7.2, 2H), 1.42 (s, 9H). ^{13}C NMR (126 MHz, $CDCl_3$): δ 168.55, 156.31, 156.28, 149.91, 140.46, 134.50, 132.75, 127.47, 126.31, 126.21, 122.61, 118.86, 107.63, 79.45, 70.09, 40.19, 39.80, 28.55, 27.93, 26.93. High resolution ESI-MS: *m*/*z* calculated for $C_{22}H_{30}N_3O_4^+$ ($[M+H]^+$): 400.2236; found 400.2220.

4-(8-(Allyloxy)quinoline-5-carboxamido)butan-1-aminium 2,2,2-trifluoroacetate (1). In a 20-mL glass vial, compound **3** (74 mg, 0.19 mmol) was dissolved in DCM (2 mL) and TFA (200 µL) was added. The mixture was stirred at room temperature for 2 h. The reaction mixture was precipitated in diethyl ether (40 mL) to yield 70 mg (91%) of a white solid. ^{1}H NMR (500 MHz, DMSO-d_6): δ 8.90 (dd, *J* = 4.1, 1.8, 1H), 8.75 (dd, *J* = 8.6, 1.7, 1H), 8.54 (t, *J* = 5.8, 1H), 7.69 (d,

J = 8.1, 1H), 7.66 (s, 3H), 7.60 (dd, *J* = 8.7, 4.1, 1H), 7.22 (d, *J* = 8.1, 1H), 6.17 (ddt, *J* = 17.4, 10.5, 5.3, 1H), 5.51 (dq, *J* = 17.3, 1.8, 1H), 5.37 – 5.30 (m, 1H), 4.83 (dt, *J* = 5.4, 1.6, 2H), 2.85 (d, *J* = 6.4, 2H), 1.62 (m, 4H). ^{13}C NMR (126 MHz, DMSO-d_6): δ 167.53, 155.33, 149.16, 139.50, 133.91, 133.36, 126.84, 126.66, 125.96, 122.31, 118.02, 108.16, 69.07, 38.71, 38.41, 26.17, 24.65. High resolution ESI-MS: *m*/*z* calculated for $C_{17}H_{22}N_3O_2^+$ ([M]$^+$): 300.1712; found 300.1707.

2-((6-Bromohexyl)oxy)naphthalene (S5). To a 3-neck 250-mL round bottom flask was added 2-naphthol (5.0 g, 35 mmol), K_2CO_3 (7.19 g, 52.0 mmol), and MeCN (50 mL). The flask was transferred to an oil bath preheated to 90 °C and stirred for 30 min. To the flask was added a solution of 1,6-dibromohexane (26.7 mL, 173 mmol) in MeCN (50 mL), and the mixture was stirred at reflux under N_2 atm for 24 h. The mixture was diluted with $CHCl_3$ (100 mL) and washed once with water (100 mL) and once with sat. aq. NaCl (100 mL). The organic layer was dried over Na_2SO_4, filtered, and concentrated by rotary evaporation. The crude was purified twice by silica gel column chromatography using a gradient elution of 100% hexane to 10% (v/v) ethyl acetate in hexane to afford 8.08 g (76 %) of a white solid. ^{1}H NMR (500 MHz, $CDCl_3$) δ 7.79 – 7.68 (m, 3H), 7.43 (m, 1H), 7.36 – 7.29 (m, 1H), 7.17 – 7.08 (m, 2H), 4.09 (t, *J* = 6.4, 2H), 3.44 (t, *J* = 6.8, 2H), 1.90 (m, 4H), 1.55 (p, *J* = 3.8, 2H). ^{13}C NMR (151 MHz, $CDCl_3$) δ 157.02, 134.60, 129.36, 128.91, 127.66, 126.70, 126.33, 123.53, 118.99, 106.55, 67.74, 33.86, 32.72, 29.10, 27.98, 25.40. High resolution ESI-MS: *m*/*z* calculated for $C_{16}H_{19}BrO^+$ ([M+H]$^+$): 307.0619; found 307.0689.

2-((6-Azidohexyl)oxy)naphthalene (S6). To a 250-mL round bottom flask equipped with a magnetic stir bar was added compound **S5** (5.00 g, 19.4 mmol), sodium azide (1.59 g, 24.5 mmol),

and DMF (75 mL). The mixture was transferred to an oil bath preheated to 60 °C and stirred for 24 h. The mixture was diluted with ethyl ether (100 mL) and washed five times with water (50 mL) and once with sat. aq. NaCl (50 mL). The organic layer was dried over Na_2SO_4, filtered, and concentrated by rotary evaporation to afford 3.87 g (88%) of a yellow liquid. ^{1}H NMR (500 MHz, $CDCl_3$) δ 7.82 – 7.67 (m, 3H), 7.43 (ddd, *J* = 8.2, 6.8, 1.3, 1H), 7.33 (ddd, *J* = 8.1, 6.9, 1.3, 1H), 7.15 (m, 2H), 4.09 (t, *J* = 6.4, 2H), 3.31 (t, *J* = 6.9, 6.3, 2H), 1.87 (p, *J* = 8.1, 6.5, 2H), 1.67 (p, *J* = 12.3, 7.6, 4.4, 2H), 1.62 – 1.41 (m, 4H). ^{13}C NMR (151 MHz, $CDCl_3$) δ 157.02, 134.61, 129.37, 128.92, 127.66, 126.71, 126.34, 123.53, 118.99, 106.55, 67.73, 51.42, 29.15, 28.85, 26.57, 25.79. High resolution ESI-MS: *m*/*z* calculated for $C_{16}H_{20}N_3O^+$ ($[M+H]^+$): 270.1528; found 270.1563.

6-(Naphthalen-2-yloxy)hexan-1-amine (2). To a 300-mL round bottom flask equipped with a magnetic stir bar was added compound **S6** (1.53 g, 6.98 mmol), PPh_3 (1.79 g, 6.82 mmol), and 4:1 THF/H_2O (25 mL). The mixture was stirred at room temperature for 16 h. The mixture was concentrated by rotary evaporation, diluted with DCM (20 mL) and HCl (20 mL, 1 M aq. soln.) and allowed to sit overnight. The mixture was filtered by vacuum filtration to afford 1.37 g (86%) of a white solid. ^{1}H NMR (600 MHz, $CDCl_3$) δ 7.79 – 7.68 (m, 3H), 7.42 (t, *J* = 7.5, 1H), 7.32 (t, *J* = 7.5, 1H), 7.17 – 7.10 (m, 2H), 4.08 (t, *J* = 6.5, 2H), 2.73 (t, *J* = 7.0, 2H), 1.86 (dt, *J* = 14.5, 6.6, 2H), 1.52 (tt, *J* = 14.0, 7.2, 5H), 1.47 – 1.38 (m, 2H). ^{13}C NMR (151 MHz, $CDCl_3$) δ 157.07, 134.62, 129.33, 128.89, 127.65, 126.70, 126.31, 123.49, 119.02, 106.54, 77.25, 77.03, 76.82, 67.88, 42.12, 33.57, 29.25, 26.70, 26.03. High resolution ESI-MS: *m*/*z* calculated for $C_{16}H_{21}NO^+$ ($[M+H]^+$): 244.1623; found 244.1694.

General procedure for RAFT polymerization. In a 20 mL glass vial equipped with a magnetic stir bar, 46 mg of 2-(dodecylthiocarbonothioylthio)-2-methylpropionic acid and 2.07 mg of AIBN were dissolved in 2.5 mL of 1,4-dioxane. To this mixture was added 2.07 mL of pentafluorophenyl acrylate, and the vial was degassed using three cycles of freeze-pump-thaw. The vial was transferred to an oil bath preheated to 70 °C and stirred for 6.5 h. The solution was diluted with 3 mL of THF and precipitated from 10 mL of MeOH. This process was repeated three times, and the solid was dried under high vac at 40 °C for 2 d to obtain the polymer.

Post-polymerization functionalization of P1. This procedure was adapted from that reported by Palmans, Meijer, and coworkers.[6] In a 20-mL glass vial, poly(pentafluorophenyl acrylate) (200 mg, 8.4 μmol) and compound **1** (69.4 mg, 168 μmol) were dissolved in dry THF (1 mL) and DMF (1 mL), and DIPEA (50 μL) was added. The mixture was stirred at 50 °C for 4 h. The progress of the reaction was checked by ^{19}F NMR in $CDCl_3$ to confirm the intended degree of functionalization. Compound **2** (48.6 mg, 200 μmol) and DIPEA (50 μL) were added to the mixture and stirred at 50 °C for 4 h. The progress of the reaction was checked by ^{19}F NMR. An excess of Jeffamine M-1000 (200 μL of 750 mg/mL solution in THF) was added to the vial and stirred at 50 °C for 16 h. The polymer was dialyzed against methanol in 1 kDa cutoff dialysis tubing for 2 d followed by dialysis in 5 kDa cutoff dialysis tubing in water for 2 d. The polymer solution was freeze-dried in a lyophilizer to yield 265 mg of a light brown gel. GPC (0.1 M LiBr in DMF): M_n = 54.8 kDa, M_w = 67.9 kDa, $Đ$ = 1.2.

Small molecule catalyst Ru1. In a 4-mL glass vial, compound **3** (20.3 mg, 50.9 μmol) was dissolved in MeCN (0.5 mL). In a separate 4-mL glass vial,

tris(acetonitrile)cyclopentadienylruthenium(II) hexafluorophosphate (22.1 mg, 50.9 μmol) was dissolved in MeCN (0.5 mL). The solution of compound **3** was added to the Ru solution. The mixture was stirred at room temperature for 1 h. The reaction mixture was added dropwise to diethyl ether (45 mL) in a 50-mL centrifuge tube, and a yellow solid was collected by centrifugation. The pellet was washed twice with diethyl ether (35 mL). The product was collected by centrifugation and dried under vacuum to afford 13.1 mg (36%) of a yellow solid. ^{1}H NMR (500 MHz, CD_3CN): δ 9.22 (dd, *J* = 8.7, 1.2, 1H), 8.65 (dd, *J* = 5.2, 1.2, 1H), 7.65 (d, *J* = 8.3, 1H), 7.57 (dd, *J* = 8.7, 5.1, 1H), 6.94 (s, 1H), 6.86 (d, *J* = 8.3, 1H), 5.95 (s, 5H), 5.31 (s, 1H), 4.51 (tt, *J* = 10.8, 6.2, 1H), 4.41 (d, *J* = 10.9, 1H), 4.14 (d, *J* = 11.0, 1H), 4.12 (dd, J = 6.1, 2.9, 1H), 4.09 (dd, *J* = 6.3, 2.8, 1H), 3.38 – 3.32 (m, 2H), 3.05 (q, *J* = 6.5, 2H), 1.57 (q, *J* = 7.1, 6.5, 2H), 1.54 – 1.46 (m, 2H), 1.39 (s, 9H). ^{13}C NMR (126 MHz, CD_3CN): δ 172.49, 168.01, 156.67, 146.78, 139.81, 131.45, 130.42, 125.22, 119.08, 114.95, 99.66, 96.78, 69.62, 66.28, 63.91, 40.74, 40.01, 28.63, 28.25, 27.54, 15.63. MALDI-TOF: *m*/*z* calculated for $C_{27}H_{34}N_3O_4Ru^+$ ($[M]^+$): 565.7; found 565.3.

Small molecule catalyst Ru2. In a 4-mL glass vial, compound **S4** (27.6 mg, 114 μmol) was dissolved in MeCN (0.5 mL). In a separate 4-mL glass vial, tris(acetonitrile)-cyclopentadienylruthenium(II) hexafluorophosphate (49.3 mg, 114 μmol) was dissolved in MeCN (0.5 mL). The solution of compound **S4** was added to the Ru solution. The mixture was stirred at room temperature for 1 h. The reaction mixture was added dropwise to diethyl ether (45 mL) in a 50-mL centrifuge tube, and a yellow solid was collected by centrifugation. The pellet was washed twice with diethyl ether (35 mL). The product was collected by centrifugation and dried under vacuum to afford 49.7 mg (79%) of a yellow solid. ^{1}H NMR (500 MHz, CD_3CN): δ 9.62 (dd, *J* = 8.8, 1.2, 1H), 8.68 (dd, *J* = 5.1, 1.2, 1H), 8.21 (d, *J* = 8.6, 1H), 7.65 (dd, *J* = 8.8, 5.1, 1H), 6.91 (d,

J = 8.6, 1H), 5.98 (s, 5H), 4.54 (tt, *J* = 10.7, 6.2, 1H), 4.44 (d, *J* = 11.0, 1H), 4.18 (d, *J* = 10.8, 1H), 4.17 – 4.11 (m, 2H), 3.88 (s, 3H). ^{13}C NMR (126 MHz, CD_3CN): 175.10, 167.04, 164.62, 156.66, 139.61, 136.72, 131.81, 126.14, 115.63, 111.62, 99.98, 96.90, 69.69, 64.43, 52.41. MALDI-TOF: *m*/*z* calculated for $C_{19}H_{18}NO_3Ru^+$ ($[M]^+$): 409.4; found 409.2.

Polymer Ru-P1. In a 1.5-mL glass vial, polymer **P1** (1.95 mg) was dissolved in degassed MeCN (0.2 mL). In a separate 1.5-mL glass vial, the tris(acetonitrile)cyclo-pentadienylruthenium(II) hexafluorophosphate was dissolved in degassed MeCN (0.2 mL). To the polymer solution was added the Ru solution (60 µL, 0.8 µmol). The mixture was stirred at room temperature for 20 h. The amount of Ru coordinated to the polymer was determined via UV-vis using a calibration curve from the Ru complex **Ru1** in MeCN. Polymer **Ru-P1** was used without further purification.

Allyl carbamate protected coumarin (4). In a 4-mL glass vial, 7-amino-4-methylcoumarin (101 mg, 577 µmol) was dissolved in DMF (2.0 mL). Pyridine (93 µL, 1.15 mmol) was added and the mixture was stirred in an ice bath. To the ice-cold mixture, allyl chloroformate (72.8 µL, 685 µmol) was added dropwise and the mixture was allowed to stir at 0°C for 4 h and at room temperature for 12 h. HCl (4 mL, 5% (v/v) aq. soln.) and ethyl acetate (10 mL) were added to the mixture. The aqueous layer was extracted twice with ethyl acetate (5 mL) and the combined organic layers were washed twice with sat. aq. $NaHCO_3$ soln. (5 mL). Volatiles were removed under rotary evaporation and the crude was purified by silica gel column chromatography using a gradient elution of 100% hexane to 20% (v/v) ethyl acetate in hexane to afford 28 mg (19%) of a white solid. ^{1}H NMR (500 MHz, $CDCl_3$): δ 7.53 (d, *J* = 8.6, 1H), 7.43 (d, *J* = 2.1, 1H), 7.37 (dd, *J* = 8.6, 2.2, 1H), 6.85 (s, 1H), 6.19 (s, 1H), 6.03 – 5.92 (m, 1H), 5.39 (dq, *J* = 17.1, 1.7, 1H), 5.32 – 5.27 (m, 1H), 4.71 (dd,

J = 5.8, 1.6, 2H), 2.41 (t, J = 0.9, 3H). ^{13}C NMR (126 MHz, $CDCl_3$): δ 161.11, 154.68, 152.77, 152.23, 141.43, 132.13, 125.53, 118.94, 115.78, 114.50, 113.45, 106.14, 66.49, 18.70. High resolution ESI-MS: m/z calcd for $C_{14}H_{14}NO_4^+$ ($[M+H]^+$): 260.0923; found 260.0915.

Fluorescence Studies

General procedure for critical micelle concentration studies. To sixteen 7-mL glass vials was added 100 μL of a Nile Red solution (5 μM) in DCM. The vials were left uncapped and the DCM was evaporated. In a separate 7-mL glass vial, a 2 mg/mL solution of polymer **P1** or **Ru-P1** was prepared in 10 mM PBS pH = 7.4. To each vial was added aliquots of a polymer solution and the corresponding volume of PBS to yield 0.5 mL of varying concentrations of the polymer. The vials were capped and stirred at room temperature for 20 h to equilibrate. The fluorescence spectra were measured for each polymer solution with λ_{ex} = 553 nm. A plot of the relative fluorescence intensity at 619 nm versus the log of polymer concentrations in mg/mL produced a non-linear curve. A linear curve was fitted to the static data points belonging to the low polymer concentrations and a second linear curve was fitted to the data points showing steady increase of fluorescence intensity. The critical micelle concentration was calculated as the point of inflection.

General procedure for Ru-catalyzed cleavage of allylcarbamate groups. Stock solutions of GSH (20 mM in water), pro-fluorophore **4** (1 mM in DMSO), **Ru-P1** (500 μM in Ru in MeCN), and **Ru2** (500 μM in MeCN) were prepared. All reactions were conducted in a final volume of 500 μL of 10 mM PBS pH = 7.4. To each reaction mixture was added 3, 5, or 10 μL of **Ru-P1** or **Ru2** (3, 5, and 10 μM final concentration), 7.5 μL GSH (300 μM final concentration), and 10 μL

of **4** (20 μM final concentration). The increase in fluorescence was measured using a fluorometer with λ_{ex} = 355 nm and λ_{em} = 450 nm. The fluorescence was recorded every 10 s for 20 min. The percent conversions were determined by using a linear regression curve from the linear correlation between fluorescence intensity and yield of coumarin **5**. The initial rates were calculated from the first derivative of the slope tangent of each timepoint between 1 and 2 min of reaction.

2.6 References

1. Garcia, E. S.; Xiong, T. M.; Lifschitz, A.; Zimmerman, S. C. Tandem Catalysis Using an Enzyme and a Polymeric Ruthenium-Based Artificial Metalloenzyme. *Submitted* **2021**.
2. Tanaka, S.; Saburi, H.; Murase, T.; Yoshimura, M.; Kitamura, M. Catalytic Removal of N-Allyloxycarbonyl Groups Using the [CpRu(IV)(π-C_3H_5)(2-quinolinecarboxylato)]PF_6 Complex. A New Efficient Deprotecting Method in Peptide Synthesis. *J. Org. Chem.* **2006**, *71*, 4682–4684.
3. Völker, T.; Dempwolff, F.; Graumann, P. L.; Meggers, E. Progress Towards Bioorthogonal Catalysis with Organometallic Compounds. *Angew. Chem. Int. Ed. Engl.* **2014**, *53*, 10536–10540.
4. Völker, T.; Meggers, E. Chemical Activation in Blood Serum and Human Cell Culture: Improved Ruthenium Complex for Catalytic Uncaging of Alloc-Protected Amines. *ChemBioChem* **2017**, *18*, 1083-1086.
5. Das, A.; Theato, P. Multifaceted Synthetic Route to Functional Polyacrylates by Transesterification of Poly(pentafluorophenyl acrylates). *Macromolecules* **2015**, *48*, 8695-8707.
6. Liu, Y.; Pauloehrl, T.; Presolski, S. I.; Albertazzi, L.; Palmans, A. R. A.; Meijer, E. W.

Modular Synthetic Platform for the Construction of Functional Single-Chain Polymeric Nanoparticles: From Aqueous Catalysis to Photosensitization. *J. Am. Chem. Soc.* **2015**, *137*, 13096-13105.

7. Bonvoisin, J.; Ciofini, I. Spectral Signature of a Ru(II, III, IV) Complex: A Combined Experimental and Theoretical Investigation. *Dalton Trans.* **2013**, *42*, 7943-7951.
8. Mavila, S.; Eivgi, O.; Berkovich, I.; Lemcoff, N. G. Intramolecular Cross-Linking Methodologies for the Synthesis of Polymer Nanoparticles. *Chem. Rev.* **2016**, *116*, 878-961.
9. Pomposo, J. A., Ed. *Single-Chain Polymer Nanoparticles: Synthesis, Characterization, Simulations, and Applications*; John Wiley & Sons, 2017.
10. Chen, R.; Berda, E. B. 100th Anniversary of Macromolecular Science Viewpoint: Re-examining Single-Chain Nanoparticles. *ACS Macro. Lett.* **2020**, *9*, 1836-1843.
11. Barbee, M. H.; Wright, Z. M.; Allen, B. P.; Taylor, H. F.; Patteson, E. F.; Knight, A. S. Protein-Mimetic Self-Assembly with Synthetic Macromolecules. *Macromolecules* **2021**, *54*, 3585-3612.
12. Terashima, T.; Sugita, T.; Fukae, K.; Sawamoto, M. Synthesis and Single-Chain Folding of Amphiphilic Random Copolymers in Water. *Macromolecules* **2014**, *47*, 589-600.
13. Hattori, G.; Hirai, Y.; Sawamoto, M.; Terashima, T. Self-Assembly of PEG/Dodecyl-Graft Amphiphilic Copolymers in Water: Consequences of the Monomer Sequence and Chain Flexibility on Uniform Micelles. *Polym. Chem.* **2017**, *8*, 7248-7259.
14. Shibata, M.; Matsumoto, M.; Hirai, Y.; Takenaka, M.; Sawamoto, M.; Terashima, T. Intramolecular Folding or Intermolecular Self-Assembly of Amphiphilic Random

Copolymers: On-Demand Control by Pendant Design. *Macromolecules* **2018**, *51*, 3738-3745.

15. Fowler, S. D.; Greenspan, P. Application of Nile Red, a Fluorescent Hydrophobic Probe, for the Detection of Neutral Lipid Deposits in Tissue Sections: Comparison with Oil Red O. *J. Histochem. Cytochem.* **1985**, *33*, 833-836.

16. Greenspan, P.; Mayer, E. P.; Fowler, S. D. Nile Red: A Selective Fluorescent Stain for Intracellular Lipid Droplets. *J. Cell Biol.* **1985**, *100*, 965-973.

17. Stuart, M. C. A.; van de Pas, J. C.; Engberts, J. B. F. N. The Use of Nile Red to Monitor the Aggregation Behavior in Ternary Surfactant-Water-Organic Solvent Systems. *J. Phys. Org. Chem.* **2005**, *18*, 929-934.

18. Liu, Y.; Pauloehrl, T.; Presolski, S. I.; Albertazzi, L.; Palmans, A. R. A.; Meijer, E. W. Modular Synthetic Platform for the Construction of Functional Single-Chain Polymeric Nanoparticles: From Aqueous Catalysis to Photosensitization. *J. Am. Chem. Soc.* **2015**, *137*, 13096-13105.

19. Chen, J.; Wang, J.; Li, K.; Wang, Y.; Gruebele, M.; Ferguson, A. L.; Zimmerman, S. C. Polymeric "Clickase" Accelerates the Copper Click Reaction of Small Molecules, Proteins, and Cells. *J. Am. Chem. Soc.* **2019**, *141*, 9693-9700.

20. Chen, J.; Wang, J.; Bai, Y.; Li, K.; Garcia, E. S.; Ferguson, A. L.; Zimmerman, S. C. Enzyme-like Click Catalysis by a Copper-Containing Single-Chain Nanoparticle. *J. Am. Chem. Soc.* **2018**, *140*, 13695-13702.

21. Kanaoka, Y.; Takahashi, T.; Nakayama, H.; Ueno, T.; Sekine, T. Synthesis of a New Fluorogenic Substrate for Cystine Aminopeptidase. *Chem. Pharm. Bull.* **1982**, *30*, 1485-1487.

22. Schiller, R.; Scozzafava, G.; Tumber, A.; Wickens, J. R.; Bush, J. T.; Rai, G.; Lejeune, C.; Choi, H.; Yeh, T.-L.; Chan, M. C.; Mott, B. T.; McCullagh, J. S. O.; Maloney, D. J.; Schofield, C. J.; Kawamura, A. A Cell-Permeable Ester Derivative of the JmjC Histone Demethylase Inhibitor IOX_1. *ChemMedChem* **2014**, *9*, 566–571.

23. Beenakker, T. J. M.; Wander, D. P. A.; Offen, W. A.; Artola, M.; Raich, L.; Ferraz, M. J.; Li, K.-Y.; Houben, J. H. P. M.; van Rijssel, E. R.; Hansen, T.; van Der Marel, G. A.; Codée, J. D. C.; Aerts, J. M. F. G.; Rovira, C.; Davies, G. J.; Overkleeft, H. S. Carba-Cyclophellitols are Neutral Retaining-Glucosidase Inhibitors. *J. Am. Chem. Soc.* **2017**, *139*, 6534–6537.

CHAPTER 3: MODULAR APPROACH TO SINGLE CHAIN NANOPARTICLES VIA HYDROPHOBIC INTERACTIONS

Part of this chapter has been adapted and modified from the following publication: **Xiong, T. M.**; Garcia, E. S.; Chen, J.; Alzona, A. J.; Zimmerman, S. C. Enzyme-Like Catalysis by Single Chain Nanoparticles that Use Transition Metal Cofactors. *Submitted* **2021**.

3.1 Design and Synthesis of Polymers

The second strategy to obtain transition metal SCNPs utilizes a modular approach in which the SCNP is not covalently attached to the catalyst but is able to selectively bind the catalyst and its substrates for higher catalytic activity.[1] I synthesized random amphiphilic polymers **P1** and **P2**

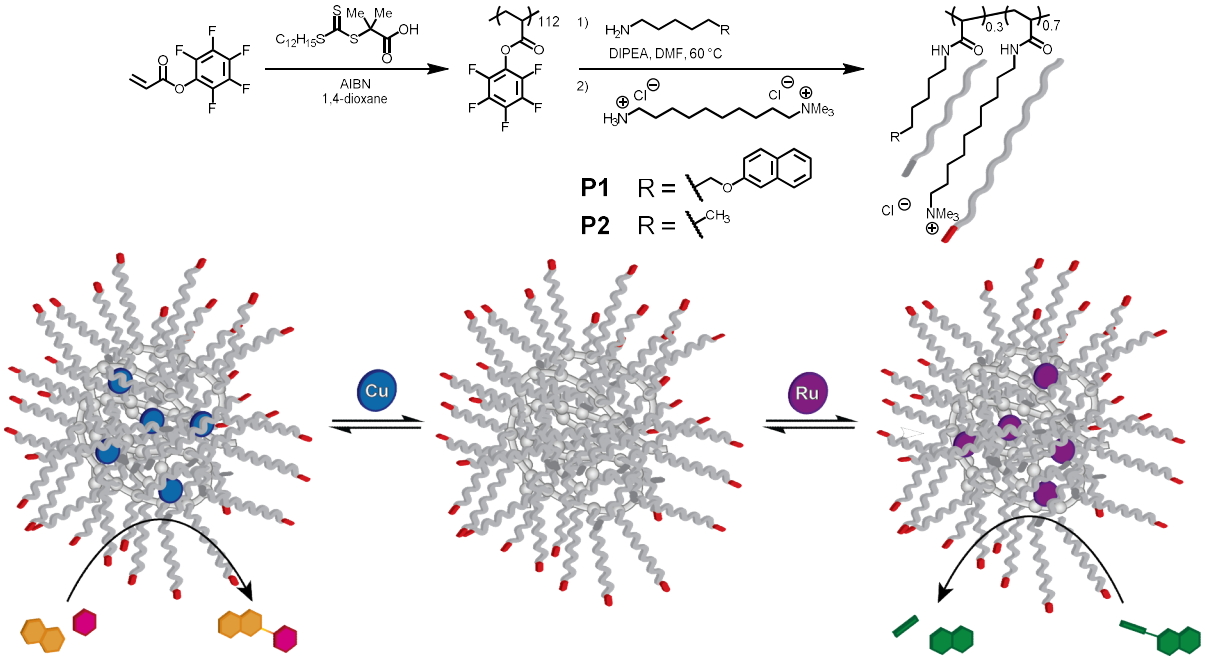

Scheme 3.1 Synthetic scheme for polymer **P1** and **P2** using RAFT polymerization of pentafluorophenyl acrylate and post-polymerization functionalization of poly(pentafluorophenyl acrylate).

from precursor poly(pentafluorophenyl acrylate), which was obtained from reversible addition-fragmentation chain-transfer (RAFT) polymerization (Scheme 3.1).[2] The degree of polymerization (DP) of the poly(pentafluorophenyl acrylate) was controlled by carefully controlling the ratio of monomer to chain transfer agent. The percent conversion was monitored by ^{1}H NMR and the polymer was characterized by gel permeation chromatography (GPC) and ^{1}H NMR (Experimental Section, Supplementary Figure 3.1). The GPC elution curve indicated a dispersity value, $Đ = 1.12$

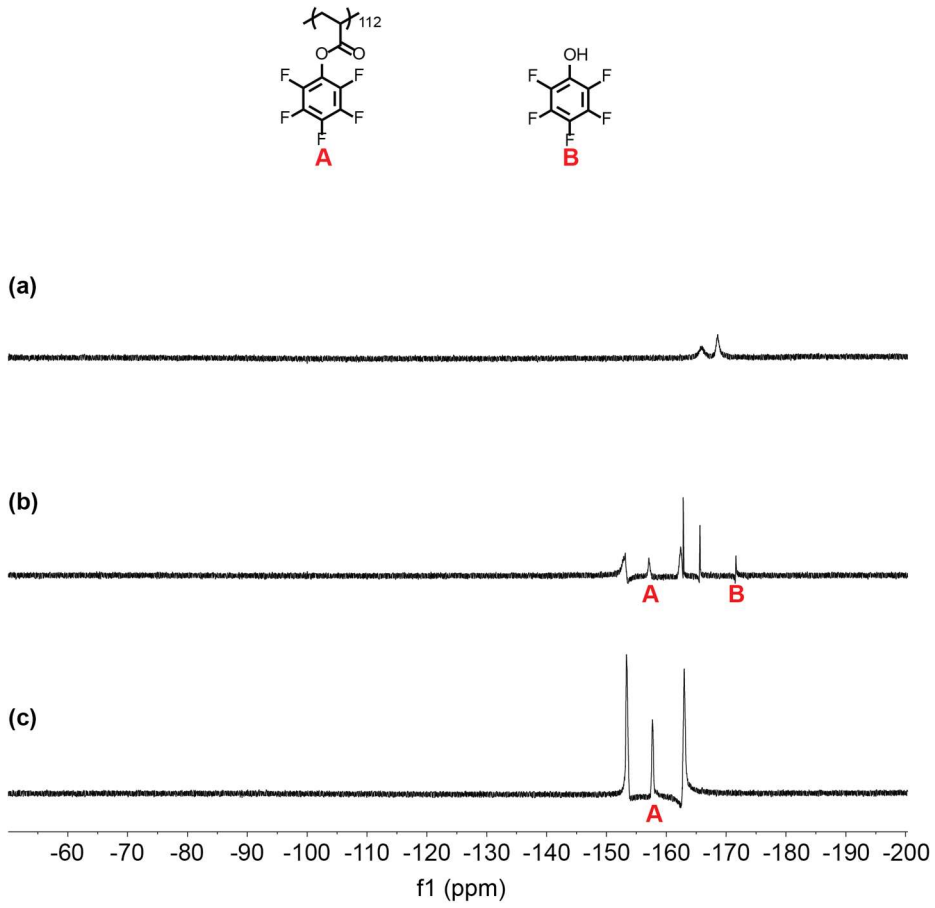

Figure 3.1 Stacked ^{19}F NMR spectra of **P1** (a) 12 h after addition of 10-trimethyl-ammonium-1-decylamine (100% conversion, d_6-DMSO) (b) 4 h after addition of 6-(2-naphthyloxy)-1-hexylamine (27% conversion, $CDCl_3$) and (c) before addition of amines (0% conversion, $CDCl_3$).

and molecular weight, M_n = 27 kDa, which corresponded to a DP of 112. The pendant activated ester groups readily undergo substitution in the presence of a hard nucleophile, such as an amine. This flexible and efficient approach to SCNPs was developed by Palmans, Meijer, and coworkers[3] and I have employed it for developing several artificial metalloenzymes. Thus, amphiphilic polyacrylamides were obtained through post-polymerization functionalization using 10-trimethyl-ammonium-1-decylamine, and either 6-(2-naphthyloxy)-1-hexylamine for polymer **P1** or hexylamine for polymer **P2**.

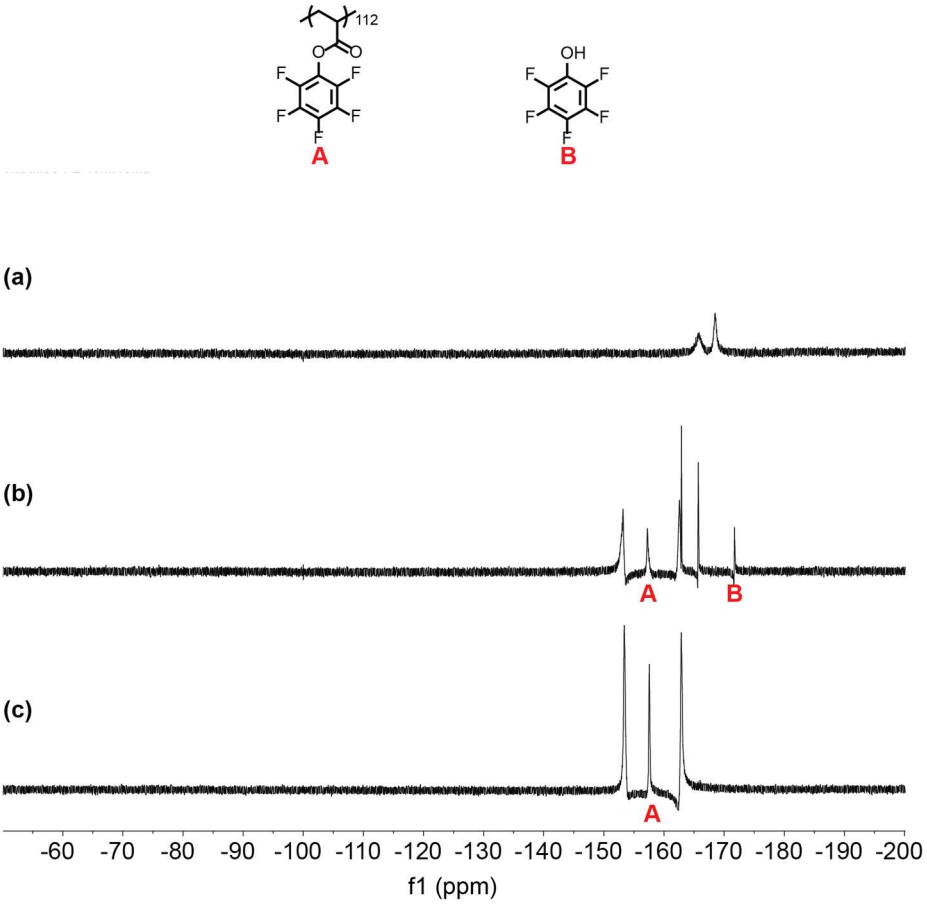

Figure 3.2 Stacked ^{19}F NMR spectra of **P2** (a) 12 h after addition of 10-trimethyl-ammonium-1-decylamine (100% conversion, d_6-DMSO) (b) 4 h after addition of hexylamine (23% conversion, $CDCl_3$) and (c) before addition of amines (0% conversion, $CDCl_3$).

The hydrophilic trimethylammonium ion groups were designed to provide water solubility whereas the decyl linker, hexyl, and naphthyl groups assist folding and provide a hydrophobic interior for substrate binding. The target ratio of hydrophilic/hydrophobic groups was 70:30. The percent conversion was monitored by ^{19}F NMR to give a ratio of 73:27 for polymer **P1** (Figure 3.1) and 77:23 for polymer **P2** (Figure 3.2). The polymers were also characterized by ^{1}H NMR to give a ratio of 72:28 for polymer **P1** and 75:25 for polymer **P2** (Experimental Section, Supplementary Figure 3.2 and 3.3). The results from both characterization methods were

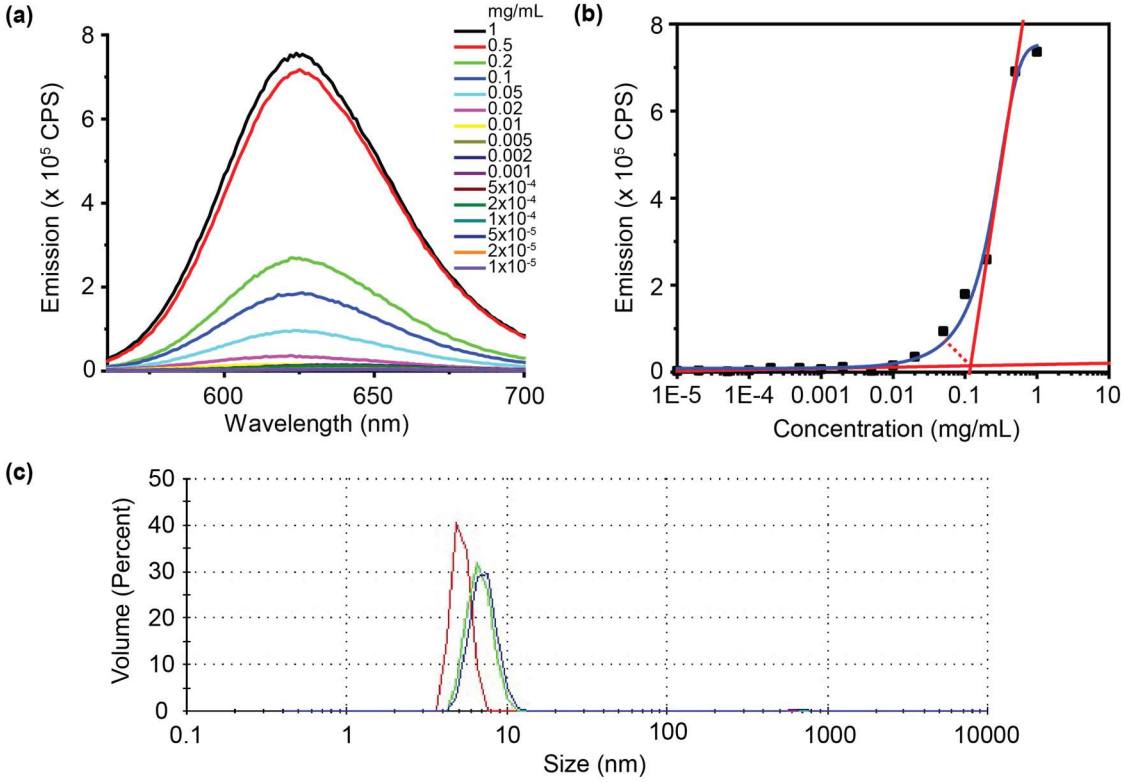

Figure 3.3 (a) Plot of fluorescence emission vs wavelength for Nile red with 1 mg/mL (33 μM) to 10 ng/mL (330 pM) polymer **P1** in water. [Nile red] = 1 μM. (b) Plot of fluorescence emission (λ_{em} = 619 nm) vs concentration. Critical micelle concentration was calculated as 0.05 mg/mL (1.6 μM) polymer **P1**. [Nile red] = 1 μM. (c) DLS size distribution by volume for 0.03 mg/mL (1 μM) polymer **P1** in water. Curves are from technical replicates.

consistent with each other. The functionalized polymers were purified by precipitation from diethyl ether and dialysis against water and used in the next step to produce SCNPs.

3.2 Characterization of SCNPs

To establish whether SCNPs are formed by intramolecular folding of amphiphilic polymer **P1** and its potential for intermolecular aggregation, fluorescence spectroscopy was used to determine the critical micelle concentration (CMC) of polymer **P1**. Samples of polymer **P1** with 1

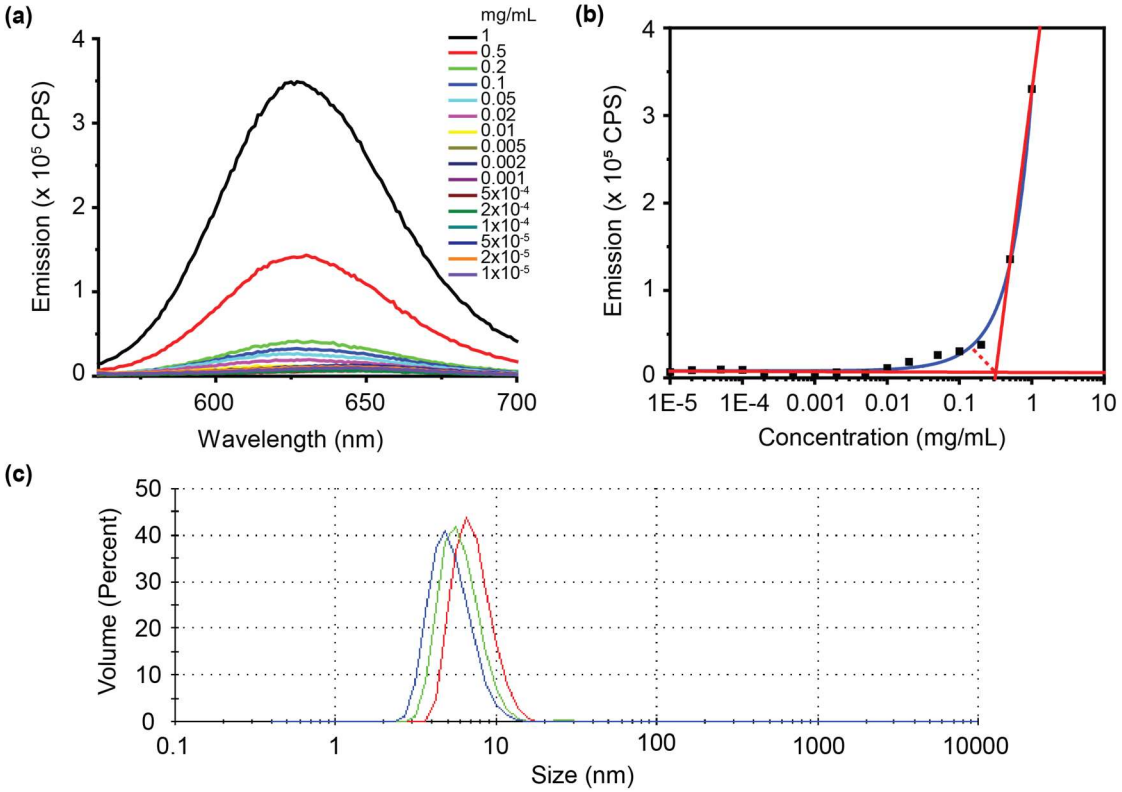

Figure 3.4 (a) Plot of fluorescence emission vs wavelength for Nile red with 1 mg/mL (33 μM) to 10 ng/mL (330 pM) polymer **P2** in water. [Nile red] = 1 μM. (b) Plot of fluorescence emission (λ_{em} = 619 nm) vs concentration. Critical micelle concentration was calculated as 0.13 mg/mL (4.3 μM) polymer **P2**. [Nile red] = 1 μM. (c) DLS size distribution by volume of 0.03 mg/mL (1 μM) polymer **P2** in water.

μM Nile red were prepared with concentrations ranging from 1 mg/mL (33 μM) to 10 ng/mL (330 pM). The fluorescence emission was measured (Figure 3.3a). Nile red does not fluoresce in polar solvents, but it exhibits strong fluorescence in hydrophobic environments.[4] Little to no fluorescence is observed before significant aggregation of unimolecular micelles, but fluorescence emission increases exponentially after assembly of aggregates. The CMC, or the point at which this change occurs, was calculated as 0.05 mg/mL (1.6 μM) polymer (Figure 3.3b). A sample with 0.03 mg/mL (1 μM) polymer **P1**, a concentration below the CMC, was characterized by dynamic light scattering (DLS) (Figure 3.3c). A single peak at 6.4 ± 1.1 nm was observed (error is standard deviation with n = 3), which suggested the formation of monodisperse SCNPs with a relatively small average hydrodynamic diameter. This size is consistent with that of previously reported SCNPs of comparable molecular weight.[5] I repeated these studies for polymer **P2** and obtained a CMC of 0.13 mg/mL (4.3 μM) using fluorescence spectroscopy and a hydrodynamic diameter of 6.2 ± 1.0 nm using DLS (Figure 3.4). The following catalytic studies used 1 μM amphiphilic polymer.

3.3 SCNP Catalysis of the CuAAC Reaction Using a Modular Cofactor Approach

I analyzed the ability of polymers **P1** and **P2** to increase the activity of transition metal catalysts. CuAAC is a robust reaction that proceeds under mild conditions. The Wu group reported biocompatible tris(triazolylmethyl)amine ligands with faster rates of reaction.[6, 7] A bulky *tert*-butyl substituent on two of the triazole rings was found to prevent the polymerization of copper acetylides and the formation of unreactive side products. Based on this work, I synthesized ligand **L1** with a naphthyloxyhexyl side chain and ligand **L2** with a hexyl side chain (Figure 3.5b). The catalytic activity of Cu-**L1** and Cu-**L2** with polymers **P1** and **P2** was studied using the

cycloaddition reaction between 3-azido-7-hydroxycoumarin (**1**) and 1-ethynyl-4-methoxybenzene (**2**) (Figure 3.5a). Compound **1** is non-fluorescent but formation of the triazole ring activates the fluorescence of coumarin.[8, 9] By using fluorescence as a "turn on" property, the progress of the cycloaddition reaction was monitored by fluorescence spectroscopy. Polymer **P1** or **P2**, Cu catalyst, sodium ascorbate (NaAsc), azide **1**, and alkyne **2** were added to PBS buffer, and fluorescence emission curves of the cycloaddition reaction were obtained over 30 min (Figure

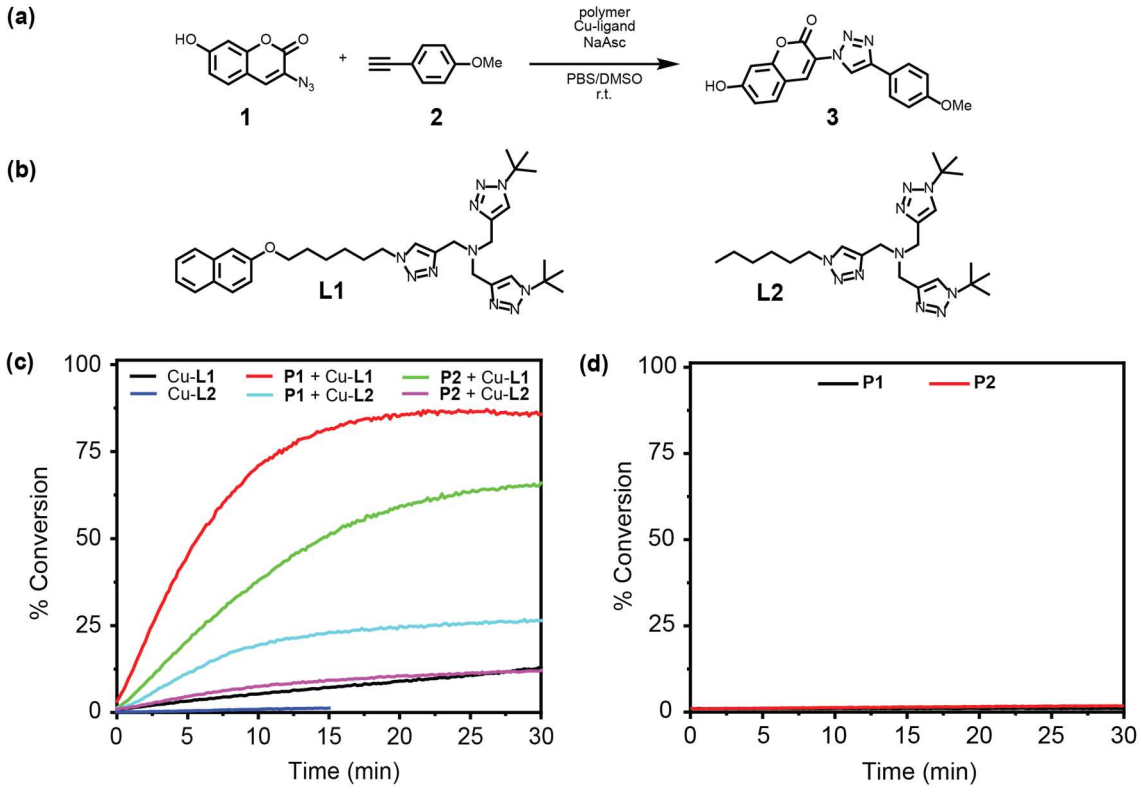

Figure 3.5 (a) CuAAC activity was measured by reaction between 3-azido-7-hydroxycoumarin (**1**, 20 μM) and 1-ethynyl-4-methoxybenzene (**2**, 40 μM) with polymer **P1** or **P2** (1 μM), Cu catalyst (5 μM), and NaAsc (2 mM). (b) Structures of bis(*tert*-butyltriazolyl) ligands **L1** and **L2**. (c) Increase in fluorescence emission intensity at λ_{em} = 480 nm of CuAAC in PBS buffer vs. time. (d) Fluorescence emission curves at λ_{em} = 480 nm of cycloaddition reaction without Cu catalyst in PBS buffer vs. time.

3.5c). In the presence of polymer **P1** and Cu-**L1**, 86% conversion was observed after 15 min compared to polymer **P2** and Cu-**L1** with 66% conversion. Free Cu-**L1** achieved 13% conversion. Lower activity was observed with Cu-**L2** in the presence of polymer **P1** (26% conversion) and polymer **P2** (12% conversion). Control reactions with polymer **P1** or **P2** without catalyst did not generate an increase in fluorescence emission, indicating that the polymers alone do not have measurable activity (Figure 3.5d). The faster initial rate of reaction and higher percent conversion observed for the catalyst in the presence of the SCNP can be rationalized by the binding of both substrates and catalyst within the SCNP, achieving high local concentrations of each. Previous work in our group, in which a Cu-SCNP catalyzes the CuAAC reaction between azide **1** and different alkynes, has demonstrated that substrate charge and hydrophobicity affect the reaction.[10] Substrates with increasing aliphatic chain length and negatively charged substrates resulted in faster initial rates of reaction. The SCNP may also help protect the catalyst from side reactions that occur in the bulk environment.[11, 12] Because higher catalytic activity was observed with polymer **P1** compared to **P2**, subsequent studies used polymer **P1**.

3.4 Characterization of Polymer-Ligand Interactions by NOESY

To obtain evidence for catalyst binding to the amphiphilic polymer, Nuclear Overhauser Effect Spectroscopy (NOESY) was performed.[13] I first identified proton peaks with unique chemical shifts in the ^{1}H NMR spectra of polymer **P1** and ligand **L1** (Figure 3.6). The experiment was conducted without Cu because the addition of paramagnetic Cu(II) led to wide chemical shifts and broadened signals such that the ligand was not observed. The ^{1}H NMR spectrum of polymer **P1** has distinct and well-resolved peaks at δ 0.9–1.8 ppm, which correspond to the polymer backbone and alkyl side chains, and at δ 3.1 ppm for the trimethyl ammonium groups. The ^{1}H

NMR spectrum of ligand **L1** has distinct peaks at δ 1.6 ppm for the *tert*-butyl groups and at δ 7.9 ppm for the triazole rings. NOESY of polymer **P1** was conducted and cross-peaks were observed from the trimethyl ammonium groups and naphthyl groups to the polymer backbone and alkyl side chains (Figure 3.7). This indicates through-space interactions between protons on the amphiphilic polymer that may arise from intramolecular folding and intermolecular aggregation. No cross-peaks were observed for ligand **L1** (Figure 3.8). When ligand **L1** was added to polymer **P1**, new cross-peaks were observed between the ligand triazole rings and both the polymer backbone and alkyl side chains (Figure 3.9). New cross-peaks in the aromatic region suggest some pi-pi stacking

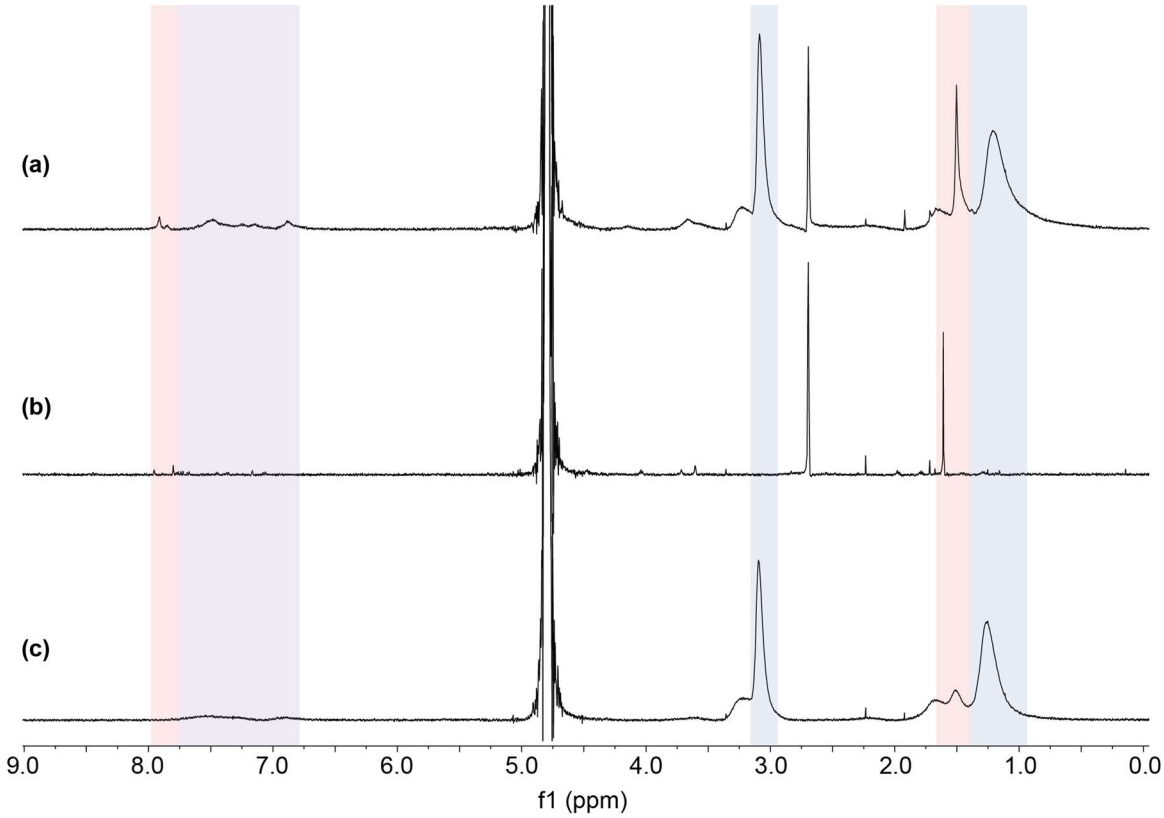

Figure 3.6 Stacked ^{1}H NMR spectra (D_2O) of (a) polymer **P1** and ligand **L1**, (b) ligand **L1**, and (c) polymer **P1**. Proton peaks identified from left to right: **L1** triazole (red), **P1** and **L1** naphthalene (purple), **P1** trimethylammonium ion (blue), **L1** tert-butyl (red), and **P1** backbone and alkyl side chains (blue).

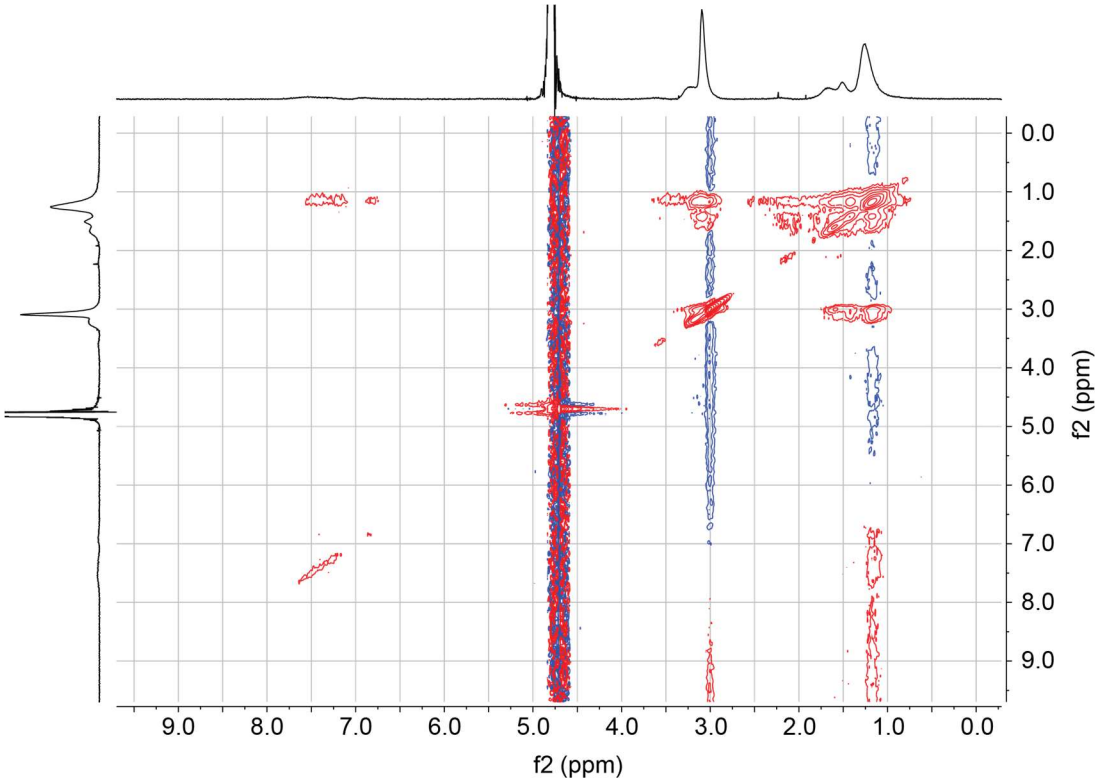

Figure 3.7 NOESY spectrum (D_2O) of polymer **P1**.

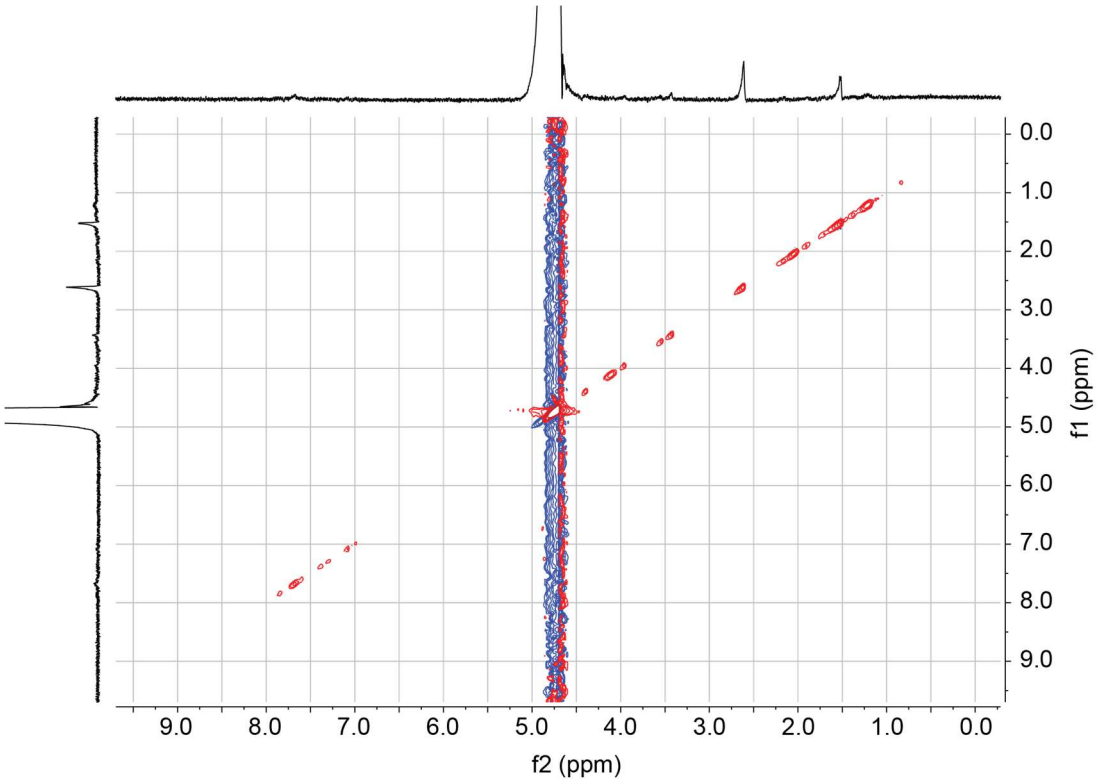

Figure 3.8 NOESY spectrum (D_2O) of ligand **L1**.

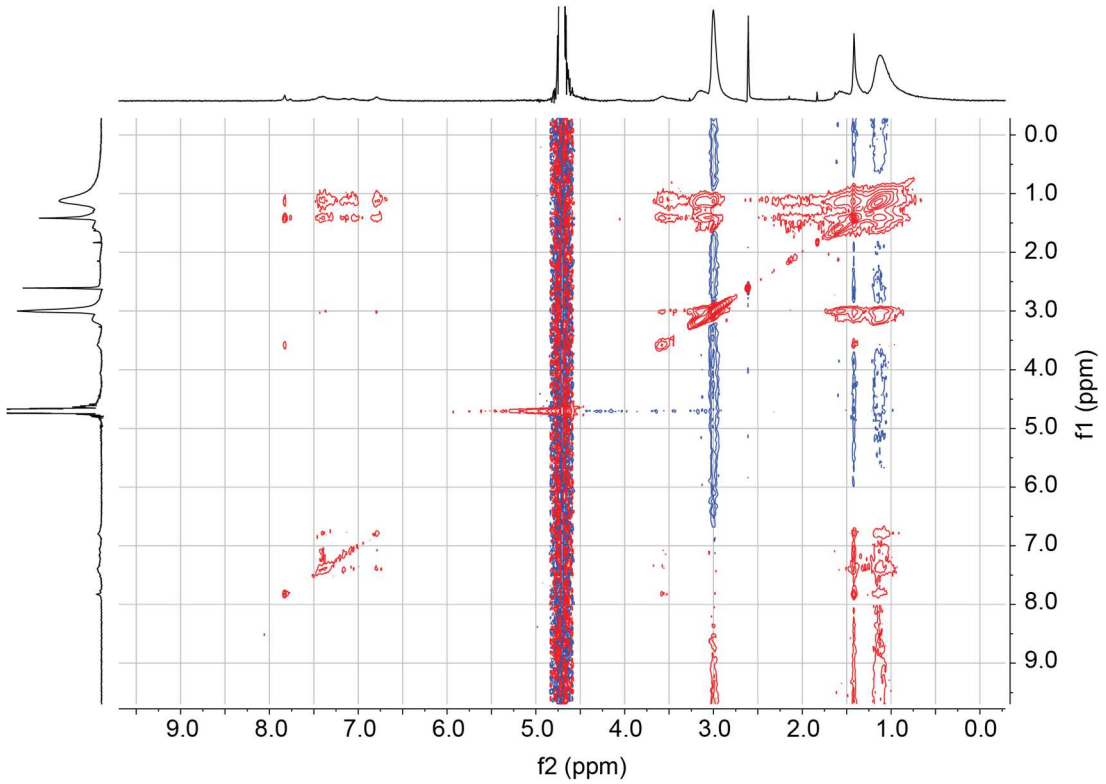

Figure 3.9 NOESY spectrum of polymer **P1** and ligand **L1**.

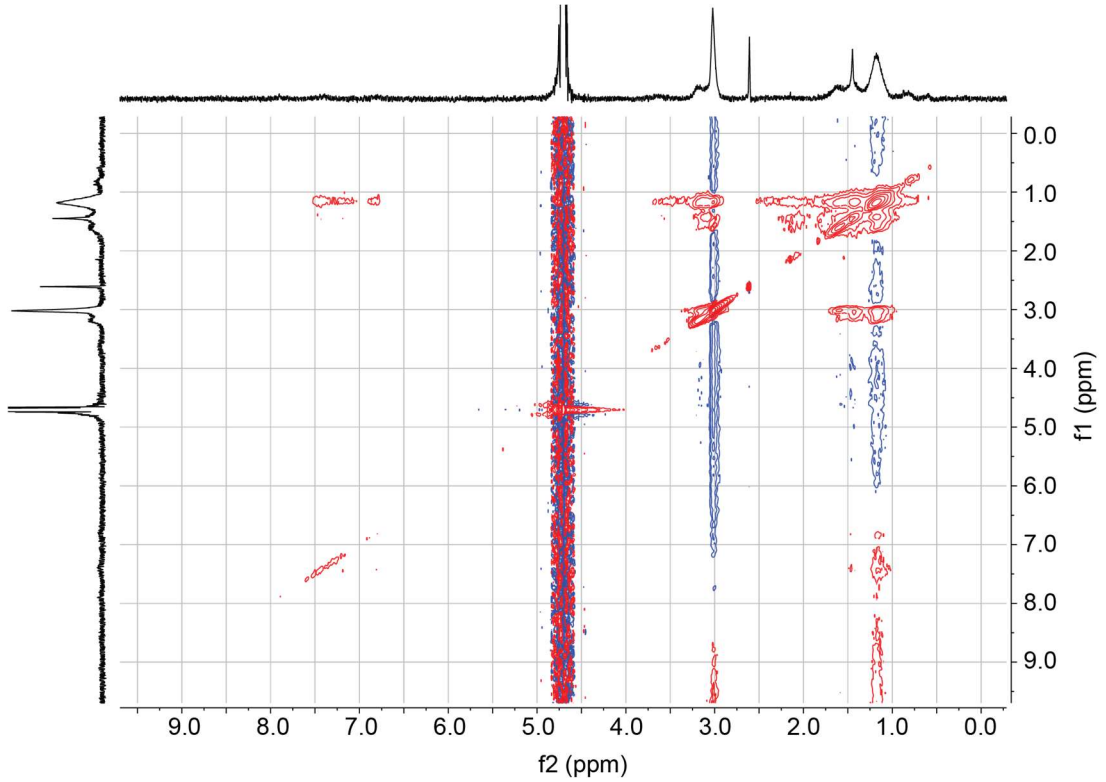

Figure 3.10 NOESY spectrum (D_2O) of polymer **P1** and ligand **L2**.

occurs between the naphthyl groups on the polymer and ligand. Unfortunately, the signal-to-noise required the concentration of polymer **P1** in each of the NOESY experiments to be above the CMC, but the data does indicate the potential both for intramolecular folding of polymer **P1** and its interaction with ligand **L1**. Other cross-peaks were observed but overlapping chemical shifts made it challenging to distinguish between the polymer and the ligand. NOESY was also conducted for polymer **P1** and ligand **L2** (Figure 3.10), however, no new distinguishable cross-peaks were observed.

3.5 Characterization of Polymer-Ligand Interactions by STD NMR

Another technique to observe and quantify binding is saturation-transfer difference (STD) NMR.[14] STD NMR has been used for ligand screening and characterization of protein binding. In

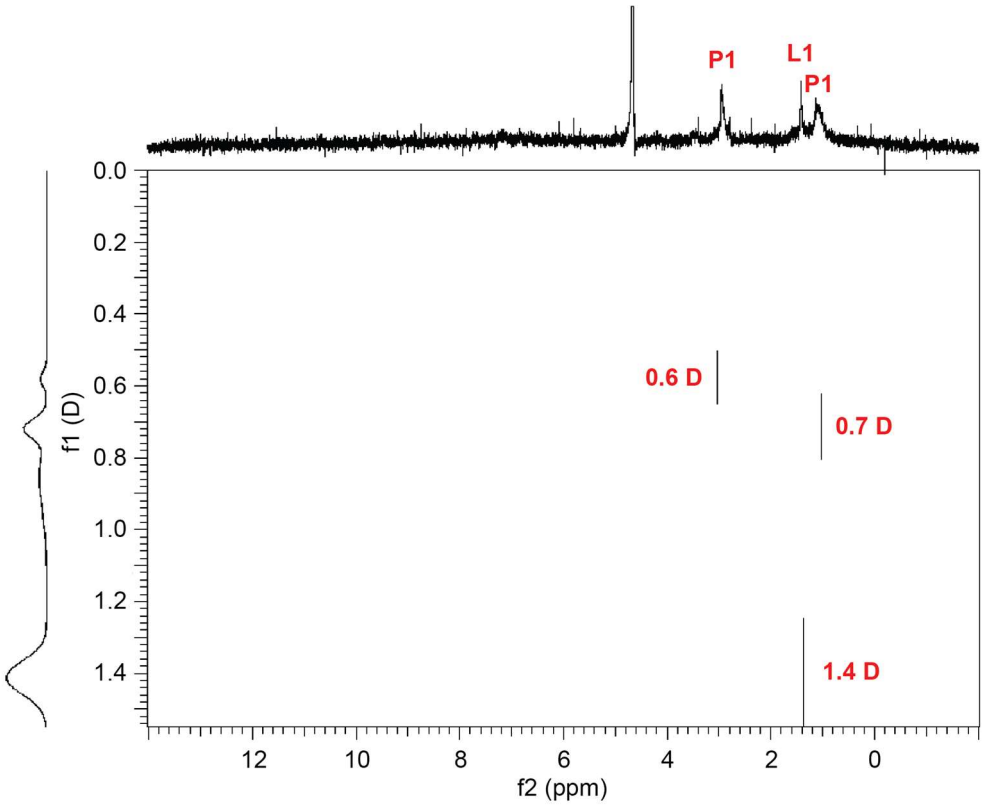

Figure 3.11 DOSY spectrum (D_2O) of polymer **P1** and ligand **L1** (D = 10 x 10^{-10} m^2/s).

this experiment, a spectrum in which the polymer is selectively saturated (*on-resonance* spectrum) is subtracted from one without polymer saturation (*off-resonance* spectrum) to obtain a difference spectrum. Only the ligands that bind to and receive saturation transfer from the polymer are observed. A practical advantage of this technique in the present case was the ability to work below the CMC. In the *off-resonance* spectrum with 1 μM polymer **P1** and 250 μM ligand **L1**, the ligand proton peaks undergo a slight chemical shift. Diffusion ordered spectroscopy (DOSY) was conducted to obtain the diffusion coefficients of the polymer and ligand and determine whether the ligand proton peaks correspond to free ligand or bound ligand (Figure 3.11). Polymer proton peaks at δ 3.03 and δ 1.03 ppm had a diffusion coefficient of 0.6 ± 0.02 D (D = 10 x 10^{-10} m^2/s). The ligand proton peak at δ 1.37 ppm had a diffusion coefficient of 1.4 ± 0.04 D. Although I observe a 100% difference between the polymer and ligand diffusion coefficients, the smaller than

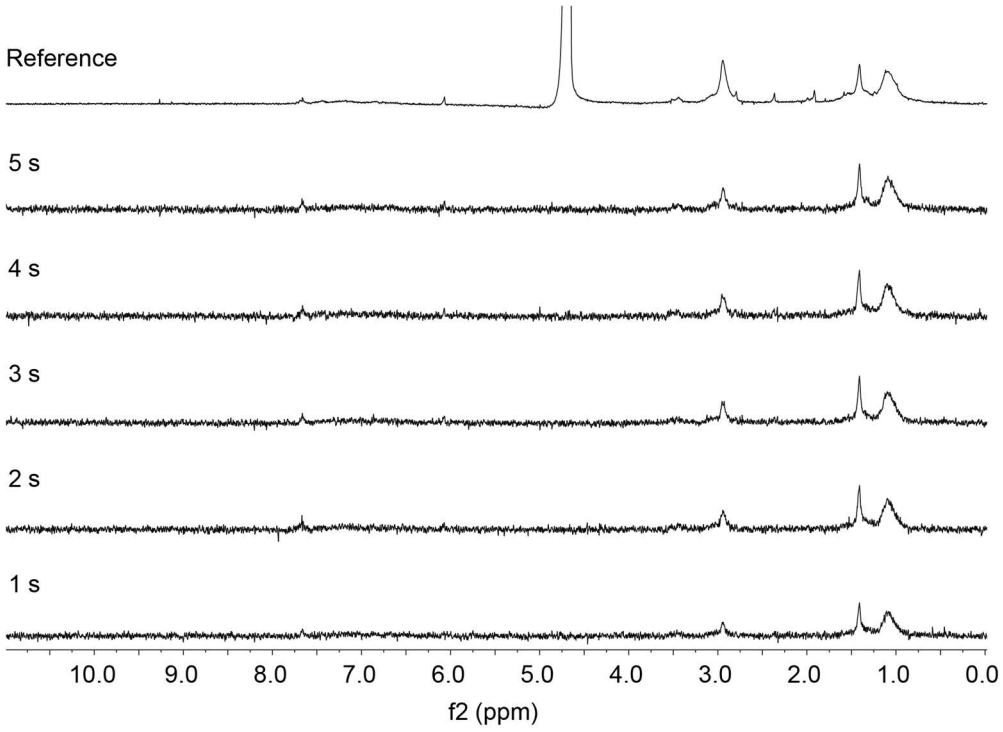

Figure 3.12 Stacked *off-resonance* spectrum of polymer **P1** and ligand **L1** and STD difference spectra with 5, 4, 3, 2, and 1 s saturation time.

expected diffusion coefficient of the ligand suggests that this value reflects an average of bound ligand and free ligand. STD NMR was conducted with peak irradiation at δ 0.4 ppm with 1, 2, 3, 4, and 5 s saturation time (Figure 3.12). The STD amplification factor (A_{STD}), which can be depicted as the average number of ligands saturated per polymer, was calculated for triazole and *tert*-butyl proton peaks at δ 7.7 and δ 1.4 ppm, respectively (Figure 3.13). The triazole proton peak has a low signal-to-noise ratio and as a result integration of this peak may have produced inflated values. In general, I obtained A_{STD} equal to the molar ratio of ligand in excess relative to the polymer with saturation times greater than or equal to 2 s. I attempted to map the ligand moieties important for interaction, which is calculated by setting the largest A_{STD} to 100% and calculating other A_{STD} with the same saturation time accordingly. At 2 s, the triazole proton experiences 100% interaction with the polymer whereas the *tert*-butyl protons only experience 85% interaction with the polymer. Taking into consideration possible error with the triazole proton, the triazole and *tert*-butyl protons are in similar proximity to the polymer. Unfortunately, I was unable to map the ligand naphthyl protons because their chemical shift overlaps with those from the polymer.

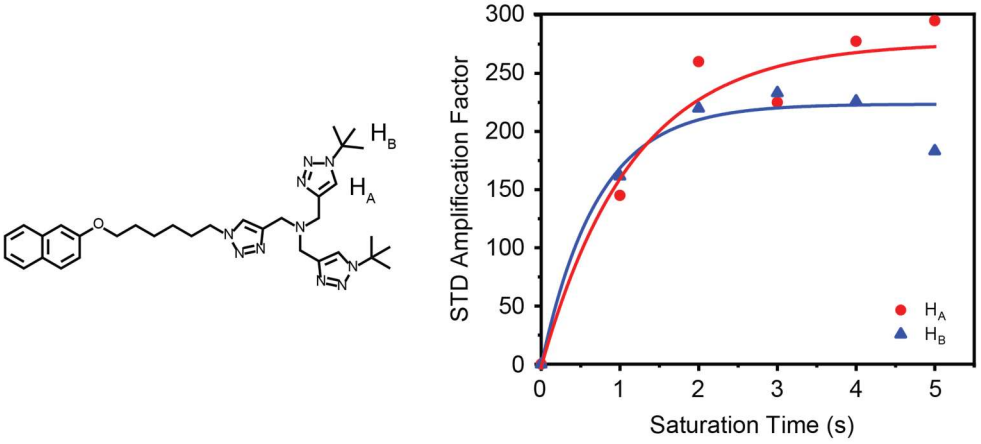

Figure 3.13 Graph of A_{STD} vs saturation time for triazole and *tert*-butyl proton peaks at δ 7.7 and δ 1.4 ppm, respectively.

3.6 Library of Cofactors for CuAAC Reaction

I obtained by NOESY and STD NMR data that is consistent with ligand **L1** binding to the polymer via the *tert*-butyl substituted triazole rings. To study how the structure of the third side chain affects interactions with the SCNP and CuAAC catalysis, my collaborators and I synthesized additional ligands **L3** to **L7** (Figure 3.14a). The library included neutral ligands **L1** to **L4**, anionic ligand **L5**, and cationic ligands **L6** to **L7**, and their catalytic activity was again analyzed using the fluorogenic click reaction in Figure 3.2a. Polymer **P1**, Cu catalyst, NaAsc, coumarin azide, and alkyne were added to water, and fluorescence emission curves of the cycloaddition reaction were

(a)

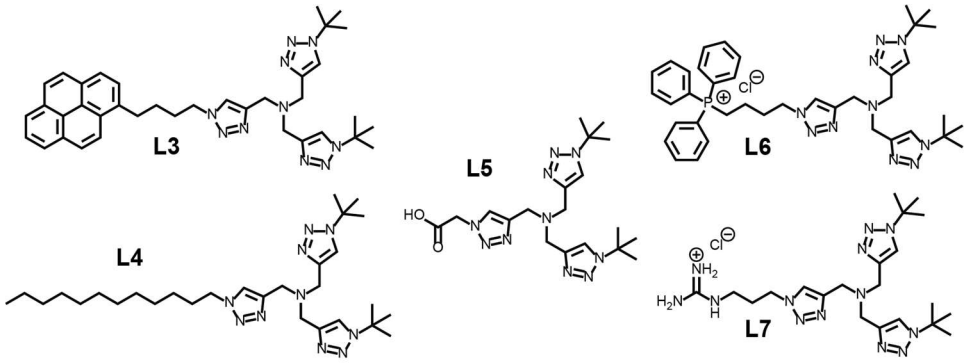

(b)

Catalyst	Initial Rate (nM/s)		% Conversion	
	w/o **P1**	w/ **P1**	w/o **P1**	w/ **P1**
Cu-**L1**	0.4	36 ± 5	2 ± 0.5	86 ± 0.4
Cu-**L2**	0.6 ± 0.4	38 ± 1	2 ± 0.2	87 ± 1
Cu-**L3**	0.4 ± 0.3	26 ± 2	2 ± 0.5	74 ± 2
Cu-**L4**	2.1 ± 0.3	23 ± 7	7 ± 0.5	83 ± 12
Cu-**L5**	0.8 ± 0.5	88 ± 9	1 ± 0.1	90 ± 1
Cu-**L6**	0.9 ± 0.6	26 ± 8	2 ± 0.4	84 ± 3
Cu-**L7**	1.0 ± 0.4	14 ± 3	1 ± 0.2	58 ± 5

Figure 3.14 (a) A library of bis(*tert*-butyltriazolyl) ligands with different chain lengths and charges was synthesized. (b) Observed percent conversions and initial rates obtained from fluorescence emission curves of ligands **L1** through **L7** in water. Standard deviation calculated from n = 3.

obtained over 15 min (Figure 3.14b). The largest enhancement in initial rate and percent conversion was observed for ligand **L5** (BTTAA), which is anionic under the working conditions. I rationalize that it may bind tighter to the positively-charged SCNP through favorable electrostatic interactions.[15] The cationic ligands performed the worst in the presence of polymer **P1** but still demonstrated higher activity than the free catalyst. In comparison, a moderate improvement in initial rate and percent conversion was observed for the more hydrophobic ligands, consistent with their tighter binding to the hydrophobic pockets of the SCNP and a resultant higher local concentration seen by the alkyne and azide substrates.

3.7 SCNP Catalysis of a Ru-Mediated Deprotection Using a Modular Cofactor Approach

I demonstrated the plug-and-play cofactor approach of our system by conveniently generating a structure-activity relationship using different Cu catalysts. To extend this approach, we sought to use a second transition metal catalyst as a cofactor with polymer **P1**. I was attracted to the Ru-catalyzed cleavage of allylcarbamate groups as a widely used bioorthogonal reaction that can be utilized to generate fluorophores from non-fluorescent precursors and active drugs from pro-drugs. Tanaka and coworkers reported the first example of a Ru catalyst for the cleavage of *N*-allyloxycarbonyl groups.[16] In 2017, the Meggers group optimized the Ru catalyst and demonstrated its catalytic activity under biologically relevant conditions.[17] Ru-**L8** was prepared using the reported procedures and Ru-**L9** was prepared from 6-(naphthalen-2-yloxy)hexan-1-amine (Figure 3.15b). Evaluation of their catalytic activity used the *N*-allyloxycarbonyl-caged coumarin shown in Figure 3.15a as a fluorogenic reporter.[18] The caged substrate is non-fluorescent but cleavage of the allylcarbamate group results in fluorescence. Polymer **P1**, Ru catalyst, glutathione (GSH), and caged coumarin **4** were added to water and fluorescence emission curves

of the cleavage reaction were obtained over 20 min (Figure 3.15c). GSH was chosen as the reducing agent because of its biocompatibility and bioavailability. The catalytic activity of Ru-**L8** did not change significantly with and without polymer **P1** (Figure 3.15d). In contrast, the catalytic activity of Ru-**L9** significantly increased in the presence of polymer **P1** with observed percent conversion increasing from 30% to 84% conversion and initial rate increasing more than 16-fold. These results are generally consistent with the trends I observed with the Cu catalysts where

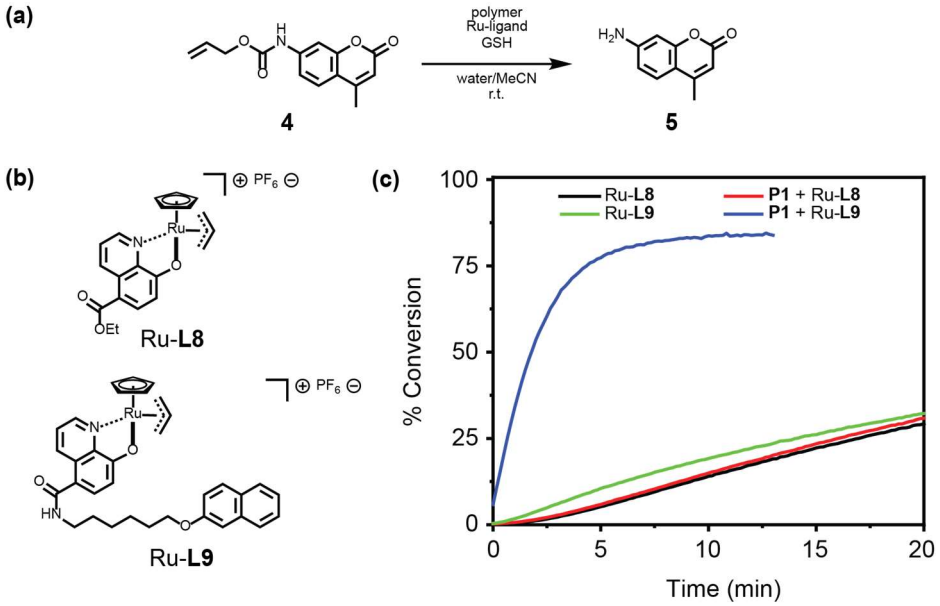

(d)

Catalyst	Initial Rate (nM/s)		% Conversion	
	w/o **P1**	w/ **P1**	w/o **P1**	w/ **P1**
Ru-**L8**	5 ± 0.3	6 ± 1	28 ± 3	31 ± 3
Ru-**L9**	6 ± 1	100 ± 4	30 ± 5	84 ± 2

Figure 3.15 (a) Ru-catalyzed cleavage of allylcarbamate groups was measured by the deprotection of *N*-(allyloxycarbonyl)aminocoumarin (20 μM) with polymer **P1** (1 μM), Ru catalyst (5 μM), and GSH (300 μM). (b) Structures of catalysts Ru-**L8** and Ru-**L9**. (c) Increase in fluorescence emission intensity at λ_{em} = 440 nm of Ru-catalyzed cleavage of allylcarbamate groups in water vs. time. (d) Observed percent conversions and initial rates obtained from kinetic study. Standard deviation calculated from n = 3.

catalysts modified with hydrophobic side chains exhibited a greater enhancement in both percent conversion and initial rate with polymer **P1** in comparison to free catalysts.

3.8 Conclusions

In summary I have developed a modular approach to transition metal-SCNPs that features a folded amphiphilic polymer to bind to transition metal catalysts in a plug-and-play cofactor approach. This simple and versatile system was utilized to generate different Cu-SCNPs for the CuAAC reaction and Ru-SCNPs for the cleavage of allylcarbamate groups. Faster initial rates of reaction and higher percent conversions were observed for catalysts with hydrophobic or anionic ligands in the presence of the SCNP compared to free catalysts. In addition, important ligand moieties for binding to the polymer were identified by NOESY and STD NMR. The structure of the catalyst can be optimized to increase binding to the polymer and increase initial rates of reaction in the presence of the SCNP. The transition metal-SCNP functions under mild conditions and has potential to be used for biological applications such as therapy or diagnostics.

3.9 Experimental Section

General Experimental Procedures

BTTAA (**L5**) was purchased from Sigma-Aldrich. For additional information, see Chapter 2. 2. 5 Experimental Section.

Synthetic Procedures

General procedure for RAFT polymerization. In a 20 mL glass vial equipped with a magnetic stir bar, 46 mg of 2-(dodecylthiocarbonothioylthio)-2-methylpropionic acid and 2.07 mg of AIBN were dissolved in 2.5 mL of 1,4-dioxane. To this mixture was added 2.07 mL of pentafluorophenyl acrylate, and the vial was degassed using three cycles of freeze-pump-thaw. The vial was transferred to an oil bath preheated to 70 °C and stirred for 6.5 h. The solution was diluted with 3 mL of THF and precipitated from 10 mL of MeOH. This process was repeated three times, and the solid was dried under high vac at 40 °C for 2 d to obtain the polymer.

General procedure for post-polymerization functionalization. To a 20 mL glass vial was added 50-100 mg of poly(pentafluorophenyl acrylate)[2] and appropriate equivalents of hexylamine, 6-(naphthalen-2-yloxy)hexan-1-amine (**S3**), and mono(10-(14-azaneyl)-*N*,*N*,*N*-trimethyldecan-1-aminium)dichloride.[15] The vial was purged with N_2, and 5 mL of DMF and 100-200 eq of DIPEA were added. The vial was transferred to a hot plate preheated to 60 °C and stirred for 24 h. The progress of the reaction was monitored by ^{19}F NMR. The product was precipitated from Et_2O, redissolved in DMSO, and dialyzed (1 kD) against H_2O for 2 d. The aqueous solution was freeze-dried on a lyophilizer to obtain the functionalized polymer as an off-white solid.

General procedure for synthesis of bis(*tert*-butyltriazolyl) ligands L1-L4. To a 20 mL glass vial was added 1 eq *N,N*-bis((1-(*tert*-butyl)-1*H*-1,2,3-triazol-4-yl)methyl)prop-2-yn-1-amine[6] and 1.15 eq substituted azide dissolved in 1:1:1 *tert*-butanol/H_2O/THF. To this vial was added 0.05 eq $CuSO_4 \cdot 5H_2O$ and 0.2 eq NaAsc, and the mixture was stirred overnight at room temperature under

N_2 atm. The mixture was concentrated by rotary evaporation, dissolved in 20 mL of EtOAc, and washed with 20 mL of H_2O and 10 mL of saturated aqueous solution of sodium chloride. The organic layer was dried over Na_2SO_4, filtered, and concentrated by rotary evaporation. The product was purified by silica gel column chromatography (10% MeOH/DCM).

2-((6-Bromohexyl)oxy)naphthalene (S1). To a 3-neck 250 mL round-bottom flask was added 5.0 g 2-naphthol, 7.19 g K_2CO_3, and 50 mL of MeCN. The flask was transferred to an oil bath preheated to 90 °C and stirred for 30 min. To this flask was added a solution of 26.7 mL 1,6-dibromohexane dissolved in 50 mL MeCN, and the mixture was stirred at reflux under N_2 atm for 24 h. The mixture was partitioned between 100 mL H_2O and 100 mL $CHCl_3$. The organic layer was washed with 100 mL saturated aqueous solution of sodium chloride, dried over Na_2SO_4, and concentrated by rotary evaporation. The product was purified twice by silica gel column chromatography using gradient elution (100% hexane to 10% EtOAc/hexane) to obtain a white solid (8.08 g, 76% yield). ^{1}H NMR (500 MHz, $CDCl_3$) δ 7.79 – 7.68 (m, 3H), 7.43 (m, 1H), 7.36 – 7.29 (m, 1H), 7.17 – 7.08 (m, 2H), 4.09 (t, J = 6.4, 2H), 3.44 (t, J = 6.8, 2H), 1.90 (m, 4H), 1.55 (p, J = 3.8, 2H). ^{13}C NMR (151 MHz, $CDCl_3$) δ 157.02, 134.60, 129.36, 128.91, 127.66, 126.70, 126.33, 123.53, 118.99, 106.55, 67.74, 33.86, 32.72, 29.10, 27.98, 25.40. High resolution ESI-MS: m/z calcd for $C_{16}H_{19}BrO^+$ ($[M+H]^+$): 307.0692; found 307.0689.

2-((6-Azidohexyl)oxy)naphthalene (S2). To a 250 mL round-bottom flask was added 5.0 g compound **S1**, 1.29 g sodium azide, and 75 mL DMF. The flask was transferred to an oil bath preheated to 60 °C and stirred under N_2 atm overnight. The mixture was diluted with 100 mL Et_2O and washed with H_2O (5 x 50 mL) and 50 mL saturated aqueous solution of sodium chloride. The

organic layer was dried over Na_2SO_4, filtered, and concentrated by rotary evaporation to obtain a yellow liquid (3.87 g, 88% yield). ^{1}H NMR (500 MHz, $CDCl_3$) δ 7.82 – 7.67 (m, 3H), 7.43 (ddd, *J* = 8.2, 6.8, 1.3, 1H), 7.33 (ddd, *J* = 8.1, 6.9, 1.3, 1H), 7.15 (m, 2H), 4.09 (t, *J* = 6.4, 2H), 3.31 (t, *J* = 6.9, 6.3, 2H), 1.87 (p, *J* = 8.1, 6.5, 2H), 1.67 (p, *J* = 12.3, 7.6, 4.4, 2H), 1.62 – 1.41 (m, 4H). ^{13}C NMR (151 MHz, $CDCl_3$) δ 157.02, 134.61, 129.37, 128.92, 127.66, 126.71, 126.34, 123.53, 118.99, 106.55, 67.73, 51.42, 29.15, 28.85, 26.57, 25.79. High resolution ESI-MS: *m*/*z* calcd for $C_{16}H_{20}N_3O^+$ ($[M+H]^+$): 270.1601; found 270.1563.

6-(Naphthalen-2-yloxy)hexan-1-amine (S3). To a 50 mL round-bottom flask was added 1.00 g compound **S2**, 1.17 g PPh_3, and 20 mL 4:1 THF/H_2O solution, and the mixture was stirred for 16 h. The mixture was concentrated by rotary evaporation and resuspended with 20 mL DCM and 20 mL 1 M aqueous HCl. The precipitate was collected by vacuum filtration and partitioned between 25 mL DCM and 25 mL H_2O. To the biphasic mixture was added KOH pellets until pH > 14. The organic layer was dried over Na_2SO_4, filtered, and concentrated by rotary evaporation. The solid was recrystallized from hot EtOAc and hexane to obtain a white solid (0.52 g, 58% yield). ^{1}H NMR (600 MHz, $CDCl_3$) δ 7.79 – 7.68 (m, 3H), 7.42 (t, *J* = 7.5, 1H), 7.32 (t, *J* = 7.5, 1H), 7.17 – 7.10 (m, 2H), 4.08 (t, *J* = 6.5, 2H), 2.73 (t, *J* = 7.0, 2H), 1.86 (dt, *J* = 14.5, 6.6, 2H), 1.52 (tt, *J* = 14.0, 7.2, 5H), 1.47 – 1.38 (m, 2H). ^{13}C NMR (151 MHz, $CDCl_3$) δ 157.07, 134.62, 129.33, 128.89, 127.65, 126.70, 126.31, 123.49, 119.02, 106.54, 67.88, 42.12, 33.57, 29.25, 26.70, 26.03. High resolution ESI-MS: *m*/*z* calcd for $C_{16}H_{21}NO^+$ ($[M+H]^+$): 244.1696; found 244.1694.

4-(1-Pyrenyl)-1-butanol tosylate (S4). To a 25 mL round-bottom flask was added 0.47 g 4-(pyren-1-yl) butan-1-ol in 10 mL DCM. To the flask was added 0.36 g 4-methylbenzenesulfonyl

chloride, and the mixture was chilled in an ice bath. To the flask was added 0.38 g KOH over 10 min and the mixture was stirred for 3 h. The mixture was washed with 20 mL H_2O, and the aqueous layer was washed with DCM (2 x 20mL). The combined organic layers were washed with 20 mL saturated aqueous solution of sodium chloride, dried over Na_2SO_4, filtered, and concentrated by rotary evaporation to give the product (0.17 g, 23% yield). ^{1}H NMR (600 MHz, $CDCl_3$) δ 8.23 – 8.13 (m, 3H), 8.13 – 8.06 (m, 2H), 8.03 (s, 2H), 8.00 (t, *J* = 7.6, 1H), 7.79 (d, *J* = 7.7, 1H), 7.75 (d, *J* = 7.9, 2H), 7.25 (d, *J* = 7.8, 2H), 4.08 (t, *J* = 6.3, 2H), 3.31 (t, *J* = 7.6, 2H), 2.36 (s, 3H), 1.89 (p, *J* = 7.5, 2H), 1.80 (p, *J* = 6.4, 2H). ^{13}C NMR (151 MHz, $CDCl_3$) δ 144.68, 135.83, 133.09, 131.43, 130.87, 129.93, 129.80, 128.59, 127.86, 127.49, 127.38, 127.20, 126.73, 125.90, 125.09, 124.99, 124.98, 124.79, 123.19, 70.38, 60.42, 32.71, 28.76, 27.48, 21.57, 14.22. High resolution ESI-MS: *m*/*z* calcd for $C_{27}H_{25}O_3S^+$ ($[M+H]^+$): 429.1519; found 429.1503.

1-(4-Azido-butyl)-pyrene (S5). To a 20 mL glass vial was added 150 mg compound **S4**, 50 mg sodium azide, and 2.5 mL DMF. The vial was transferred to a well plate preheated to 60 °C and stirred under N_2 atm overnight. The mixture was diluted with 12 mL Et_2O and washed with H_2O (5 x 6 mL) and 6 mL saturated aqueous solution of sodium chloride. The organic layer was dried over Na_2SO_4, filtered, and concentrated by rotary evaporation. The product was purified by silica gel column chromatography using gradient elution (10% EtOAc/hexane to 20% EtOAc/hexane) to obtain a white solid (40 mg, 25% yield). ^{1}H NMR (600 MHz, $CDCl_3$) δ 8.26 (d, *J* = 9.2, 1H), 8.19 – 8.15 (m, 2H), 8.12 (d, *J* = 8.5, 2H), 8.03 (d, *J* = 2.4, 2H), 8.00 (t, *J* = 7.6, 1H), 7.87 (d, *J* = 7.7, 1H), 3.39 (t, *J* = 7.8, 2H), 3.34 (t, *J* = 6.9, 2H), 1.96 (p, *J* = 7.7, 2H), 1.78 (dt, *J* = 14.5, 7.0, 2H). ^{13}C NMR (151 MHz, $CDCl_3$) δ 136.10, 131.45, 130.90, 129.94, 128.62, 127.52, 127.39,

127.23, 126.71, 125.88, 125.13, 125.03, 124.96, 124.84, 124.78, 123.23, 51.41, 33.01, 28.91, 28.85. High resolution ESI-MS: *m*/*z* calcd for $C_{20}H_{18}N_3^+$ ($[M+H]^+$): 300.1501; found: 300.1455.

L1. *N,N*-Bis((1-(*tert*-butyl)-1*H*-1,2,3-triazol-4-yl)methyl)prop-2-yn-1-amine and compound **S2** were reacted according to the general procedure to obtain an off-white solid (0.32 g, 43% yield). ^{1}H NMR (400 MHz, $CDCl_3$) δ 7.86 (m, 3H), 7.78 – 7.68 (m, 3H), 7.42 (t, *J* = 7.7, 1H), 7.32 (t, *J* = 7.4, 1H), 7.16 – 7.09 (m, 2H), 4.39 (t, *J* = 7.0, 2H), 4.06 (t, *J* = 6.4, 2H), 3.77 (m, 6H), 2.00 (p, *J* = 7.8, 2H), 1.85 (p, *J* = 7.5, 2H), 1.69 (s, 18H), 1.45 (p, *J* = 7.4, 2H). ^{13}C NMR (151 MHz, $CDCl_3$) δ 156.98, 134.59, 129.35, 128.90, 127.63, 126.71, 126.31, 123.51, 121.09, 118.97, 106.54, 67.62, 59.26, 50.24, 46.95, 30.31, 30.06, 29.04, 26.36, 25.66. High resolution ESI-MS: *m*/*z* calcd for $C_{33}H_{47}N_{10}O^+$ ($[M+H]^+$): 599.3929; found 599.3947.

L2. *N,N*-Bis((1-(*tert*-butyl)-1*H*-1,2,3-triazol-4-yl)methyl)prop-2-yn-1-amine and 1-azidohexane were reacted according to the general procedure to obtain a white solid (0.26 g, 78% yield). ^{1}H NMR (500 MHz, $CDCl_3$) δ 7.85 (s, 3H), 4.35 (t, *J* = 7.3, 2H), 3.78 (s, 2H), 3.76 (s, 4H), 1.91 (t, *J* = 7.5, 2H), 1.69 (s, 18H), 1.31 (broad s, 6H), 0.93 – 0.82 (m, 3H). ^{13}C NMR (151 MHz, $CDCl_3$) δ 121.08, 59.26, 50.37, 47.05, 46.94, 31.17, 30.31, 30.06, 26.21, 22.44, 13.96. High resolution ESI-MS: *m*/*z* calcd for $C_{23}H_{41}N_{10}^+$ ($[M+H]^+$): 457.3510; found 457.3510.

L3. *N,N*-Bis((1-(*tert*-butyl)-1*H*-1,2,3-triazol-4-yl)methyl)prop-2-yn-1-amine and compound **S5** were reacted according to the general procedure to obtain a viscous oil (24 mg, 29% yield). ^{1}H NMR (500 MHz, $CDCl_3$) δ 8.22 (d, *J* = 9.0, 1H), 8.16 (d, *J* = 7.7, 2H), 8.10 (d, *J* = 8.1, 2H), 8.02 (s, 2H), 7.98 (t, *J* = 7.6, 1H), 7.85 (s, 1H), 7.83 (s, 1H), 7.80 (s, 2H), 4.41 (t, *J* = 7.0, 2H), 3.75 (s,

2H), 3.73 (s, 4H), 3.39 (t, J = 7.6, 2H), 2.13 – 2.08 (m, 2H), 1.91 (t, J = 8.0, 2H), 1.67 (s, 18H). ^{13}C NMR (126 MHz, $CDCl_3$) δ 135.65, 131.39, 130.84, 129.96, 128.56, 127.48, 127.46, 127.24, 126.71, 125.87, 125.07, 124.95, 124.85, 124.79, 123.12, 50.28, 46.66, 42.67, 32.74, 30.15, 29.99, 28.51. High resolution ESI-MS: m/z calcd for $C_{37}H_{45}N_{10}^+$ ($[M+H]^+$): 629.3823; found 629.3829.

L4. *N,N*-Bis((1-(*tert*-butyl)-1*H*-1,2,3-triazol-4-yl)methyl)prop-2-yn-1-amine and 1-azidododecane were reacted according to the general procedure to obtain a white solid (90 mg, 57% yield). ^{1}H NMR (500 MHz, $CDCl_3$) δ 7.84 (s, 3H), 4.34 (t, J = 7.4, 2H), 3.78 (s, 2H), 3.76 (s, 4H), 1.91 (broad s, 2H), 1.69 (s, 18H), 1.28 (m, 18H), 0.87 (t, J = 6.9, 3H). ^{13}C NMR (151 MHz, $CDCl_3$) δ 121.08, 59.21, 50.37, 46.93, 31.91, 30.36, 30.06, 29.61, 29.53, 29.41, 29.34, 29.03, 26.55, 22.70, 14.14. High resolution ESI-MS: m/z calcd for $C_{29}H_{53}N_{10}^+$ ($[M+H]^+$): 541.4449; found 541.4453.

L6. To a 20 mL glass vial was added 0.40 g (4-bromobutyl)triphenylphosphonium azide,[19] 0.33 g *N,N*-bis((1-(*tert*-butyl)-1*H*-1,2,3-triazol-4-yl)methyl)prop-2-yn-1-amine,[15] 25 mg $CuSO_4 \cdot 5H_2O$, and 12 mL of 1:1 H_2O/DMSO. To the mixture was added 40 mg NaAsc under N_2 atm. The mixture was stirred at 60 °C for 20 h. To the mixture was added 50 mL of 1 M aqueous EDTA and the mixture was extracted with 50 mL of DCM. The organic layer was washed with 50 mL of H_2O and 50 mL of saturated aqueous solution of sodium chloride, dried over Na_2SO_4, filtered, and concentrated by rotary evaporation. The crude product was purified by silica gel column chromatography using gradient elution (100% DCM to 10% MeOH/DCM) to obtain a yellow solid (0.56 g, 71% yield). ^{1}H NMR (500 MHz, $CDCl_3$) δ 8.13 (s, 1H), 7.92 (s, 2H), 7.80 – 7.71 (m, 9H), 7.63 (td, J = 7.8, 3.4, 6H), 4.61 (t, J = 6.4, 2H), 3.86 (td, J = 13.0, 6.6, 2H), 3.72 (s, 2H), 3.67 (s, 4H), 2.38 (p, J = 6.7, 2H), 1.66 (s, 18H), 1.63 – 1.53 (m, 2H). ^{13}C NMR (126 MHz, $CDCl_3$) δ

144.67, 143.70, 135.44, 135.41, 133.96, 133.88, 130.83, 130.73, 124.56, 121.37, 118.29, 117.61, 59.52, 48.98, 48.19, 47.56, 30.35, 22.59, 22.18, 19.45. High resolution ESI-MS: *m*/*z* calcd for $C_{39}H_{50}N_{10}P^+$: 689.3952; found 689.3951.

L7. To a 20 mL glass vial was added 0.18 g *N*-(3-azidopropyl)-guanidinium chloride,[20] 0.33 g *N,N*-bis((1-(*tert*-butyl)-1*H*-1,2,3-triazol-4-yl)methyl)prop-2-yn-1-amine,[15] 25 mg $CuSO_4$•$5H_2O$, and 12 mL of 1:1 H_2O/DMSO. To the mixture was added 40 mg NaAsc under N_2 atm. The mixture was stirred at 60 °C for 24 h. To the mixture was added 50 mL of 1 M aqueous EDTA and the mixture was extracted with a solution of 2:1 DCM/IPA (3 x 50 mL). The combined organic layers were washed with 50 mL of brine, dried over Na_2SO_4, filtered, and concentrated by rotary evaporation. The crude product was purified by silica gel column chromatography using gradient elution (100% DCM to 1% NH_4OH, 15% MeOH in DCM) to obtain a yellow solid (0.11 g, 20% yield). ^{1}H NMR (500 MHz, $CDCl_3$) δ 8.40 (s, 1H), 8.16 (s, 1H), 7.93 (s, 2H), 7.78 (broad s, 2H), 4.57 (t, *J* = 7.0, 2H), 3.72 (s, 6H), 3.47 – 3.32 (m, 2H), 3.10 (broad s, 2H), 2.31 – 2.18 (m, 2H), 1.64 (s, 18H). ^{13}C NMR (126 MHz, $CDCl_3$) δ 158.03, 143.78, 142.98, 125.29, 121.90, 59.90, 47.55, 47.10, 38.81, 30.27, 29.89. High resolution ESI-MS: *m*/*z* calcd for $C_{21}H_{38}N_{13}^+$: 472.3368; found 472.3370.

8-Hydroxyquinoline-5-carboxylic acid (S6). To a 250 mL round-bottom flask was added 5.5 g 3-amino-4-hydroxybenxoic acid and 100 mL 6 M HCl. The suspension was magnetically stirred at 40 °C in an oil bath. To the suspension was added 3.3 mL acrolein dropwise via an addition funnel over 30 min. The mixture was refluxed at 105 °C for 2 h. The dark brown mixture was vacuum filtered. The pH of the dark brown filtrate was adjusted to pH = 9 with 28% w/w aqueous

NH_4OH. The basic solution was vacuum filtered. The pH of the dark brown filtrate was adjusted to pH = 7 using 10 M HCl and vacuum filtered. The pH of the filtrate was adjusted to pH = 6 with 10 M HCl and vacuum filtered. The addition of 10 M HCl was repeated dropwise until solid crashed out and consequently filtered. This process was repeated until an orange solid was obtained (usually pH = 4-5). The pH = 5 filtrate was extracted with EtOAc and more yellow solid precipitated out. The combined orange solids were washed with DCM twice and dried under vacuum to obtain a bright orange powdery solid (1.02 g, 17% yield). ^{1}H NMR (500 MHz, DMSO-d_6): δ 9.47 (dd, J = 8.8, 1.6, 1H), δ 8.90 (dd, J = 4.0, 1.6, 1H), δ 8.24 (d, J = 8.2, 1H), δ 7.69 (dd, J = 8.8, 4.1, 1H), δ 7.12 (d, J = 8.2, 1H). ^{13}C NMR (125 MHz, DMSO-d_6): δ 167.63, 157.75, 148.11, 138.21, 134.51, 133.39, 128.05, 123.21, 116.68, 110.11. High resolution ESI-MS: m/z calcd for $C_{10}H_8NO_3^+$ ($[M+H]^+$): 190.0499; found 190.0495.

Allyl 8-(allyloxy)quinoline-5-carboxylate (S7). To a 50 mL round-bottom flask was added 1.0 g compound **S6**, 4.4 g potassium carbonate, and 15 mL DMF. The mixture was stirred, and 1.8 mL allyl bromide was added dropwise. The mixture was stirred at 50 °C for 16 h. To the mixture was added 20 mL H_2O and 20 mL EtOAc. The organic layer was collected and the aqueous layer was extracted with EtOAc (2 x 20 mL). The combined organic layers were washed with H_2O (4 x 20 mL) and 20 mL saturated aqueous solution of sodium chloride, dried over Na_2SO_4, and concentrated by rotary evaporation. The product was purified by silica gel column chromatography (30% EtOAc/hexane) to afford a pale yellow solid. The solid was washed with a minimal amount of Et_2O to remove the yellow impurity and obtain a white solid (0.55 g, 39% yield). ^{1}H NMR (500 MHz, $CDCl_3$): δ 9.47 (dd, J = 8.8, 1.7, 1H), 8.98 (dd, J = 4.1, 1.7, 1H), 8.35 (d, J = 8.4, 1H), 7.55 (dd, J = 8.8, 4.1, 1H), 7.06 (d, J = 8.4, 1H), 6.20 (ddt, J = 17.3, 10.7, 5.5, 1H), 6.09 (ddt, J = 17.3,

10.5, 5.7, 1H), 5.47 (m, 2H), 5.35 (m, 2H), 4.94 (dt, *J* = 5.6, 1.5, 2H), 4.88 (dt, *J* = 5.6, 1.5, 2H). ^{13}C NMR (126 MHz, $CDCl_3$): δ 165.91, 158.30, 149.43, 140.17, 134.53, 132.57, 132.33, 128.78, 123.05, 118.97, 118.38, 118.05, 107.51, 77.22, 70.07, 65.49. High resolution ESI-MS: *m*/*z* calcd for $C_{16}H_{16}NO_3^+$ ($[M+H]^+$): 270.1125; found 270.1118.

8-(Allyloxy)-7,8-dihydroquinoline-5-carboxylic acid (S8). To a 20 mL glass vial was added 460 mg compound **S7**, 717 mg $LiOH \cdot H_2O$, 2 mL THF, 2 mL methanol, and 1 mL H_2O. The mixture was stirred at room temperature for 12 h. Volatiles were removed by rotary evaporation and the solid was resuspended in 5 mL H_2O. The pH of the slurry was adjusted to pH = 3 with 1 M aqueous HCl and filtered to afford a white solid (374 mg, 95% yield). ^{1}H NMR (500 MHz, DMSO-*d*$_6$): δ 12.95 (s, 1H), 9.41 (dd, *J* = 8.8, 1.7, 1H), 8.91 (dd, *J* = 4.0, 1.7, 1H), 8.27 (d, *J* = 8.4, 1H), 7.67 (dd, *J* = 8.7, 4.0, 1H), 7.27 (d, *J* = 8.4, 1H), 6.18 (ddt, *J* = 17.1, 10.7, 5.4, 1H), 5.53 (dq, *J* = 17.2, 1.6, 1H), 5.35 (dq, *J* = 10.5, 1.5, 1H), 4.85 (dt, *J* = 5.4, 1.5, 2H). ^{13}C NMR (126 MHz, DMSO-*d*$_6$): δ 167.56, 157.68, 149.02, 139.55, 133.89, 133.10, 132.54, 127.98, 123.06, 118.30, 118.28, 108.13, 69.17. High resolution ESI-MS: *m*/*z* calcd for $C_{13}H_{12}NO_3^+$ ($[M+H]^+$): 230.0812; found 230.0808.

Methyl 8-(allyloxy)quinoline-5-carboxylate (S9). To a 25 mL round-bottom flask was added 300 mg compound **S8** and 7.5 mL dry DCM, and 11.5 μL DMF and 285 μL oxalyl chloride were added. The mixture was stirred at room temperature for 1 h. Volatiles were removed by rotary evaporation and the resulting solid was washed with dry THF. The solid was dissolved in 10 mL methanol and stirred at room temperature for 16 h. Volatiles were removed by rotary evaporation and the resulting solid was dissolved in 10 mL EtOAc and washed with 10 mL sat. aqueous $NaHCO_3$. The organic layer was dried over Na_2SO_4, filtered, and concentrated by rotary evaporation. The product

was purified by silica gel column chromatography (50% EtOAc/hexane) to obtain a pale yellow oil. The oil was washed with hexane to afford a white crystalline solid (164 mg, 52% yield). ^{1}H NMR (500 MHz, acetone-d_6): δ 9.43 (dd, J = 8.8, 1.7, 1H), 8.92 (dd, J = 4.0, 1.7, 1H), 8.32 (d, J = 8.4, 1H), 7.65 (dd, J = 8.8, 4.0, 1H), 7.26 (d, J = 8.4, 1H), 6.23 (ddt, J = 17.3, 10.5, 5.2, 1H), 5.59 (dq, J = 17.2, 1.7, 1H), 5.34 (dq, J = 10.6, 1.5, 1H), 4.90 (dt, J = 5.1, 1.6, 2H), 3.94 (s, 3H). ^{13}C NMR (126 MHz, acetone-d_6): δ 166.28, 158.66, 149.00, 140.33, 133.71, 133.12, 132.47, 128.40, 122.95, 117.91, 117.28, 107.83, 69.41, 51.30. High resolution ESI-MS: m/z calcd for $C_{14}H_{14}NO_3^+$ ([M+H]$^+$): 244.0968; found 244.0962.

Ru-**L8.** To a 4 mL glass vial was added 27.6 mg compound **S9** and 0.5 mL MeCN. To a different 4 mL glass vial was added 49.3 mg tris(acetonitrile)cyclopentadienylruthenium(II) and 0.5 mL MeCN. The solution of compound **S9** was added to the ruthenium solution. The mixture was stirred at room temperature for 1 h. The mixture was added dropwise to 45 mL Et_2O in a 50 mL centrifuge tube, and a yellow solid was collected by centrifugation. The pellet was washed with Et_2O (2 x 35 mL). The product was collected by centrifugation and dried under vacuum to afford a yellow solid (50 mg, 79% yield). ^{1}H NMR (500 MHz, CD_3CN): δ 9.62 (dd, J = 8.8, 1.2, 1H), 8.68 (dd, J = 5.1, 1.2, 1H), 8.21 (d, J = 8.6, 1H), 7.65 (dd, J = 8.8, 5.1, 1H), 6.91 (d, J = 8.6, 1H), 5.98 (s, 5H), 4.54 (tt, J = 10.7, 6.2, 1H), 4.44 (d, J = 11.0, 1H), 4.18 (d, J = 10.8, 1H), 4.17 – 4.11 (m, 2H), 3.88 (s, 3H). ^{13}C NMR (126 MHz, CD_3CN): 175.10, 167.04, 164.62, 156.66, 139.61, 136.72, 131.81, 126.14, 115.63, 111.62, 99.98, 96.90, 69.69, 64.43, 52.41. MALDI-TOF: m/z calcd for $C_{19}H_{18}NO_3Ru^+$ ([M]$^+$): 409.4; found 409.2.

8-Hydroxy-*N*-(6-(naphthalen-2-yloxy)hexyl)-7,8-dihydroquinoline-5-carboxamide (S10). To a 20 mL glass vial was added 400 mg compound **S6**, 490 mg EDC, 390 mg HOBt, 620 mg compound **S3**, and 5 mL DMF. To the mixture was added 0.88 mL triethylamine and the mixture was stirred at room temperature for 16 h. The mixture was diluted with 15 mL H_2O and extracted with EtOAc (3 x 15 mL). The combined organic layers were washed with H_2O (3 x 10 mL). The organic layer was dried over Na_2SO_4, filtered, and concentrated by rotary evaporation. The crude product was purified by silica gel column chromatography (5% methanol/DCM) to afford a white solid (230 mg, 26% yield). ^{1}H NMR (500 MHz, $CDCl_3$) δ 8.97 (dd, *J* = 8.7, 1.6, 1H), 8.80 (dd, *J* = 4.2, 1.6, 1H), 7.77 – 7.69 (m, 3H), 7.65 (d, *J* = 7.9, 1H), 7.51 (dd, *J* = 8.7, 4.2, 1H), 7.45 – 7.40 (m, 1H), 7.32 (ddd, *J* = 8.0, 6.8, 1.2, 1H), 7.15 – 7.08 (m, 3H), 5.99 (s, 1H), 4.10 (t, *J* = 6.4, 2H), 3.54 (td, *J* = 7.2, 5.8, 2H), 1.94 – 1.84 (m, 2H), 1.72 (p, *J* = 7.3, 2H), 1.66 – 1.58 (m, 4H). ^{13}C NMR (126 MHz, $CDCl_3$) δ 168.32, 157.15, 154.59, 148.43, 138.31, 135.32, 134.73, 129.50, 129.05, 127.79, 127.35, 126.83, 126.76, 126.48, 124.51, 123.67, 123.01, 119.09, 108.39, 106.71, 67.90, 40.14, 29.90, 29.29, 26.94, 26.05. High resolution ESI-MS: m/z calcd for $C_{26}H_{27}N_2O_3^+$ ($[M+H]^+$): 415.2016; found 415.2025.

8-(Allyloxy)-N-(6-(naphthalen-2-yloxy)hexyl)-7,8-dihydroquinoline-5-carboxamide (S11). To a 20 mL glass vial was added 120 mg compound **S10**, 80 mg potassium carbonate, and 3 mL dry DMF. To the mixture was added 31 μL allyl bromide and the mixture was stirred at room temperature for 20 h. The mixture was diluted with 20 mL H_2O and extracted with EtOAc (3 x 15 mL). The combined organic layers were washed with H_2O (3 x 15 mL). The organic layer was dried over Na_2SO_4, filtered, and concentrated by rotary evaporation. The crude product was purified by silica gel column chromatography (10% methanol/DCM) to afford a white solid (68

mg, 51% yield). ^{1}H NMR (500 MHz, $CDCl_3$): δ 8.97 (dd, *J* = 4.1, 1.7, 1H), 8.84 (dd, *J* = 8.6, 1.7, 1H), 7.78 – 7.69 (m, 3H), 7.58 (d, *J* = 8.1, 1H), 7.48 (dd, *J* = 8.6, 4.1, 1H), 7.43 (ddd, *J* = 8.1, 6.8, 1.3, 1H), 7.33 (ddd, *J* = 8.1, 6.9, 1.2, 1H), 7.16 – 7.10 (m, 2H), 6.93 (d, *J* = 8.1, 1H), 6.18 (ddt, *J* = 17.4, 10.7, 5.5, 1H), 5.97 (s, 1H), 5.46 (dq, *J* = 17.3, 1.5, 1H), 5.35 (dq, *J* = 10.6, 1.4, 1H), 4.86 (dt, *J* = 5.4, 1.6, 2H), 4.10 (t, *J* = 6.4, 2H), 3.55 (td, *J* = 7.1, 5.8, 2H), 1.94 – 1.86 (m, 2H), 1.72 (p, *J* = 7.3, 2H), 1.62 (p, *J* = 6.9, 2H), 1.58 – 1.51 (m, 2H). ^{13}C NMR (126 MHz, $CDCl_3$): δ 168.50, 157.15, 156.27, 149.93, 140.45, 134.74, 134.47, 132.74, 129.51, 129.05, 127.79, 127.44, 126.83, 126.49, 126.40, 126.12, 123.69, 122.62, 119.10, 118.86, 107.61, 106.71, 70.06, 67.87, 40.13, 29.83, 29.26, 26.87, 26.02. High resolution ESI-MS: m/z calcd for $C_{29}H_{31}N_2O_3^+$ ($[M+H]^+$): 455.2329; found 455.2325.

Ru-**L9.** To a 4 mL glass vial was added 42.7 mg compound **S11**, 40.0 mg tris(acetonitrile)cyclopentadienylruthenium(II) hexafluorophosphate, and 2 mL dry DCM. The mixture was stirred at room temperature for 3 h. The crude product was precipitated by dropwise addition to 12 mL Et_2O and collected by centrifugation (5000 rpm, 5 min). The pellet was resuspended in 1 mL acetone and precipitated by dropwise addition to 13 mL Et_2O. The product was collected by centrifugation (5000 rpm, 5 min) and dried under vacuum to obtain a shimmery brown solid (53 mg, 75% yield). ^{1}H NMR (500 MHz, CD_3CN): δ 9.22 (dd, *J* = 8.7, 1.2, 1H), 8.63 (dd, *J* = 5.1, 1.2, 1H), 7.81 – 7.73 (m, 3H), 7.65 (d, *J* = 8.3, 1H), 7.55 (dd, *J* = 8.7, 5.1, 1H), 7.45 (ddd, *J* = 8.2, 6.8, 1.3, 1H), 7.34 (ddd, *J* = 8.1, 6.8, 1.2, 1H), 7.24 (d, *J* = 2.6, 1H), 7.12 (dd, *J* = 9.0, 2.5, 1H), 6.88 (s, 1H), 6.85 (d, *J* = 8.3, 1H), 5.95 (s, 5H), 4.50 (tt, *J* = 10.6, 6.2, 1H), 4.41 (d, *J* = 10.9, 1H), 4.17 – 4.07 (m, 5H), 3.38 (q, *J* = 6.6, 2H), 1.88 – 1.81 (m, 2H), 1.64 (p, *J* = 7.1, 2H), 1.60 – 1.52 (m, 2H), 1.52 – 1.45 (m, 2H). ^{13}C NMR (126 MHz, CD_3CN): 172.48, 168.00, 158.12,

156.66, 146.80, 139.83, 135.79, 131.43, 130.43, 130.28, 129.88, 128.54, 127.65, 127.43, 125.22, 124.58, 119.83, 119.23, 115.00, 107.70, 99.71, 96.80, 69.69, 68.86, 63.92, 40.33, 30.27, 29.87, 27.46, 26.54. MALDI-TOF: m/z calcd for $C_{34}H_{35}N_2O_3Ru^+$ ($[M]^+$): 620.7; found 620.4.

Allyl (4-methyl-2-oxo-2*H*-chromen-7-yl)carbamate (4). To a 4 mL glass vial was added 101 mg 7-amino-4-methylcoumarin and 2.0 mL DMF. To the mixture was added 93 μL pyridine and the mixture was chilled in an ice bath. To the mixture was added 72.8 μL allyl chloroformate dropwise and the mixture was allowed to stir at 0 °C for 4 h and at room temperature for 12 h. The mixture was partitioned between 4 mL 5% (v/v) aqueous HCl and 10 mL EtOAc. The aqueous layer was extracted with EtOAc (2 x 5 mL) and the combined organic layers were washed with sat. aqueous $NaHCO_3$ (2 x 5 mL). Volatiles were removed by rotary evaporation and the product was purified by silica gel column chromatography using gradient elution (100% hexane to 20% EtOAc/hexane) to afford a white solid (28 mg, 19% yield). ^{1}H NMR (500 MHz, $CDCl_3$): δ 7.53 (d, *J* = 8.6, 1H), 7.43 (d, *J* = 2.1, 1H), 7.37 (dd, *J* = 8.6, 2.2, 1H), 6.85 (s, 1H), 6.19 (s, 1H), 6.03 – 5.92 (m, 1H), 5.39 (dq, *J* = 17.1, 1.7, 1H), 5.32 – 5.27 (m, 1H), 4.71 (dd, *J* = 5.8, 1.6, 2H), 2.41 (t, *J* = 0.9, 3H). ^{13}C NMR (126 MHz, $CDCl_3$): δ 161.11, 154.68, 152.77, 152.23, 141.43, 132.13, 125.53, 118.94, 115.78, 114.50, 113.45, 106.14, 66.49, 18.70. High resolution ESI-MS: *m*/*z* calcd for $C_{14}H_{14}NO_4^+$ ($[M+H]^+$): 260.0917; found 260.0915.

Polymer Characterization

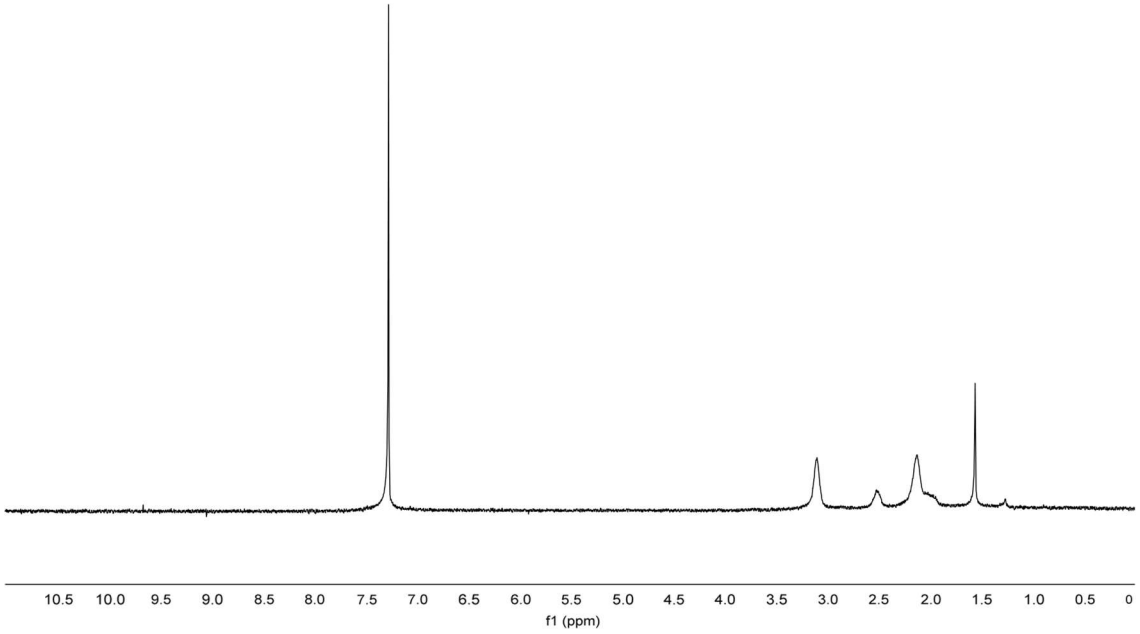

Supplementary Figure 3.1 ^{1}H NMR spectrum ($CDCl_3$) of poly(pentafluorophenyl acrylate).

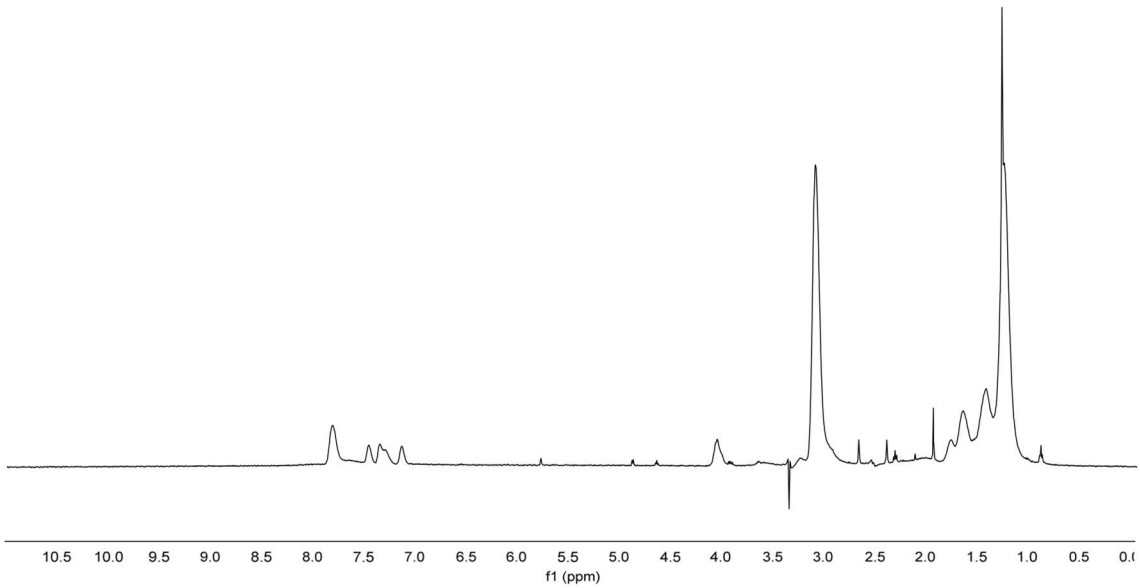

Supplementary Figure 3.2 ^{1}H NMR spectrum (DMSO-d_6, H_2O suppression) of polymer **P1**.

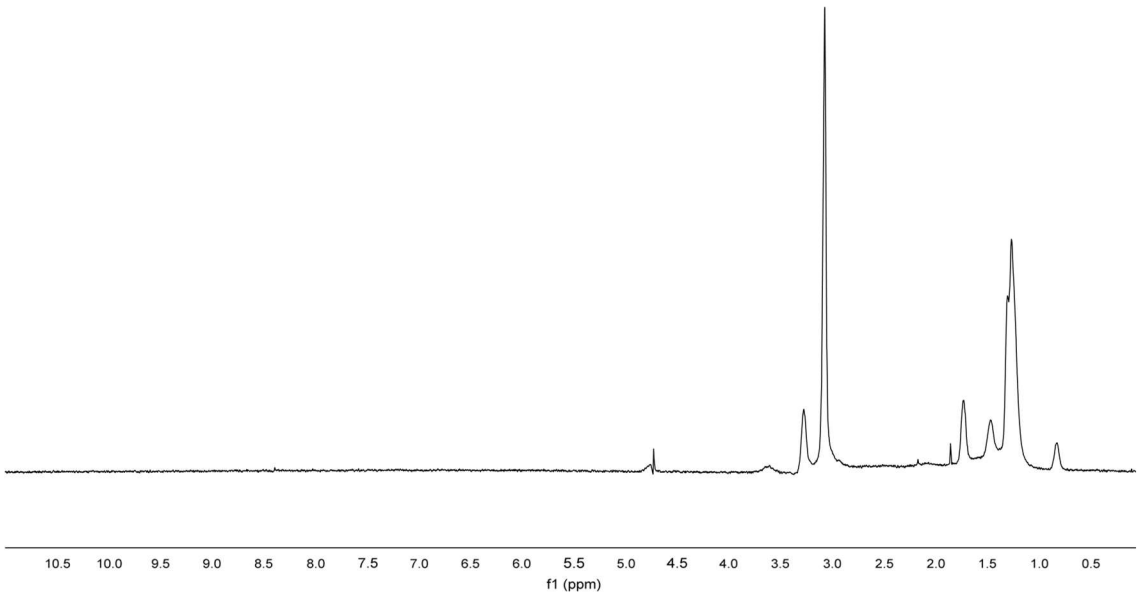

Supplementary Figure 3.3 ^{1}H NMR spectrum (DMSO-d_6, H_2O suppression) of polymer **P2**.

NMR Procedures

Nuclear overhauser effect spectroscopy (NOESY). To an NMR tube was added polymer **P1**, ligand **L1**, or **L2**, and D_2O to obtain final concentrations of 5 μM polymer and 100 μM ligand, and ^1H NMR and NOESY were conducted.

Diffusion ordered spectroscopy (DOSY). To an NMR tube was added polymer **P1**, ligand **L1**, and D_2O to obtain final concentrations of 1 μM polymer and 250 μM ligand. DOSY was conducted using relaxation time of 100 ms and bipolar pulse pair stimulated echo (Dbppste) sequence.

Saturation-transfer difference (STD) NMR. To an NMR tube was added polymer **P1**, ligand **L1**, and D_2O to obtain final concentrations of 1 μM polymer and 250 μM ligand. STD NMR was conducted using irradiation at 0.4 ppm and saturation times of 1, 2, 3, 4, and 5 s. Ligand proton peaks at 7.66 and 1.41 ppm were integrated and the integrations were normalized to the *off-resonance* spectrum. STD amplification factor (A_{STD}) was calculated using Equation 3.1, where I_0 is the *off-resonance* intensity, I_{SAT} is the *on-resonance* intensity, $[L]_T$ is the ligand concentration, and [P] is the polymer concentration. A_{STD} was plotted against saturation time. Ligand mapping was achieved by setting the largest A_{STD} to 100% and calculating other A_{STD} with the same saturation time accordingly.

$$A_{STD} = \frac{I_0 - I_{SAT}}{I_0} x \frac{[L]_T}{[P]} \qquad \textbf{Equation 3.1}$$

Fluorescence Studies

General procedure for critical micelle concentration study. To 16 1-dram glass vials were added aliquots from stock solutions of Nile red and polymer to obtain final concentrations of 1 μM Nile red and 1 mg/mL (33 μM) to 10 ng/mL (330 pM) polymer. To the vials were added magnetic stir bars and the mixtures were stirred for 24 h. The fluorescence emission was measured on a fluorometer using excitation wavelength = 553 nm, scan emission wavelengths = 561 to 700 nm, and slit width = 3 nm. The fluorescence emission at 619 nm was plotted against polymer concentration and the point of inflection was calculated using OriginPro.

General procedure for CuAAC. To a 500 μL glass cuvette was added aliquots from stock solutions of polymer, $CuSO_4 \cdot 5H_2O$ and ligand, azide **1**,[8] alkyne **2**, NaAsc, and PBS buffer or water to obtain final concentrations of 0 – 1 μM polymer, 0 – 5 μM Cu catalyst, 20 μM azide **1**, 40 μM alkyne **2**, and 2 mM NaAsc. The cuvette was capped and the mixture was stirred by pulsing on a vortex machine. CuAAC activity was monitored by measuring the increase in fluorescence on a fluorometer using λ_{ex} = 410 nm, λ_{em} = 480 nm, and slit width = 1.5 nm at room temperature for 30 min or 15 min. The % conversion was calculated based on a standard curve for coumarin click product **3**. The initial rate was calculated by averaging the second derivative values of the linear segment of the fluorescence emission curves. Experiments were performed in triplicate and standard deviation was calculated for n = 3.

General procedure for Ru-catalyzed cleavage of allylcarbamate groups. To a 500 μL glass cuvette was added aliquots from stock solutions of polymer, Ru catalyst, caged coumarin **4**, GSH,

and water to obtain final concentrations of 0 – 1 μM polymer, 0 – 5 μM Ru catalyst, 20 μM caged coumarin **4**, and 300 μM GSH. The cuvette was stirred by pulsing on a vortex machine. Ru-catalyzed cleavage of allylcarbamate groups was monitored by measuring the increase in fluorescence on a fluorometer using λ_{ex} = 375 nm, λ_{em} = 440 nm, and slit width = 2 nm at room temperature for 20 min. The % conversion was calculated based on a standard curve for the decaged coumarin product **5**. The initial rate was calculated by averaging the second derivative values of the linear segment of the fluorescence emission curves. Experiments were performed in triplicate and standard deviation was calculated for n = 3.

3.10 References

1. Xiong, T. M.; Garcia, E. S.; Chen, J.; Alzona, A. J.; Zimmerman, S. C. Enzyme-Like Catalysis by Single Chain Nanoparticles that Use Transition Metal Cofactors. *Submitted* **2021**.
2. Das, A.; Theato, P. Multifaceted Synthetic Route to Functional Polyacrylates by Transesterification of Poly(pentafluorophenyl acrylates). *Macromolecules* **2015**, *48*, 8695-8707.
3. Liu, Y.; Pauloehrl, T.; Presolski, S. I.; Albertazzi, L.; Palmans, A. R. A.; Meijer, E. W. Modular Synthetic Platform for the Construction of Functional Single-Chain Polymeric Nanoparticles: From Aqueous Catalysis to Photosensitization. *J. Am. Chem. Soc.* **2015**, *137*, 13096-13105.
4. Daban, J.-R.; Samsó, M.; Bartolomé, S. Use of Nile Red as a Fluorescent Probe for the Study of the Hydrophobic Properties of Protein-Sodium Dodecyl Sulfate Complexes in Solution. *Anal. Biochem.* **1991**, *199*, 162-168.

5. Pomposo, J. A.; Rubio-Cervilla, J.; Moreno, A. J.; Lo Verso, F.; Bacova, P.; Arbe, A.; Colmenero, J. Folding Single Chains to Single-Chain Nanoparticles via Reversible Interactions: What Size Reduction Can One Expect? *Macromolecules* **2017**, *50*, 1732-1739.

6. Soriano del Amo, D.; Wang, W.; Jiang, H.; Besanceney, C.; Yan, A. C.; Levy, M.; Liu, Y.; Marlow, F. L.; Wu, P. Biocompatible Copper(I) Catalysts for In Vivo Imaging of Glycans. *J. Am. Chem. Soc.* **2010**, *132*, 16893-16899.

7. Besanceney-Webler, C.; Jiang, H.; Zheng, T.; Feng, L.; Soriano del Amo, D.; Wang, W.; Klivansky, L. M.; Marlow, F. L.; Liu, Y.; Wu, P. Increasing the Efficacy of Bioorthogonal Click Reactions for Bioconjugation: a Comparative Study. *Angew. Chem. Int. Ed. Engl.* **2011**, *50*, 8051-8056.

8. Sivakumar, K.; Xie, F.; Cash, B. M.; Long, S.; Barnhill, H. N.; Wang, Q. A Fluorogenic 1,3-Dipolar Cycloaddition Reaction of 3-Azidocoumarins and Acetylenes. *Org. Lett.* **2004**, *6*, 4603-4606.

9. Zhou, Z.; Fahrni, C. J. A Fluorogenic Probe for the Copper(I)-Catalyzed Azide−Alkyne Ligation Reaction: Modulation of the Fluorescence Emission via $^{3}(n,\pi^*)$–$^{1}(\pi,\pi^*)$ Inversion. *J. Am. Chem. Soc.* **2004**, *126*, 8862-8863.

10. Chen, J.; Wang, J.; Bai, Y.; Li, K.; Garcia, E. S.; Ferguson, A. L.; Zimmerman, S. C. Enzyme-like Click Catalysis by a Copper-Containing Single-Chain Nanoparticle. *J. Am. Chem. Soc.* **2018**, *140*, 13695-13702.

11. Artar, M.; Souren, E. R. J.; Terashima, T.; Meijer, E. W.; Palmans, A. R. A. Single Chain Polymeric Nanoparticles as Selective Hydrophobic Reaction Spaces in Water. *ACS Macro Lett.* **2015**, *4*, 1099-1103.

12. Liu, Y.; Turunen, P.; De Waal, B. F. M.; Blank, K. G.; Rowan, A. E.; Palmans, A. R. A.; Meijer, E. W. Catalytic Single-Chain Polymeric Nanoparticles at Work: from Ensemble Towards Single-Particle Kinetics. *Mol. Syst. Des. Eng.* **2018**, *3*, 609-618.

13. Neuhaus, D.; Williamson, M. P. *The Nuclear Overhauser Effect in Structural and Conformational Analysis*. 2nd ed.; Wiley-VCH: New York, 2000.

14. Viegas, A.; Manso, J.; Nobrega, F. L.; Cabrita, E. J. Saturation-Transfer Difference (STD) NMR: a Simple and Fast Method for Ligand Screening and Characterization of Protein Binding. *J. Chem. Educ.* **2011**, *88*, 990-994.

15. Chen, J.; Wang, J.; Li, K.; Wang, Y.; Gruebele, M.; Ferguson, A. L.; Zimmerman, S. C. Polymeric "Clickase" Accelerates the Copper Click Reaction of Small Molecules, Proteins, and Cells. *J. Am. Chem. Soc.* **2019**, *141*, 9693-9700.

16. Tanaka, S.; Saburi, H.; Murase, T.; Yoshimura, M.; Kitamura, M. Catalytic Removal of *N*-Allyloxycarbonyl Groups Using the [CpRu(IV)(π-C_3H_5)(2-quinolinecarboxylato)]PF_6 Complex. A New Efficient Deprotecting Method in Peptide Synthesis. *J. Org. Chem.* **2006**, *71*, 4682-4684.

17. Völker, T.; Meggers, E. Chemical Activation in Blood Serum and Human Cell Culture: Improved Ruthenium Complex for Catalytic Uncaging of Alloc-Protected Amines. *ChemBioChem* **2017**, *18*, 1083-1086.

18. Volker, T.; Dempwolff, F.; Graumann, P. L.; Meggers, E. Progress Towards Bioorthogonal Catalysis with Organometallic Compounds. *Angew. Chem. Int. Ed. Engl.* **2014**, *53*, 10536-10540.

19. Han, X.; Wang, R.; Song, X.; Yu, F.; Lv, C.; Chen, L. A Mitochondrial-Targeting Near-Infrared Fluorescent Probe for Bioimaging and Evaluating Endogenous Superoxide Anion

Changes during Ischemia/reperfusion Injury. *Biomaterials* **2018**, *156*, 134-146.

20. Budhathoki-Uprety, J.; Peng, L.; Melander, C.; Novak, B. M. Synthesis of Guanidinium Functionalized Polycarbodiimides and Their Antibacterial Activities. *ACS Macro Lett.* **2012**, *1*, 370-374.

CHAPTER 4: INTRODUCTION TO SELF-PROTECTING COATINGS

4.1 Self-Protecting Coatings

Coatings are applied to surfaces for decoration or to change their physical and chemical properties, such as adhesion, wettability, and corrosion resistance. For example, anticorrosion coatings are used in many industries to protect metal substrates from corrosion damage. They may contain an anticorrosion active agent, such as a metal phosphate, dispersed throughout the polymer matrix.[1] However, this strategy suffers from multiple disadvantages, including uncontrollable release of the compound and leaching by environmental factors such as rain.[2] A potential solution is to encapsulate the active agents within microcapsules for stimuli-responsive release, at which time the compounds can form a protective layer via absorption on the surface of the metal substrate.[3] Previously, Sottos and coworkers reported self-protecting coatings embedded with microcapsules containing lawsone.[4] This system is dependent on mechanical damage of the microcapsule shell wall for the cargo to be released.

We envision a system in which the microcapsules can respond to other external triggers, such as pH. In a corrosive environment, a decrease in pH occurs with the anodic corrosion half reaction.[5] Thus, we designed a ketal-based cross-linked polyamide microcapsule that would protect and stabilize the core content in a neutral environment until exposure to low pH in a corrosive environment triggers shell wall degradation and cargo release. Microcapsules that demonstrate pH-responsive anticorrosion behavior have been previously reported,[6-9] however, there are few examples of robust microcapsules that can survive solvent-based commercial coatings. We demonstrate the compatibility of our material with a variety of commercial coatings and explore their anticorrosion ability under different acidic conditions.

4.2 References

1. Montemor, M. F. Functional and Smart Coatings for Corrosion Protection: A Review of Recent Advances. *Surf. Coatings Technol.* **2014**, *258*, 17–37.
2. Jämsä, S.; Mahlberg, R.; Holopainen, U.; Ropponen, J.; Savolainen, A.; Ritschkoff, A. C. Slow Release of a Biocidal Agent from Polymeric Microcapsules for Preventing Biodeterioration. *Prog. Org. Coatings* **2013**, *76*, 269–276.
3. Chen, Y.; Wei, W.; Zhu, Y.; Luo, J.; Liu, R.; Liu, X. Synthesis of Temperature/pH Dual-Stimuli-Response Multicompartmental Microcapsules via Pickering Emulsion for Preprogrammable Payload Release. *ACS Appl. Mater. Interfaces* **2020**, *12*, 4821–4832.
4. Odarczenko, M.; Thakare, D.; Li, W.; Yang, K.; Tang, S.; Venkateswaran, S. P.; Sottos, N. R.; White, S. R. Self-Protecting Epoxy Coatings with Anticorrosion Microcapsules. *ACS Omega* **2018**, *3*, 14157–14164.
5. Zheludkevich, M. L.; Shchukin, D. G.; Yasakau, K. A.; Möhwald, H.; Ferreira, M. G. S. Anticorrosion Coatings with Self-Healing Effect Based on Nanocontainers Impregnated with Corrosion Inhibitor. *Chem. Mater.* **2007**, *19*, 402–411.
6. Tavandashti, N. P.; Ghorbani, M.; Shojaei, A.; Mol, J. M. C.; Terryn, H.; Baert, K.; Gonzalez-Garcia, Y. Inhibitor-Loaded Conducting Polymer Capsules for Active Corrosion Protection of Coating Defects. *Corros. Sci.* **2016**, *112*, 138–149.
7. Matsuda, T.; Kashi, K. B.; Fushimi, K.; Gelling, V. J. Corrosion Protection of Epoxy Coating with pH Sensitive Microcapsules Encapsulating Cerium Nitrate. *Corros. Sci.* **2019**, *148*, 188–197.
8. Snihirova, D.; Lamaka, S. V.; Cardoso, M. M.; Condeço, J. A. D.; Ferreira, H. E. C. S.; De Fatima Montemor, M. pH-Sensitive Polymeric Particles with Increased Inhibitor-Loading

Capacity as Smart Additives for Corrosion Protective Coatings for AA2024. *Electrochim. Acta* **2014**, *145*, 123–131.

9. Kim, C.; Karayan, A. I.; Milla, J.; Hassan, M.; Castaneda, H. Smart Coating Embedded with pH-Responsive Nanocapsules Containing a Corrosion Inhibiting Agent. *ACS Appl. Mater. Interfaces* **2020**, *12*, 6451–6459.

CHAPTER 5: ACID-RESPONSIVE MICROCAPSULES FOR ANTI-CORROSION COATINGS

Part of this chapter has been adapted and modified from the following publication: Thakare, D. R.*; **Xiong, T. M.***; Flueck, I. C.; Morado, E. G.; Zimmerman, S. C.; Sottos, N. R. Acid-Responsive Anticorrosion Microcapsules for Self-Protecting Coatings. *Submitted* **2021**.

5.1 Design and Synthesis of Microcapsules

We designed ketal-based cross-linked polyamide microcapsules, which effectively degrade under acidic conditions and release an anticorrosion agent (Scheme 5.1). Fréchet and coworkers have utilized ketal-based cross-linked polyamide microcapsules for pH-responsive drug delivery.[1,2] The ketal unit's responsive behavior under mild conditions (pH < 6) makes it attractive for anticorrosion applications. Based on a previously reported procedure, I synthesized ketal-

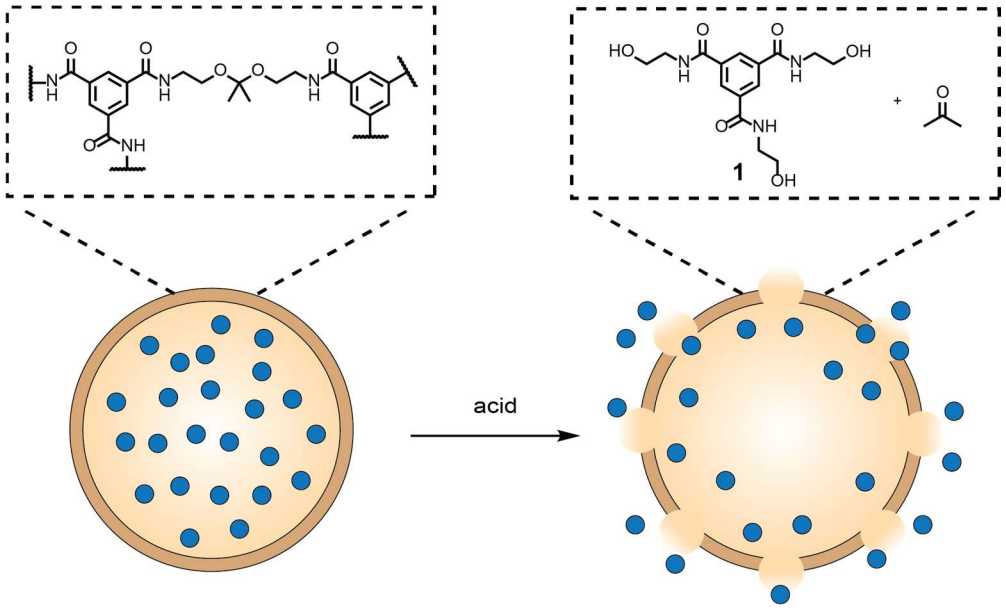

Scheme 5.1 Ketal-based cross-linked polyamide microcapsules degrade and release an anticorrosion agent under acidic conditions.

containing monomer diethylaminoketal (DEAK) in two steps on 100 g scale.[1] The microcapsules were obtained using interfacial polymerization with DEAK and cross-linking monomer trimesoyl chloride (TMC). An oil phase containing TMC, indicator dye methyl yellow, and an anticorrosive agent (6% w/v) was emulsified in 3 wt% poly(vinyl alcohol) (PVA) (M_w = 13,000 – 23,000 g/mol, 87-89% hydrolyzed) in dionized water. Then an aqueous solution of DEAK (38% v/v, pH = 9.5) was added dropwise to initiate the formation of the cross-linked polyamide shell wall. The resulting microcapsules were collected by centrifugation and freeze-dried on a lyophilizer to obtain a powder.

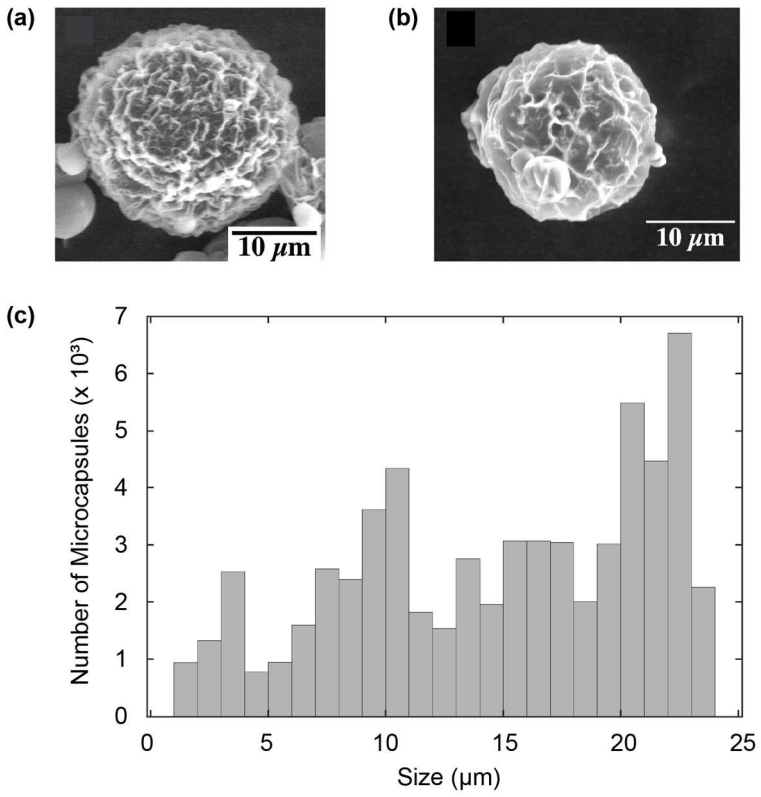

Figure 5.1 SEM images of (a) butyne-diOTMS and CTG (50% v/v) microcapsules and (b) JJB and CTG (50% v/v) microcapsules. (c) DLS size distribution by number of the microcapsules (n = 62,000).

Two different anticorrosive active agents were encapsulated using the above procedure. The first set of microcapsules contained trimethylsilyl (TMS) protected 2-butyne-1,4-diol (butyne-

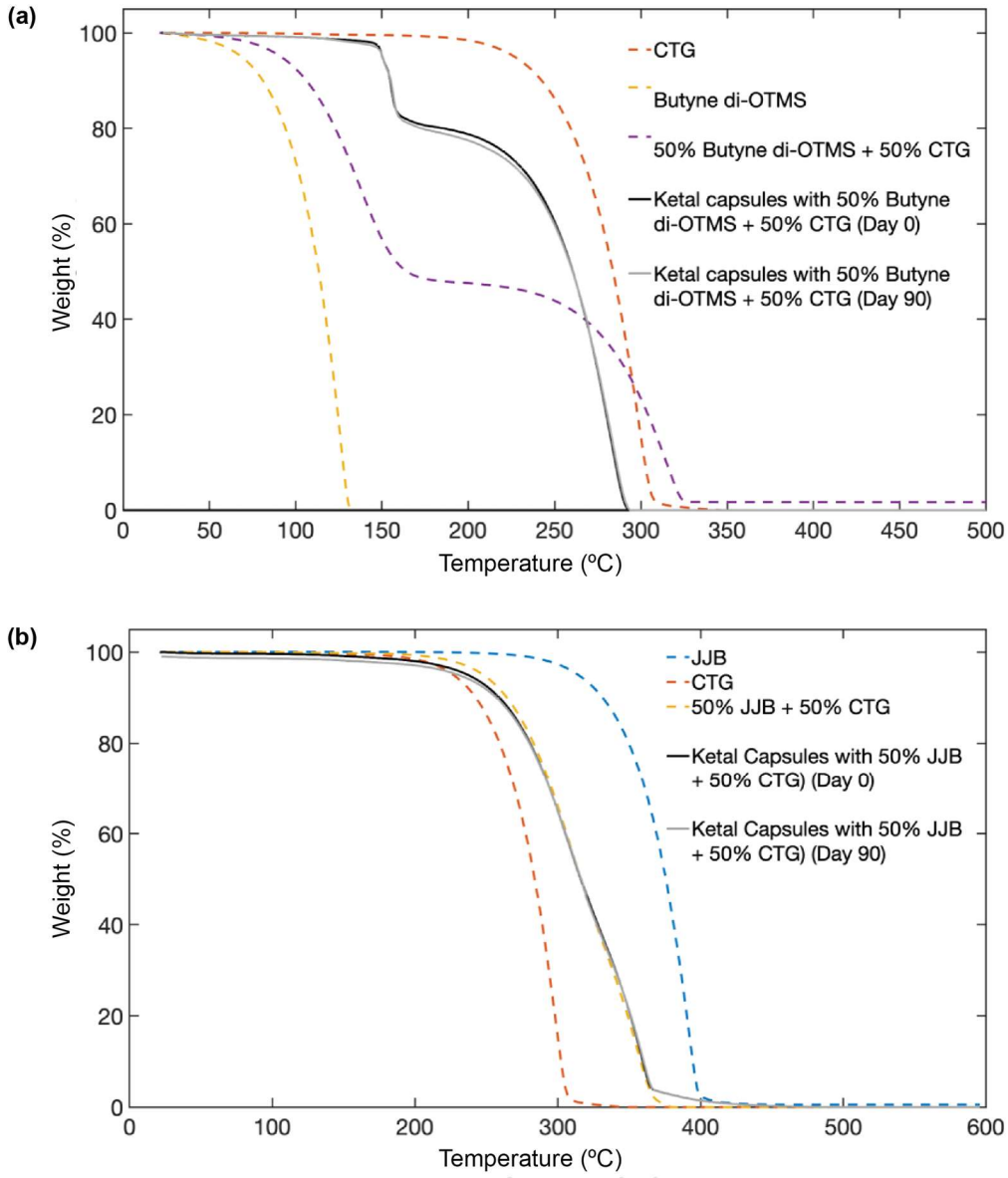

Figure 5.2 (a) TGA analysis of butyne-diOTMS and CTG (50% v/v) microcapsules on day 0 (solid black line) and day 90 (solid gray line) and the unencapsulated components (dashed lines). (b) TGA analysis of JJB and CTG (50% v/v) microcapsules on day 0 (solid black line) and day 90 (solid gray line) and the unencapsulated components (dashed lines).

diOTMS) diluted with capric/caprylic triglyceride (CTG, 50% v/v). The alcohol groups were TMS protected to increase the hydrophobicity of 2-butyne-1,4-diol (BD) for encapsulation and to prevent side reactions between BD and TMC duing interfacial polymerization. The TMS protecting group is cleaved within 1 min at pH = 5 such that BD is readily available after cargo release under the acidic conditions explored in this study. The second set of microcapsules contained greener alternative jojoba oil (JJB) diluted with CTG (50% v/v). CTG was added to improve the solubility of TMC in butyne-diOTMS and JJB. BD and JJB are reported to be effective organic corrosion inhibitors in acidic solutions.[3-6] They function by adsorbing via noncovalent bonds onto the metal substrate to form a protective layer.[4]

The microcapsule core content was determined using ^{1}H NMR with JJB microcapsules. I induced degradation of the microcapsules using DCl and quantified the amount of JJB and CTG based on the appearance of proton peaks at δ 5.5 and 5.3 ppm, respectively. The core content was determined for JJB (42 ± 1 wt%) and CTG (40 ± 1 wt%) based on their respective standard curves. The microcapsules were also characterized by scanning electron microscopy (SEM) and dynamic light scattering (DLS) (Figure 5.1). The microcapsules have an average hydrodynamic diameter of 14 μm, which falls within the optimal size range of 10 – 20 μm for coating applications.[7,8] The thermal stability of the microcapsules was determined using thermogravimetric analysis (TGA) immediately after preparation and after 90 d (Figure 5.2). The microcapsules demonstrated thermal stability up to 150 ºC and long-term stability after storage for three months at room temperature.

5.2 Characterization of Microcapsule Shell Wall Degradation and Cargo Release

Next I quantified the acid-triggered response of the microcapsules by determining the degradation profile of the shell wall and release profile of the cargo using ^{1}H NMR and gas

chromatography (GC), respectively. Microcapsules containing butyne-diOTMS and CTG (50% v/v) were used in both studies. For examining the degradation profile of the shell wall, 1 mg microcapsules was added to aqueous deuterated buffer solutions at various pD values (pD = 1, 2,

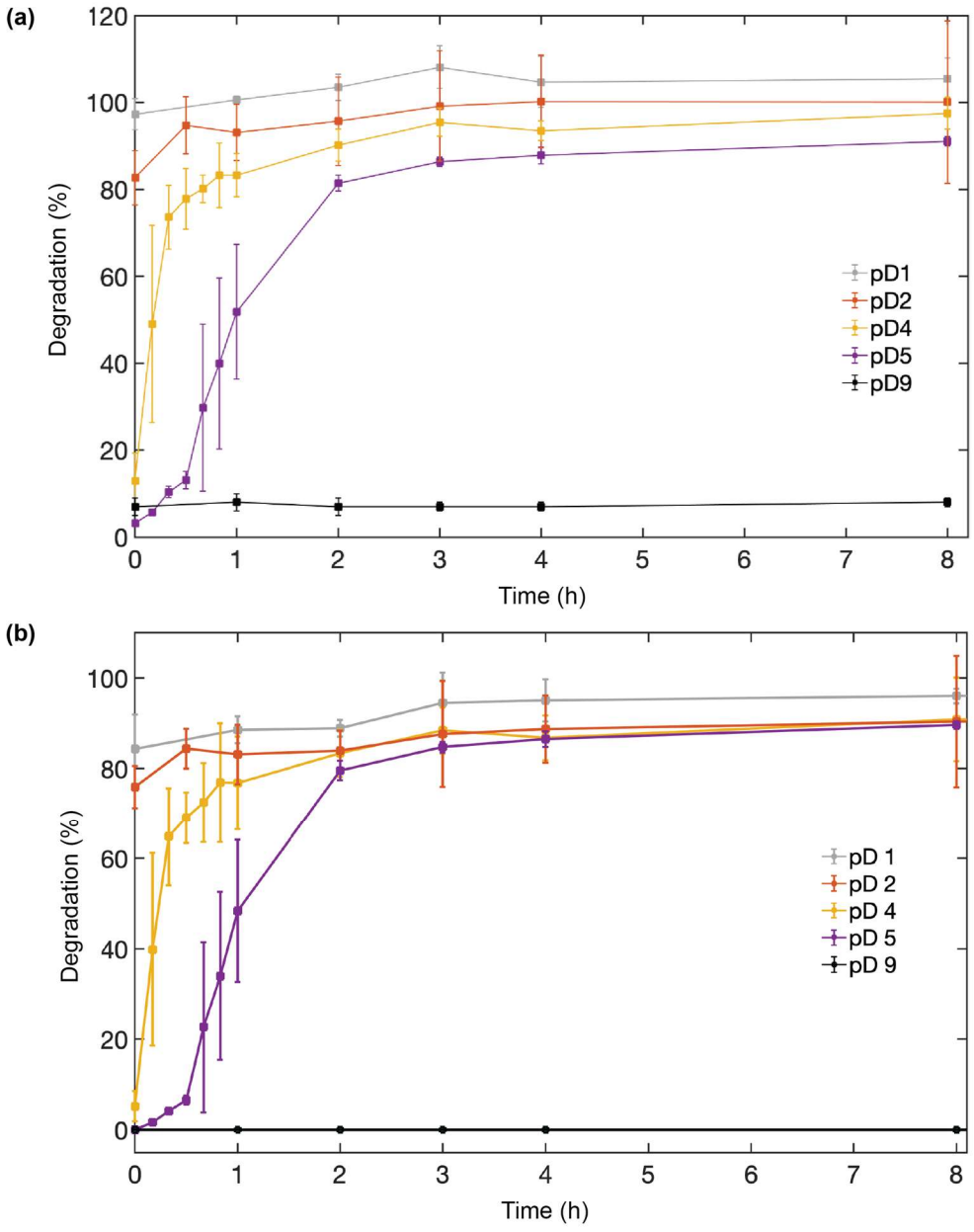

Figure 5.3 Degradation profiles of butyne-diOTMS and CTG (50% v/v) microcapsules in various deuterated aqueous buffer solutions tracking the appearance of (a) acetone and (b) triamide **1** using ^{1}H NMR. Error bars calculated from n = 3.

4, 5, and 9) and ^{1}H NMR spectra were obtained at various time points (Figure 5.3). The appearance of proton peaks at 3.4 – 3.7 ppm and 2.1 ppm corresponding to degradation products triamide **1** and acetone, respectively, were observed. The integrations of these proton peaks at each time point were converted to percent degradation values using a calibration curve. The microcapsules achieved quantitative degradation within 5 min at pD 1 and 2, >80% degradation within 2 h at pD 4 and 5, and little to no degradation within 2 d at pD 9. I observed a slightly faster rate of degradation when tracking the appearance of acetone compared to that of triamide **1**. I rationalize that acetone is a small, water-miscible compound that more readily enters the aqueous deuterated buffer solution for faster detection by ^{1}H NMR. In comparison, triamide **1** is more hydrophobic and may prefer to aggregate in or around the microcapsule fragments.

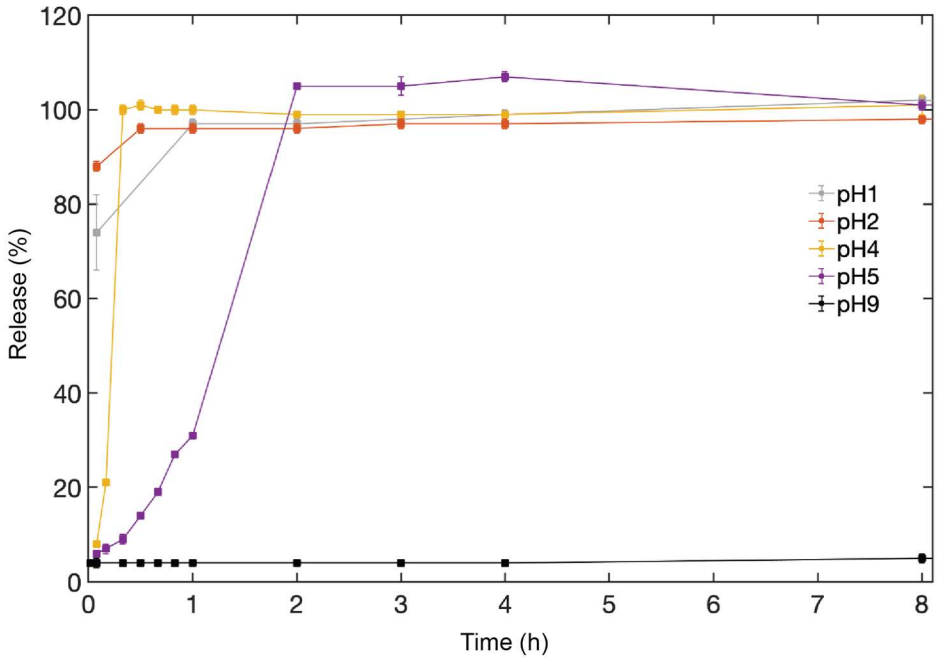

Figure 5.4 Release profile of butyne-diOTMS and CTG (50% v/v) microcapsules in biphasic toluene/aqueous buffer mixtures tracking the appearance of CTG using GC. Error bars calculated from n = 3.

For examining the release profile of the cargo, 50 mg microcapsules were suspended at the interface between toluene and an aqueous buffer solution at various pH levels (pH = 1, 2, 4, and 5) (Figure 5.4). Small aliquots of the organic layer were analyzed by GC at various time points and the appeareance of peaks corresponding to CTG were observed. The integrations of these peaks at each time point were converted to percent release values using a calibration curve. The release profile of CTG is consistent with the degradation profile of the microcapsule shell wall. I observed >80% release within 5 min at pH = 1, 2, 4, and 5 and little to no release at pH = 9. The release profile is slightly faster than the degradation profile because cargo release does not require full degradation of the microcapsule shell wall.

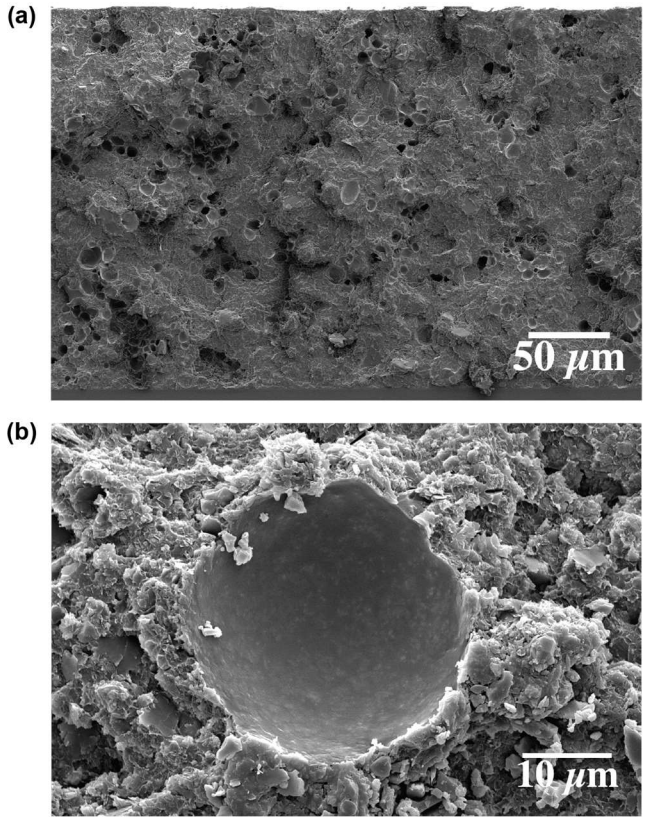

Figure 5.5 SEM images of a cross-section of a phenolic epoxy coating embedded with 10 wt% butyne-diOTMS microcapsules showing (a) even dispersion of microcapsules and (b) intact microcapsule shell.

5.3 Synthesis and Characterization of Microcapsule-Loaded Coatings

Commercially available phenolic epoxy coating was loaded with 5 or 10 wt% microcapsules containing either butyne-diOTMS or JJB and CTG (50% v/v). The coatings were diluted with a thinner composed of organic solvents including toluene, methyl ethyl ketone, and xylene. [9,10] All coatings were maintained at a constant dried film thickness of 110 μm. Cross-sections of the microcapsule-loaded coating were imaged by SEM (Figure 5.5). We observed intact microcapsules, which suggested the microcapsules are stable in a solvent-based coating environment. The images also indicate that the microcapsules are evenly dispersed throughout the coating.

5.4 Anti-Corrosive Behavior of Microcapsule-Loaded Coatings

My collaborator Dhawal Thakare examined the anticorrosion performance of the microcapsule-loaded coatings on steel substrates using electrochemical corrosion (EC) measurements based on a previously reported procedure by Odarczenko and coworkers (Figure 5.6).[7] The samples were damaged and immediately submerged in an electrolyte chamber with 5 wt% NaCl solution at pH = 1, 2, or 4. The corrosion currents for the control (I_o) and microcapsule-loaded samples (I_i) were measured and used to calculate the inhibition efficiency (IE) as shown in Equation 5.1.

$$IE(\%) = \frac{I_o - I_i}{I_o} x100 \qquad \textbf{Equation 5.1}$$

The IE measures the anticorrosion performance of a self-protecting coating through the reduction in corrosion current. We observed >70% IE with 10 wt% butyne-diOTMS microcapsules in pH =

4, 5 wt% NaCl solutions. IE decreased with decreasing pH of the salt solution and with decreasing capsule loading. We rationalize that decreasing pH accelerates the corrosion process but the amount of corrosion inhibitor remains the same. In addition, decreasing the amount of capsule loading lowers the amount of available corrosion inhibitor. In general, butyne-diOTMS microcapsules produced higher IE than JJB microcapsules. This higher anticorrosion ability may be attributed to interations between the BD triple bond and alcohol groups and the metal substrate surface.[4]

Water-based epoxies loaded with no capsules, 10 wt% butyne-diOTMS microcapsules, or 10 wt% JJB microcapsules were synthesized and used to visualize the anticorrosion performance of the microcapsule-loaded coatings (Figure 5.7). The coatings were damaged, immediately submerged in a 5 wt% NaCl solution at pH = 4 for 4 d, and then imaged. In the optical images

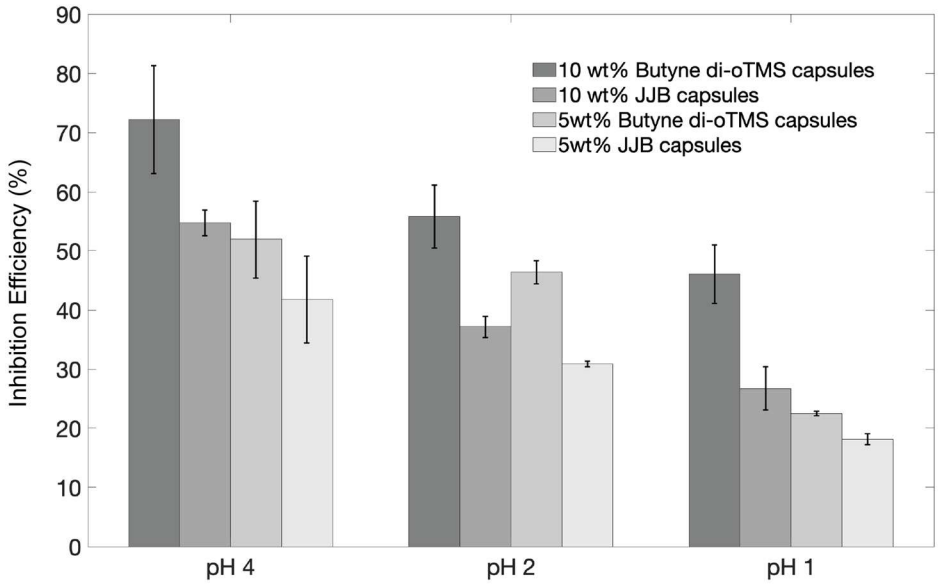

Figure 5.6 Variation of IE of phenolic epoxy coatings embedded with acid-responsive microcapsules as a function of the pH of a 5 wt% NaCl solution and microcapsule concentration. Error bars represent standard deviation for n = 3.

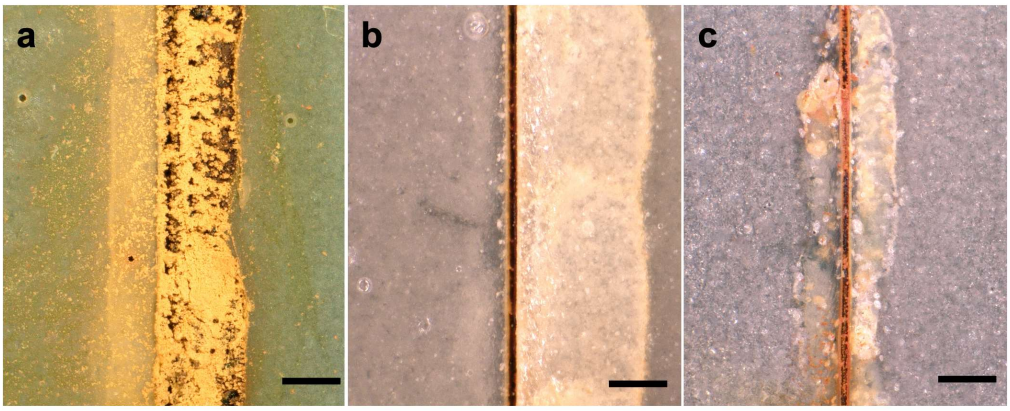

Figure 5.7 Optical images of scribed water-based epoxy coatings embedded with (a) no microcapsules, (b) 10 wt% butyne di-OTMS microcapsules, and (c) 10 wt% JJB microcapsules after being exposed to a 5 wt% NaCl solution of pH = 4. Scale-bar = 400 μm.

following exposure, the microcapsule-loaded coatings produced reduced corrosion product, which suggested they provide more protection against corrosion damage than the control coating.

5.5 Conclusions

In conclusion, we have developed acid-responsive microcapsules for self-protecting anticorrosion coatings. The ketal-based polyamide microcapsules were synthesized from interfacial polymerization and efficiently degrade and release either active agent butyne-diOTMS or JJB under acidic conditions. EC analysis on steel substrates coated with commercially available polymer resins demonstrated that the anticorrosion performance of the microcapsule-loaded coatings increases with higher microcapsule loading and higher pH values up to 5. Butyne-diOTMS microcapsules showed higher IE compared to JJB microcapsules. Future studies can focus on improving the anticorrosion performance of the microcapsule-loaded coatings by encapsulating other reported anticorrosion active agents. Further, these microcapsules are

compatible with a wide variety of commercially available polymer resins and may be incorporated into different materials for pH-responsive products.

5.6 Experimental Section

General Experimental Procedures

SEM was conducted on a Quanta 450 FEG ESEM (FEI Company, Hillsboro OR). TGA was obtained on a Q50 TA Instrument. The temperature during TGA experiments was varied from 22 ºC to 600 ºC at a rate of 10 ºC/min. GC was performed on a Shimadzu GC-2010 Plus with LabSolutions Lite software. Images were taken with a digital microscope (Keyence VHX 6000 series). Phenoline 187 Part A and B (Phenolic Epoxy) and thinner (Thinner 2) was provided as a gift sample from Carboline, MO. Epirez resin 6520-WH-53 (water-based epoxy) and Epikure curing agent 6870-W-53 were obtained from Chemical Marketing Concepts Inc. Hot rolled steel substrates following ASTM A569 were purchased from Metals Depot (Winchester, KY, USA). For additional information, see Chapter 2. 2. 5 Experimental Section.

Synthetic Procedures

2,2'-((Propane-2,2-diylbis(oxy))bis(ethane-2,1-diyl))bis(isoindoline-1,3-dione) (S1). To an oven-dried 1 L round bottom flask was added 100 g 2-(2-hydroxyethyl) isoindoline-1,3-dione, 500 mL dry toluene, 31 mL 2,2-dimethoxypropane, and 100 mg *p*-TSA. A Dean-Stark apparatus was attached, the flask was transferred to an oil bath preheated to 125 °C, and the mixture was stirred at reflux under N_2 atm overnight. Toluene/MeOH was removed azeotropically by occasionally

draining the Dean-Stark trap. The mixture was cooled to 70 °C, 146 mL TEA, and 25 mL acetic anhydride were added, and the mixture was stirred under N_2 atm for 2 h. The mixture was cooled to 30 °C and poured into 2.5 L hexane. The resulting precipitate was collected by vacuum filtration, suspended in a small volume of hot EtOAc, and filtered again to afford an off-white solid (68.33 g, 65% yield). ^{1}H NMR (acetone-d_6) δ 7.82 (m, 4H), 7.78 (m, 4H), 3.75 (t, J = 6.3, 4H), 3.57 (t, J = 6.3, 4H), 1.24 (s, 6H).

2,2'-(Propane-2,2-diylbis(oxy)) bis(ethan-1-amine) (S2). To a 1 L round bottom flask was added 63.8 g compound **S1** and 400 mL of a 3 M aq. solution of NaOH. The flask was transferred to an oil bath preheated to 110 °C, and the mixture was stirred at reflux under N_2 atm overnight. The mixture was cooled to room temperature and chilled in an ice bath. The aqueous layer was washed with DCM (6 x 500 mL). The combined organic layers were dried over Na_2SO_4, filtered, and concentrated by rotary evaporation to afford a pale-yellow liquid (9.53 g, 39% yield). ^{1}H NMR δ 3.43 (t, J = 5.3, 4H), 2.82 (t, J = 5.3, 4H), 1.34 (s, 6H).

2,2,9,9-Tetramethyl-3,8-dioxa-2,9-disiladec-5-yne (S3). To a 500 mL round bottom flask was added 6.87 g diol, 200 mL dry DCM, and 27.8 mL TEA, and the mixture was stirred at room temperature under N_2 atm for 20 min until all solids dissolved. The flask was transferred to an ice bath and stirred under N_2 atm for five min. To the chilled mixture was added 21.3 mL TMSCl via syringe, and the mixture was stirred under N_2 atm for 4 h. The mixture was poured into ~20 g ice and immediately transferred to a separatory funnel. The aqueous layer was washed with DCM (2 x 150 mL), and the combined organic layers were dried over Na_2SO_4 and filtered. To the filtrate

was added 500 mL hexane. The product was purified by a silica gel plug to obtain a clear liquid (12.38 g, 67% yield). ^{1}H NMR (500 MHz) δ 4.31 (s, 4H), 0.16 (s, 18H).

General Procedure for Quantification of Microcapsule Core Content

A stock solution of 2 mM duroquinone in toluene-d_8 was prepared and used as the internal standard. To a 20 mL glass vial was added 50 mg microcapsules, 50 μL 20 wt% aqueous DCl, and 2 mL DCM. The mixture was sonicated for 2 h and the solvent was removed by rotary evaporation. The residue was suspended in 1 mL toluene-d_8. To an NMR tube was added 10 μL 2 mM standard, 50 μL microcapsule mixture, and 450 μL toluene-d_8, and ^{1}H NMR was obtained. Experiments were performed in triplicate and standard deviation was calculated for n = 3. Ketal microcapsules containing (50% JJB and 50% CTG) were used for these studies. Core content was determined for JJB (42 ± 0.8 wt%) and CTG (40 ± 1 wt%) based on their respective standard curves. For standard curves, stock solutions of 5 mg/mL JJB and CTG in toluene-d_8 were prepared. A stock solution of 2 mM duroquinone in toluene-d_8 was prepared and used as the internal standard. ^{1}H NMR was obtained for samples containing 0, 0.5, 1.0, 1.5, 2.0, and 2.5 mg compound. The proton peaks at 5.47 and 5.32 ppm corresponding to JJB and CTG, respectively, were integrated, and the data was plotted against mass and fitted to a linear curve.

General Procedure for Degradation Profile of Microcapsules

Buffered aqueous solutions (pD = 1 and 2) were prepared by dissolving 75 mg KCl in 10 mL D_2O (100 mM) and adjusting the pH with 20 wt% aqueous DCl. Buffered aq. solutions (pD = 4, 5, 7, and 9) were prepared by dissolving 81 μL pyridine in 10 mL D_2O (100 mM) and adjusting the pH with 20 wt% aqueous DCl. All pH values were measured using a glass electrode pH meter and

adjusted using the following formula: pD = 0.4 + pH reading. Stock solutions of 100 mM and 2 mM 3-(trimethylsilyl) propionic-2,2,3,3-d_4 acid sodium salt in D_2O were prepared and used as the internal standard. To an NMR tube was added ~1 mg microcapsule, 10 μL 100 mM standard and 490 μL deuterated buffer, or 5 μL 2 mM standard and 495 μL deuterated buffer. The NMR tube was capped and ^1H NMR spectra were taken at different time points. The appearance of proton peaks at 3.4 – 3.7 ppm and 2.1 ppm corresponding to degradation products triamide **1** and acetone, respectively, were observed. Experiments were performed in triplicate and standard deviation was calculated for n = 3. To each NMR sample was added 5 μL 20 wt% aqueous DCl to induce microcapsule degradation. The integrations of these peaks were set as 100% degradation and the % degradation was calculated as a ratio of (integration at time point) / (integration of final) x 100.

General Procedure for Cargo Release of Microcapsules

Buffered aqueous solutions (pH = 1 and 2) were prepared by dissolving 0.45 g KCl in 60 mL water (100 mM) and adjusting the pH with 37 wt% aqueous HCl. Buffered aq. solutions (pH = 4, 5, 7 and 9) were prepared by dissolving 483 μL pyridine in 60 mL water (100 mM) and adjusting the pH with 37 wt% aqueous HCl. To a 20 mL glass vial was added 10 mL aq. buffer, 50 mg microcapsules, 10 μL dodecane, and 10 mL toluene. Aliquots of 50 μL were taken at different time points and analyzed by GC. Triplicates were repeated for each aqueous buffer. To each vial was added 50 μL 37 wt% aqueous HCl to induce microcapsule degradation. The integrations of these peaks were set as 100% degradation and the % degradation was calculated as a ratio of (integration at time point) / (integration of final) x 100.

General Procedure for Microcapsule-Loaded Coatings

Steel substrates (14.0 by 10.0 by 0.5 cm) were sandblasted according to ASTM D7055-09 with 180 grit aluminum oxide blast media. The blasted steel surfaces were cleaned with compressed air to remove excess grit and rinsed with acetone to remove dirt and oils. Control coatings were made by mixing Part A and B of the phenolic resin in 2:1 ratio (w/w) and the self-protecting coatings were made by adding 5 or 10 wt% microcapsules with respect to the epoxy mixture. The mixture was diluted with 10 wt% thinner to aid in dispersion and viscosity modification. The coating mixture was then applied with a micrometer-controlled doctor blade. The applied coating material was cured for 3 d at 35 °C. The dried film thickness of the coating was determined using a coating thickness gauge (PCE-CT 65, PCE Americas Inc., FL). The coatings were inflicted with uniform scribe damage with a corrocutter (Erichsen 639) affixed with a razor blade.

General Procedure for Electrochemical Corrosion Measurement

The coated steel substrate was damaged and then immediately submerged in an electrolyte chamber (5 wt% NaCl solution with pH = 1, 2, or 4). The electrolyte chamber was clamped to the coated steel substrate, with the steel substrate acting as the working electrode, a platinum wire as the counter electrode (BASi MW-1032), and a silver/silver chloride electrode as the reference (BASi MF-2052). Potentiodynamic linear polarization measurements at room temperature were performed with a Bio-Logic VSP potentiostat. The open-circuit potential was first measured for 30 min, following which, a stepwise voltage from −100 to 100 mV at a rate of 0.2 mV/s was applied with respect to the open-circuit voltage and the current was measured throughout. Tafel extrapolation was used to determine the steady-state corrosion current.[7] The corrosion current for the control (I_o) and self-protecting samples (I_i) was measured and used to calculate the IE as shown

in Equation 5.1. EC analysis was repeated three times for each of the different types of microcapsules and electrolytes.

5.7 References

1. Broaders, K. E.; Pastine, S. J.; Grandhe, S.; Fréchet, J. M. J. Acid-Degradable Solid-Walled Microcapsules for pH-Responsive Burst-Release Drug Delivery. *Chem. Commun.* **2011**, *47*, 665–667.
2. Paramonov, S. E.; Bachelder, E. M.; Beaudette, T. T.; Standley, S. M.; Lee, C. C.; Dashe, J.; Fréchet, J. M. J. Fully Acid-Degradable Biocompatible Polyacetal Microparticles for Drug Delivery. *Bioconjug. Chem.* **2008**, *19*, 911–919.
3. Meresht, E. S.; Farahani, T. S.; Neshati, J. 2-Butyne-1,4-Diol as a Novel Corrosion Inhibitor for API X65 Steel Pipeline in Carbonate/Bicarbonate Solution. *Corros. Sci.* **2012**, *54*, 36–44.
4. Muralidharan, V. S.; Mohideen, A. M. U.; Selvan, R. A. M. Mechanism of Inhibition of Iron Corrosion in HCl by Acetylenic Alcohols. *Anti-Corros. Method M.* **1995**, *42*, 17–20.
5. Bockris, J. O. M.; Yang, B. The Mechanism of Corrosion Inhibition of Iron in Acid Solution by Acetylenic Alcohols. *J. Electrochem. Soc.* **1991**, *138*, 2237-2252.
6. Jackson, J. Application of Corrosion Inhibitors for Steels in Acidic Media for the Oil and Gas Industry : A Review. *Corros. Sci.* **2014**, *86*, 17–41.
7. Odarczenko, M.; Thakare, D.; Li, W.; Yang, K.; Tang, S.; Venkateswaran, S. P.; Sottos, N. R.; White, S. R. Self-Protecting Epoxy Coatings with Anticorrosion Microcapsules. *ACS Omega* **2018**, *3*, 14157–14164.

8. Odarczenko, M.; Thakare, D.; Li, W.; Venkateswaran, S. P.; Sottos, N. R.; White, S. R. Sunlight-Activated Self-Healing Polymer Coatings. *Adv. Eng. Mater.* **2020**, *22*, 1901223.

9. Carboline Phenoline 187 https://www.carboline-me.com/products/product-details/?prod=1103.

10. Carboline Thinner 2 https://www.carboline.com/products/product-details/?prod=0522.